Design of modified steel shipping containers for ambient and elevated temperatures

by

Christian Oosthuysen

In partial fulfilment of the requirements for the degree of Master of Engineering in Structural Engineering in association with the Faculty of Engineering at Stellenbosch University

Supervisors: Prof R.S. Walls and Prof N.P.J de Koker

April 2022

Stellenbosch University https://scholar.sun.ac.za

Declaration

This thesis was written by me and in my own words, except where quotations have been used from either published or unpublished sources which are clearly acknowledged. I am aware that the inclusion of material from others work will be treated as plagiarism. The source of any illustration or material not resulting from my own experimentation is indicated. The reproduction and publication of this thesis will not infringe any third-party rights and I have not previously submitted it for obtaining any qualification.

April 2022

Date

Copyright © 2022 Stellenbosch University
All rights reserved

Stellenbosch University https://scholar.sun.ac.za

Abstract

The use of shipping containers as basic building blocks for commercial and domestic buildings is fast becoming a popular method of construction. There are numerous reasons why shipping containers are gaining popularity while the biggest drivers are linked to cost, architectural freedom and time of construction. The primary goal of this thesis is to determine the structural resistance of load bearing elements in shipping container buildings at both ambient and elevated temperatures.

The reduction in capacity of the main load bearing elements, namely the corner columns, were associated with the removal of the corrugated wall panels. An upper and lower bound capacity was determined for each corner column by considering the sheeting to be fully present and entirely absent respectively. The load bearing capacities for the back and front corner columns were 958 and 923 kN respectively for the upper bound capacity and were in good agreement with capacities determined previously according to experimental testing. A reduction in capacity of 20 and 34% occurred for the back and front corner columns for the lower bound scenario considered. Previous authors have shown that the corrugated sheeting provides significant lateral rigidity while the results from this thesis emphasise the significance of the corrugated sheeting with respect to the load bearing capacity of the main load bearing elements.

The Euler buckling capacity of the shipping container side wall was found to be 317 kN due to a monolithic load applied to the top support beam. Inclusion of plasticity in the material definition led to failure of the top side beam. Even though these capacities are considered sufficient with regard to the design loads of many shipping container building configurations, a method of strengthening the side wall was proposed by increasing the stiffness of the surrounding members and adding stiffeners at the positions of expected bearing failure.

The load bearing capacities of the corner columns reduced at an unprecedented rate when exposed to the ISO 834 standard fire curve for the unprotected case. The fitting of passive fire protection boards reduced the rate of capacity reduction considerably while even after a 2-hour standard fire exposure the corner columns were found to have considerable residual capacity. For 20 mm thick boards, the capacity of the back and front corner columns reduced by 24 and 13%. To ensure the reduced capacities of the corner columns are not exceeded it is important to prevent high thermally induced forces from occurring by permitting thermal expansion. Assuming the boards do not fail according to the integrity criteria and that thermal expansion is allowed for, the corner columns are considered to have adequate load bearing capacity to resist design loads typical for modular construction.

Stellenbosch University https://scholar.sun.ac.za

Opsomming

Die gebruik van skeepshouers as basiese boublokke vir kommersiële en huishoudelike geboue is vinnig besig om 'n gewilde konstruksiemetode te word. Daar is talle redes waarom skeepsvraghouers gewild raak terwyl die grootste dryfvere gekoppel word aan koste, argitektoniese vryheid en tyd van konstruksie. Die primêre doel van hierdie tesis is om die strukturele weerstand van lasdraende elemente in skeepsvraghouergeboue by beide omgewings en verhoogde temperature te bepaal.

Die vermindering in kapasiteit van die hoofdraende elemente, naamlik die hoekkolomme, is geassosieer met die verwydering van die geriffelde muurpanele. 'n Boonste en onderste bindingskapasiteit is vir elke hoekkolom bepaal deur die velle onderskeidelik ten volle teenwoordig en heeltemal afwesig te beskou. Die dravermoë vir die agterste en voorste hoekkolomme was onderskeidelik 958 en 923 kN vir die boonste grenskapasiteit en was in goeie ooreenstemming met kapasiteite wat voorheen volgens eksperimentele toetsing bepaal is. 'n Vermindering in kapasiteit van 20 en 34% het voorgekom vir die agterste en voorste hoekkolomme vir die ondergrens-scenario wat oorweeg is. Vorige skrywers het getoon dat die sinkplate beduidende laterale styfheid bied, terwyl die resultate van hierdie tesis die belangrikheid van die sinkplate met betrekking tot die dravermoë van die hoof-draende elemente beklemtoon.

Die Euler-knikvermoë van die skeepshouer se sywand was 317 kN as gevolg van 'n monolitiese las wat op die boonste steunbalk toegepas word. Insluiting van plastisiteit in die materiaaldefinisie het gelei tot mislukking van die boonste sybalk. Selfs al word hierdie vermoëns as voldoende beskou met betrekking tot die ontwerpladings van baie skeepshouerboukonfigurasies, is 'n metode om die sywand te versterk voorgestel deur die styfheid van die omliggende lede te verhoog en verstewigings by te voeg by die posisies van verwagte laerfaling.

Vir die onbeskermde omhulsel het die dravermoë van die hoekkolomme teen 'n ongekende tempo verminder toe dit aan die ISO 834-standaardbrandkurwe blootgestel is. Die aanbring van passiewe brandbeskermingsborde het die tempo van kapasiteitsvermindering aansienlik verminder, terwyl selfs na 'n 2-uur standaardbrandblootstelling is daar gevind dat die hoekkolomme aansienlike residuele kapasiteit het. Vir 20 mm dik borde is die kapasiteit van die agterste en voorste hoekkolomme met 24 en 13 % verminder. Om te verseker dat die verminderde kapasiteit van die hoekkolomme nie oorskry word nie, is dit belangrik om te verhoed dat hoë termies-geïnduseerde kragte voorkom deur termiese uitsetting toe te laat. Met die veronderstelling dat die borde nie misluk volgens die integriteitskriteria nie en dat termiese uitsetting toegelaat word, word die hoekkolomme beskou as voldoende in terme van dravermoë om ontwerpladings tipies vir modulêre konstruksie te weerstaan.

Stellenbosch University https://scholar.sun.ac.za

Acknowledgments

I would like to express my sincere gratitude to the following individuals who contributed to the completion of the thesis:

- Firstly, I would like to thank the Lord Jesus Christ for giving me the courage and endurance to complete this thesis, even when at times it felt as if nothing was going according to plan.

- My study leader, Prof Richard Walls not only for his guidance in the execution of this thesis but also for the valuable knowledge gained in the fire behaviour and structural fire engineering courses.

- My study leader, Prof Nico de Koker for always willing to assist me with any problems I encountered as well as providing me with the opportunity to improve my capabilities in the finite element method by appointing me as a teaching assistant for Informatics 314.

- My fellow students in the civil engineering department at Stellenbosch University, for their friendliness and support around the office.

- Finally, to my mom for her unending support in every aspect of my life.

Stellenbosch University https://scholar.sun.ac.za

Table of Content

Stellenbosch University https://scholar.sun.ac.za

Stellenbosch University https://scholar.sun.ac.za

Stellenbosch University https://scholar.sun.ac.za

Figures

Stellenbosch University https://scholar.sun.ac.za

Stellenbosch University https://scholar.sun.ac.za

Stellenbosch University https://scholar.sun.ac.za

Stellenbosch University https://scholar.sun.ac.za

Stellenbosch University https://scholar.sun.ac.za

Tables

Stellenbosch University https://scholar.sun.ac.za

Nomenclature

Take note that some of the variables listed below are applicable to more than one equation where some have been empirically derived to include a specific unit. To avoid confusion, units have been added within the chapters for empirical equations where a specific unit is required. For equations where units have not been listed for the variables it is only necessary to remain consistent with units.

Latin variables

A	Area of cross section
b	Panel width
c_p	Specific heat
C_r	Compressive resistance
C_w	Warping coefficient
$D_{x/y}$	Flexural stiffness per unit corrugation in the respective direction
E	Young's modulus
E_T	Young's modulus at temperature T
f_e	Elastic buckling stress
f_{ex}	Buckling strength about the *x*-axis
f_{ey}	Buckling strength about the *y*-axis
f_{ez}	Torsional buckling strength
f_y	Yield stress of steel
G	Shear modulus
h_c	Convective heat transfer
h_w	Height of web
I	Moment of inertia
I_c	Moment of inertia of column
I_x	Moment of inertia of one wave of corrugated sheeting about *x*-axis
J	Polar moment of inertia
k	Thermal conductivity
k_{end}	Factor to account for support end conditions
k_f	Form factor
k_g	Global shear buckling coefficient
k_s	Local shear buckling coefficient
$k_{y,T}$	Reduction factor for yield strength
K_A	Equivalent axial stiffness
K_B	Bending stiffness
$K_c(T)$	Stiffness of column at temperature
K_p	Shear stiffness of corrugated sheet
K_R	Equivalent rotational stiffness
K_s	Equivalent stiffness of surrounding elements

Stellenbosch University https://scholar.sun.ac.za

$K_{x/y/z}$	Effective length factor for the respective axes
l	Length of column
$L_{x/y/z}$	Length between lateral restraints for the respective axes
n	Buckling mode
N_T	Force induced in column because of thermal expansion
P	Critical load / Force
P_r	Axial restraint force generated at elevated temperature T
P_{ref}	Reference load
P_{total}	Current incremental load
P_0	Dead load
$\dot{q}''$	Heat flux
Q	Force
$r_{x/y}$	Radius of gyration for the respective axes
t	Time
t_w	Web plate thickness
T	Temperature
T_e	Absolute temperature of the emitting surface
T_g	Gas temperature
T_r	Absolute temperature of the receiving surface
u	Displacement
U	Strain energy
V	Shear force
V_1	Shear force between corrugated sheet and top beam
x	Distance
x_0	Perpendicular distance between shear center and y-axis
y_0	Perpendicular distance between shear center and x-axis

Greek variables

α	Thermal diffusivity
α_{exp}	Coefficient of thermal expansion
λ	Non-dimensional slenderness ratio
λ_{LPF}	Load proportionality factor
$\emptyset$	Material factor
τ	Shear stress
$\tau_{cr,l}$	Critical shear stress for local buckling
$\tau_{cr,g}$	Critical shear stress for global buckling
τ_y	Shear yield stress
υ	Poisson's ratio
$\{\sigma\}$	Stress vector
$\{\varepsilon\}$	Strain vector

Stellenbosch University https://scholar.sun.ac.za

ε_{total}	Total strain
ε_{σ}	Stress related strain
ε_{th}	Thermal strain
γ	Strain due to pure shear deformation
γ'	Strain due to linear warp distortion
Δ	Deflection
$\Delta\gamma$	Change in shear strain
Δl	Change in length
ΔT	Change in temperature
Δ_{TOTAL}	Total elongation
Δ_{THERM}	Thermal elongation
Δ_{REST}	Elongation due to axial restraint forces
Δ_{DET}	Shortening of column due to applied loads
φ	Configuration factor
ε_e	Emissivity of the emitting surface
ε_r	Emissivity of the receiving surface
δ	Displacement deformation due to pure shear
δ'	Displacement deformation due to linear warp distortion

Acronyms

CFD	Computational Fluid Dynamics
FEM	Finite Element Modelling
ISO	International Standards Organization
PDE	Partial Differential Equation

Stellenbosch University https://scholar.sun.ac.za

1 Introduction

1.1 Background

In the past, various types of building materials have been used in construction. Timber and concrete are extremely versatile and are used for many types of structures in a wide range of climates. Even though masonry construction is generally more expensive than other forms of construction, it remains popular due to its durability and attractiveness. Metal, or more specifically structural steel, remains the most common type of building material for larger commercial buildings (Stewart Lumber and Hardware, 2020). The use of structural steel as a building material for modular construction is fast becoming the construction method of choice across many countries. The reason for the increase in demand for modular construction is due to various factors such as the efficiency and speed of construction, as well as reduced costs. Another notable advantage with modular construction is the sustainable construction process involved, where eco-friendly building materials can be used while the off-site construction process means that less waste is generated.

Intermodal shipping containers are one of the most popular types of units used in modular construction. Instead of using new materials which need to be manufactured, shipping container homes use new or old shipping containers to create prefabricated structures for both residential and commercial buildings (Absolute Containers, 2021). Although originally used for combined rail and horse-drawn transport, the size and shape of a standard shipping container makes it an ideal unit to use in modular construction. By modifying shipping containers architects have a greater degree of expression and creativity in their design to expose the slenderness, strength and transparency of the container frame. As with any structural steel building, modifications to the skeleton of the container for different applications, loads or client aspirations can be achieved in ways that other framing systems simply cannot accomplish.

Due to an increase in demand for modular construction, it is necessary to investigate the structural resistance of these modified shipping container buildings. The section to follow defines the problem statement.

1.2 Problem description

The cause of failure in a steel structure is usually attributed to human error as opposed to a combination of variability in parameters affecting the capacity of the structure. Failure of steel structures is often considered to be because of one or more design flaws. The most common cause of structural failure is due to overloading or error of judgment with respect to load paths in the structure. Another downfall with steel structures, is its high thermal conductivity. Steel structures are particularly vulnerable to elevated temperatures which leads to reduced strength and stiffness, and ultimately affects structural integrity of the structure. Passive fire protection measures, such as fibre cement boards and intumescent paints, are often incorporated in designs to retard rapid increases in steel temperatures during fires and reduce the maximum temperatures reached (Buchanan and Abu, 2017).

Stellenbosch University https://scholar.sun.ac.za

Engineers focus heavily on resistance ratings to ensure safety of buildings and its occupants at both ambient and elevated temperatures. One advantage of steel structures is that they can be strengthened relatively easily. By welding additional structural elements, such as beams, angles and stiffeners, the capacity of the structure is increased to minimise the probability of structural failure (Islam *et al.*, 2019). One of the main challenges is to design a structure in such a way that the total passive fire protection required is minimised to reduce high costs without compromising the safety of the building.

From a structural engineering perspective, shipping containers are seemingly well understood due to their basic frame structure. According to Giriunas *et al.* (2012) many shipping containers used for non-shipping applications are modified from their original design. However, currently no guidelines exist for safely designing such modified structures. Similarly, a study performed by Liu *et al.* (2020) highlighted that a lack of understanding and design guidance for modular structures leads designers to underestimate the strength of the salient features, leading to overly conservative designs. From Figure 1-1, which shows a shipping container with its side and top panels removed, it is evident that the large corner posts have been designed as load bearing elements to carry the load from the vertically stacked containers above. When stacked on ships or in docks these containers may carry very high loads, typically well in excess of typical low-rise buildings. However, one of the main concerns is the way in which these shipping containers are weakened by physical removal of certain components, as well as a change in load paths due to changes in structural configurations. Limited research is currently available on both the structural and fire resistance of the load bearing elements in modified container units.

Figure 1-1: Shipping container frame (Laizhou Dingrong Steel Structure CO. LTD., 2019)

The focus of this thesis will be to investigate the buckling behaviour and capacity of load bearing elements in modified shipping container buildings. The behaviour at both ambient and elevated temperatures is of concern and therefore numerical modelling is required. The results of the analysis performed in this work can be used as guidelines for designing modular structures. The following sections include a discussion on the objectives, project scope and limitations, methodology and thesis layout.

Stellenbosch University https://scholar.sun.ac.za

1.3 Objectives

The primary goal of this thesis is to determine the structural resistance of load bearing elements in shipping container buildings at both ambient and elevated temperatures. To achieve this goal, it is necessary to divide the thesis into a series of specific objectives. These specific goals are summarised below.

- Perform an extensive literature review to gain an understanding of the behaviour of steel structures at both ambient and elevated temperatures.
- Identify possible modes of weakening in shipping container buildings as well as changes in load paths.
- Identify methods and theories currently used to determine the load capacity and stiffness of the salient features of a shipping container.
- Develop finite element models that can simulate the structural behaviour of the main load bearing elements, namely the corner columns based on the identified weakening modes.
- Develop finite element models that predict the capacity and behaviour of a shipping container subjected to an unusually applied load due to a change in load path based on the identified weakening modes.
- Perform a heat transfer analysis to gain an understanding as to what extent the salient elements of the container are exposed to temperature gradients in the event of a fire.
- Develop finite element models to determine the structural fire resistance of the corner columns.
- Compare the numerical results with analytical methods and previously published standards.

1.4 Project scope and limitations

In terms of modular construction or container-like structures, an individual modular unit can differ in terms of beam and column sizes. To remain consistent throughout this thesis it is decided to perform all analysis based on the same modular unit. This thesis will only consider the intermodal 20 ft ISO shipping container (ISO 668, 1995).

A significant amount of research with regard to modified shipping container buildings is required especially with respect to load bearing elements and load paths that conflict with the original design (i.e. not all load carried at the four corners). Limited literature is currently available on the behaviour of such structures in fire and therefore an understanding of key concepts such as thermal response, connection and mechanical behaviour of such structures is required. This thesis investigates the load bearing capacity of the corner columns as well as the

Stellenbosch University https://scholar.sun.ac.za

corrugated sheeting which arises due to a change in load paths, while the former is also studied at elevated temperature.

Both small and full-scale experimental testing is often needed to investigate the true behaviour of a structural system. According to Buchanan & Abu (2017) the demand for full scale fire testing has increased significantly over the past few decades. Limited fire experiment data is available for validating models and further testing is needed to investigate the reduced capacities at both ambient and elevated temperature because of modifications imposed on shipping containers. The computational work performed to simulate heat transfer and mechanical resistance is validated only via analytical formulations while further experimental validation is required given the complexity of the problem.

1.5 Methodology

To achieve the objectives as outlined in Section 1.3, a set of steps need to be followed as defined in the concise methodology below. The project uses analytical and numerical methods to analyse the structural resistance of load bearing elements in modified shipping containers at both ambient and elevated temperatures. The 7-step approach defined below will be adopted to reach the objectives.

1. Conduct a thorough literature review to gain an understanding of the behaviour of steel structures at ambient and elevated temperatures. Important concepts such as theoretical models, heat transfer analysis and numerical methods such as finite element analysis will be reviewed.

2. Verification based on previous studies with regard to modular container-like structures will be done. A specific focus is on reproducing previous authors results by using similar finite element software packages and comparing results to analytical methods to validate the reliability of such software and modelling approaches developed.

3. Develop finite element models that can predict the behaviour of typical load bearing elements such as corner columns in container-like structures at ambient temperature.

4. Develop finite element models that can predict the behaviour of load bearing elements that occur due to a change in load paths, e.g. points loads applied at the mid-span of a module rather than at the corners.

5. Investigate the thermal behaviour of the corner columns at elevated temperatures with specific focus on temperature gradients by developing appropriate heat transfer models.

6. Develop finite element structural models for the corner columns to predict the behaviour at elevated temperatures.

7. Validate models developed in the previous steps according to well-known theoretical principles used successfully in the past.

Stellenbosch University https://scholar.sun.ac.za

1.6 Thesis layout

Chapter 1 provided a brief introduction to modular construction while the problem statement was emphasised. The scope and limitations were discussed followed by the proposed methodology. The list below provides a summary of the sections to follow.

- Chapter 2 discusses literature relevant to the thesis. The behaviour of steel structures at both ambient and elevated temperatures is discussed with specific focus on buckling behaviour. This section concludes via a brief discussion on the finite element method.

- Chapter 3 provides technical specifications on the 20 ft ISO shipping container followed by an in-depth discussion on how shipping containers are modified with regard to removal of elements and change in load paths. Three studies applicable to the work performed in this thesis are also addressed.

- Chapter 4 discusses the development and results of the finite element models to predict the capacity of the main load bearing elements in a modified shipping container at ambient conditions.

- Chapter 5 introduces how loads can be applied to the corrugated side walls in a manner different to the original design load path of the shipping container, which influences capacity and behaviour. The capacity of members is predicted based on finite element models followed by a comparison with analytical formulations.

- Chapter 6 describes the finite element models developed to predict the capacity of the load bearing elements at elevated temperature. This section concludes by considering multistorey configurations for modular construction at elevated temperature.

- Chapter 7 concludes the thesis by providing an overview as well as project findings. Further research and recommendations are also highlighted.

Stellenbosch University https://scholar.sun.ac.za

2 Theoretical background

2.1 Introduction

This chapter discusses important concepts and theoretical background with respect to the work to follow. The first sections provide an overview of steel structures in general, specifically focusing on compression elements. Discussions include the mechanical behaviour of steel and modes of failure for columns and corrugated plates. The aim of this chapter is to provide background information on the buckling behaviour of the salient features of the 20 ft ISO shipping container as introduced in Chapter 3.

The chapter continues by providing a brief overview of steel structures in fire and discusses principles of heat transfer applicable to the research. The standard fire curve is introduced and a well-known phenomenon which occurs in steel structures, namely temperature gradients. Penultimately, the literature review briefly discusses finite element modelling and concludes by discussing previous work conducted in the field of interest.

2.2 Steel structures

In the late 19th century, steel was introduced as a building material mainly to be used for construction of large skyscraper buildings. In more recent times, steel has become a viable option form smaller buildings such as office blocks and even personal residences. Structural steel is often considered the ideal material for constructing buildings due to its innumerable benefits when compared to other construction materials (Midwest Steel, 2016). Due to the increased focus on how construction materials and methods impact the environmental footprint, an important advantage of steel is that it is recyclable and does not need to be permanently disposed. The durability and strength allows steel framed construction to resist multiple types of external pressure which cannot necessarily be resisted by other forms of construction (Frost, 2018). Steel can be converted into any desired shape which provides flexibility to architects when designing buildings and homes.

A well-known downside of steel structures is the susceptibility to corrosion which effectively reduces section thicknesses resulting in reduced resistance of members (Secer and Uzun, 2017). Even though corrosion can prevent steel structures from reaching its design life, several preventive measures such as spray on systems have been used with great success in practice. As previously mentioned, the most notable advantage of steel structures is the strength and durability that is retains at ambient temperatures. Unprotected steel has very little fire resistance in comparison to concrete as the material properties of steel reduce drastically at elevated temperatures. According to Buchanan & Abu (2017) fireproofing is often needed in steel structures to ensure that members have sufficient resistance to avoid structural collapse.

Part of the challenge when designing steel structures is predicting the types of failure associated with the structure. Two of the most important failures to consider in steel structures is that of connections and members in compression. From a steel design perspective, it is crucial that

Stellenbosch University https://scholar.sun.ac.za

members are designed to resist a certain predicted load. One of the main causes of structural failure is the omission of certain forces or unpredicted loads.

2.2.1 Steel design analysis

Before the strength of members and the stability of a structure can be satisfied, the internal forces of the structure need to be determined. EN 1993-1-1 (2005) states that the joints within a steel structure are significant and that three definitions exist. A so-called simple joint, also commonly referred to as a pinned joint, is one which does not transfer bending moments while a continuous joint transmits bending moments with the flexibility assumed to have no effect on the analysis. A semi-continuous joint transmits bending moments but the flexibility of the joint needs to be considered in the analysis. To render structural calculations, joints are either considered to be pin connected or fully fixed.

It is convenient to associate the type of joint with the design approach used. The Eurocode defines three types of approaches, namely simple design, continuous design, and semi-continuous design. The simple design approach idealises joints as perfectly pinned with zero moment transfer. The continuous design method assumes joints to be rigid with no relative rotation between members. Semi-continuous design, which is seldomly used for simple analysis, considers the true behaviour of the joint. For semi-continuous design, the characteristics of the joints are different depending on whether an elastic or plastic analysis is adopted. For the elastic case, the joints have rotational stiffness and unlike the continuous design, the joints may be semi-rigid (Steel Construction Institute, 2013). During a plastic design, the joint can have a lower moment capacity than the member itself. If the connection has sufficient rotational capacity, the joint will form a plastic hinge before the member itself reaches the plastic state.

When choosing a design method to analyse a structure, it is important to consider the assumptions regarding the boundary conditions for each method. It is essential that the true behaviour of the structural response is encapsulated as close as possible without overdesigning the structure.

2.2.2 Mechanical behaviour of steel

When a ductile material such as steel is subject to a tensile force, it undergoes several different stages before complete failure of the member occurs. Steel is considered to have a complex stress strain behaviour while its interactions with plasticity are considered important from both a theoretical and practical point of view (Wolff *et al.*, 2008).

Figure 2-1 shows the typical stress-strain relationship for mild steel. When a steel member experiences a tensile force, it will elongate proportionally with the applied force up until it reaches the elastic limit. Beyond the yield point the member will experience plastic deformation where the relationship between stress and strain is no longer proportional. Once the maximum ultimate strength of the member is reached, the member will continue to elongate with an accompanying decrease in stress until the member fails (ruptures).

Stellenbosch University https://scholar.sun.ac.za

When modelling material behaviour of steel, it is important that an analytical description is chosen for the stress strain relationship. Idealised stress strain relationships for steel members are usually adopted to simplify analysis. Two of the most common relationships used are the elasto-plastic and elastic perfectly plastic. A study performed by Cadoni *et al.* (2018) showed that the tensile and compressive yield strength of S355 steel is highly dependent on the strain rate while the tensile yield strength is generally higher than the compressive yield strength. Most analytical stress strain models assume steel to behave the same in tension and compression.

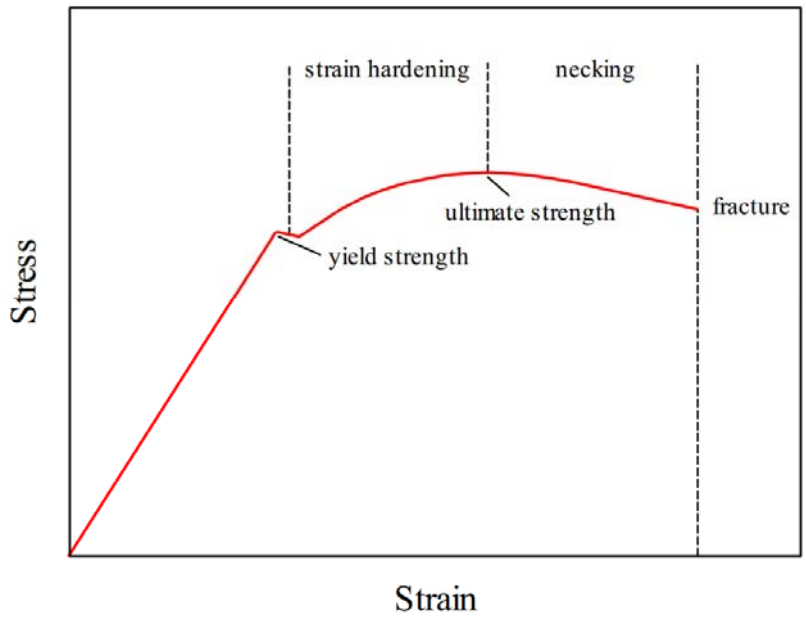

Figure 2-1: Stress-strain behaviour for typical steel adapted from Steel Construction Institute (2013)

2.3 Compression elements

The application of compression members extends far beyond normal structural columns and include bridge piers, webs in trusses and plate girders as well as braces in framed structures (Zhao *et al.*, 2005). In single and multi-storey buildings, columns act as load bearing members which are designed to safely transfer primarily vertical loads to the foundation of a structure. Theoretically, compression members are subject to pure axial compressive forces but in reality they are almost always subject to other loadings as well (Megahed, 2015). The maximum strength and mode of failure is largely dependent on the length and end support conditions. In long slender columns a structural instability known as buckling dominates where large lateral deflections make the column asymmetric to a certain extent with respect to its central axis.

What makes the buckling phenomenon hazardous is the fact that deflections often occur suddenly without providing any warning (Conor and Faraji, 2013). The collapse mechanism is heavily influenced by the moment of area and radius of gyration, and therefore need to be considered carefully to ensure the column is adequate in carrying the intended load. According to Yang and Bradford (2015), the large deflections are accompanied by significant loss in load capacity which can ultimately cause structural failure. When calculating the compressive

Stellenbosch University https://scholar.sun.ac.za

resistance of a column, various assumptions are made based on the material and geometric properties. Depending on the complexity of the problem under consideration, a linear or nonlinear elastic buckling analysis is performed using either a numerical or analytical approach. The sub-sections to follow provide a brief discussion on both linear and nonlinear elastic buckling.

2.3.1 Linear elastic buckling

Linear elastic buckling analysis predicts the theoretical buckling strength, also known as the bifurcation point, within the linear elastic region of the stress strain curve. Euler derived an equation which calculates the critical load based on the geometry of a member as well as the modulus of elasticity. Equation 2.1 below shows the equation derived by Euler.

$$P = \frac{n^2 \pi^2 EI}{(k_{end} l)^2} \tag{2.1}$$

where:

P	=	critical load
n	=	buckling mode
E	=	Young's modulus
I	=	moment of inertia
k_{end}	=	factor to account for support end conditions
l	=	length of column

Examining the formula postulated by Euler it is evident that the behaviour of a column to resist buckling is dependent on the fixity of the support conditions as well as the flexural rigidity of the column. The critical load P is occasionally incorrectly defined as the load which causes the column to buckle solely about the axis having the smallest moment of inertia. Even though the critical load is dependent on the moment of inertia for a specific axis, it should be determined in conjunction with the effective length of the axis under consideration. Equation 2.1 allows the critical load to be determined quickly and is computationally cheaper than performing a nonlinear elastic buckling analysis. As an example of how this can be applied in modelling, Fazzolari (2017) performed a series of linear buckling analyses on sandwich structures to estimate the load at onset of buckling as well as the possible buckling mode shapes before proceeding with a nonlinear elastic buckling analysis.

Unfortunately, the formulation derived by Euler is idealised for a perfectly elastic column. For more complex problems, linear elastic plastic behaviour and imperfections need to be accounted for to have a better understanding of the buckling behaviour (Paul, 2014).

2.3.2 Nonlinear elastic buckling

Once the maximum stress within a column exceeds the yield stress, displacements begin to vary nonlinearly with respect to the load due to plastic deformation. As opposed to linear elastic buckling, the stiffness varies with load and large displacements and changes in geometry are

Stellenbosch University https://scholar.sun.ac.za

to be accounted for.

In contrast to the assumptions for Euler buckling theory, most structural steel members possess some form of initial geometric imperfections because of manufacturing, transporting and handling processes. Geometric imperfections in steel members can either be local or global. Local imperfections refer to cross-sectional distortion while global imperfections are defined as distortion in terms of lengthwise straightness (Amouzegar *et al.*, 2015). Geometric imperfections are usually predicted from finite element models by conducting a linear elastic buckling analysis to find the worst-case buckling modes for both local and global buckling. The deflected shape from the linear elastic analysis is then scaled by a factor and used as an input for the nonlinear elastic analysis.

The second type of imperfection that steel members dominate is that of material imperfection. During the manufacturing process of steel, residual stresses produce internal member forces and moments within the member. The residual stress arises due to the uneven cooling of parts of the cross-section after hot rolling. Parts of the section that cool quicker result in compressive stress while the opposite is true for the steel portions that take longer to cool (Ellobody, 2014). There is not much than can be done to compensate for residual stresses occurring during the manufacturing process of steel. Nevertheless, it is an important component of the imperfection model to consider ensuring that the performance of structural steel is met.

According to Skotny (2019), a linear elastic buckling analysis typically predicts capacities up to 15% higher than a nonlinear buckling analysis. For buckling problems with complex effective lengths, the extent to which a linear elastic buckling analysis overpredicts the capacity can be significantly greater. Even though a nonlinear elastic buckling analysis is more complicated to perform and requires more computational time, it provides a safer and more realistic prediction of the capacity for members in compression.

2.3.3 Analytical methods

As discussed later in this section, numerical methods such as the finite element method have become popular for solving complex engineering problems due to the advancement in computer capabilities. Even though analytical methods provide exact solutions, it becomes tedious when solving larger and more complex problems. Some of the main advantages of performing an analytical analysis is that it serves as a validation check and computational software is not necessarily needed.

The analytical model described here determines the capacity of a column based on its slenderness which typically determines the mode of failure. The slenderness of a column is defined as the ratio between the length and radius of gyration of the cross section of the column. In general, short columns fail via yield stress while more slender columns fail according to one or more possible modes of buckling. The non-dimensional slenderness ratio is a parameter used to calculate the compressive resistance of a column by accounting for buckling. The equation for the non-dimensional slenderness is given below and is calculated based on the smallest elastic buckling strength.

Stellenbosch University https://scholar.sun.ac.za

$$\lambda = \sqrt{\frac{f_y}{f_e}} \tag{2.2}$$

where:

λ	=	non-dimensional slenderness ratio
f_y	=	yield stress
f_e	=	elastic buckling stress

As previously mentioned, the type of buckling that occurs is highly dependent on the geometry of the cross section. Sections commonly used in practice for designing steel structures have well defined geometries and the type of buckling can be predicted beforehand. Sometimes a unique member subjected to a high compressive force needs to be analysed for buckling but the type of buckling likely to govern is uncertain. For sections that have complex geometries with no axis of symmetry, it is preferable to compute the elastic buckling stress according to the equation below (SABS, 2011a), which will be applied later when considering asymmetric corner columns of containers.

$$\begin{aligned}(f_e - f_{ex})(f_e - f_{ey})(f_e - f_{ez}) - {f_e}^2(f_e - f_{ey})\left(\frac{x_0}{\overline{r_0}}\right)^2 \\ - {f_e}^2(f_e - f_{ex})\left(\frac{y_0}{\overline{r_0}}\right)^2 = 0\end{aligned} \tag{2.3}$$

with:

$$f_{ex} = \frac{\pi^2 E}{\left(\frac{K_x L_x}{r_x}\right)^2} \tag{2.4}$$

$$f_{ey} = \frac{\pi^2 E}{\left(\frac{K_y L_y}{r_y}\right)^2} \tag{2.5}$$

$$f_{ez} = \left(\frac{\pi^2 E C_w}{{K_z}^2 {L_z}^2} + GJ\right)\frac{1}{A\overline{{r_0}^2}} \tag{2.6}$$

$$\overline{{r_0}^2} = {x_0}^2 + {y_0}^2 + {r_x}^2 + {r_y}^2 \tag{2.7}$$

where:

f_{ex}	=	buckling strength about the adjusted *x*-axis
f_{ey}	=	buckling strength about the adjusted *y*-axis
f_{ez}	=	torsional buckling strength
x_0	=	perpendicular distance between shear centre and *y*-axis

Stellenbosch University https://scholar.sun.ac.za

y_0	=	perpendicular distance between shear centre and x-axis
$K_{x/y/z}$	=	effective length factor for the respective axis
$L_{x/y/z}$	=	length between lateral restraints for the respective axis
$r_{x/y}$	=	radius of gyration for the respective axis
C_w	=	warping coefficient
G	=	shear modulus
J	=	polar moment of inertia
A	=	area of cross section

Once the elastic buckling stress is known, the non-dimensional slenderness ratio can be calculated according to Equation 2.2 which is then used to calculate the compressive resistance of the column according to Equation 2.8.

$$C_r = \emptyset A f_y (1 + \lambda^{2n})^{-1/n} \qquad 2.8$$

where:

C_r	=	compressive resistance
$\emptyset$	=	material factor
n	=	1.34

Figure 2-2 below shows the compressive resistance as a function of slenderness for a typical steel column. The graphical representation captures previous discussions well, as Euler buckling should only be used for slender columns as opposed to short columns where the yield strength governs. Even though Equation 2.8 does directly not include geometric and material non-linearity, but rather does it through empricial calibration, it is a simplistic way to determine the capacity of a column taking into account both the slenderness and yield strength.

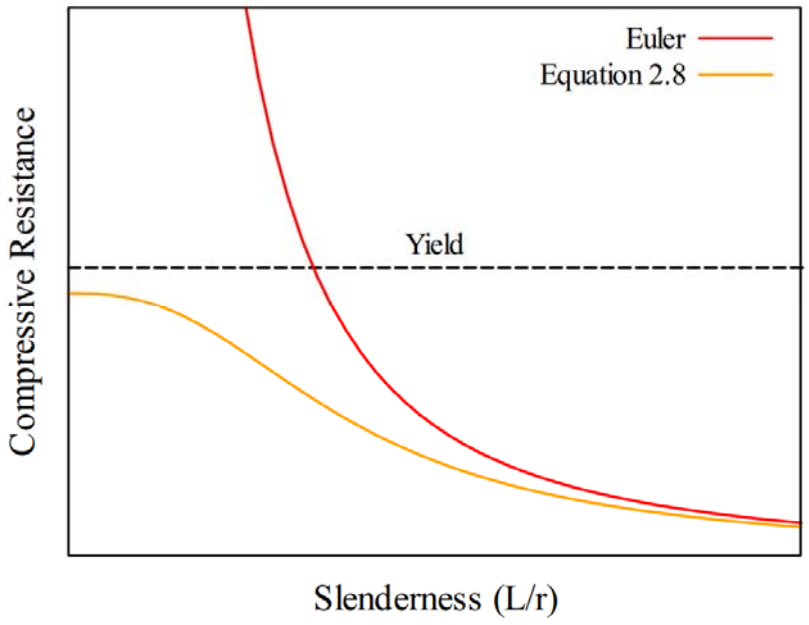

Figure 2-2: Compressive resistances according to different buckling capacities.

Stellenbosch University https://scholar.sun.ac.za

2.4 Corrugated plates

The use of corrugated plates in buildings and bridges is an innovation which has many advantages over other ways of designing these structures. Sinusoidal and trapezoidal corrugated steel plates have recently been introduced as a shear wall alternative for multi-storey buildings. The corrugated walls have good ductility and are considered an economic solution as opposed to normal stiffened and unstiffened plates (Hosseinpour *et al.*, 2015). Corrugated plates have also recently been adopted in composite bridge girder design. This innovation has not only led to an improvement in the aesthetics of the structure but also a reduction in cost (Sayed-Ahmed *et al.*, 2003). An example of such a bridge is the Hondani Bridge which was constructed in Japan. The bridge is a composite box girder with corrugated steel webs which has top and bottom prestressed concrete flanges. Figure 2-3 shows a schematic of the Hondani Bridge.

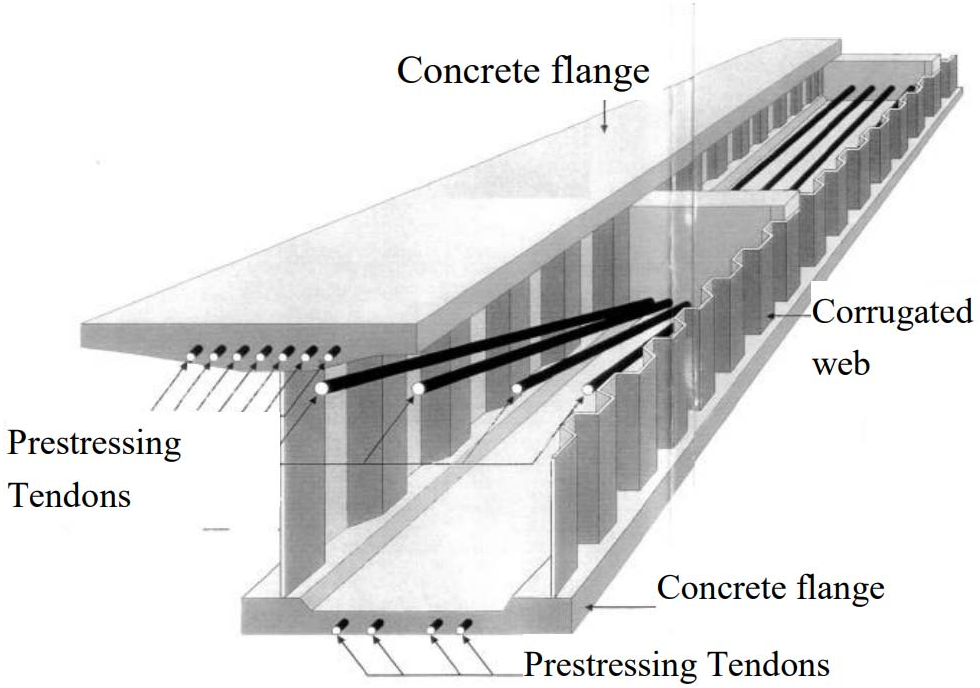

Figure 2-3: schematic of the Hondani Bridge (Sayed-Ahmed *et al.*, 2003).

2.4.1 Failure modes

The most common profiles used for these steel plates are sinusoidal and trapezoidal corrugations. According to Driver *et al.* (2006) corrugated webs of plate girders do not carry significant longitudinal stresses from the primary flexure of the girders. As a result of this it is reasonable to assume that bending moments are carried entirely by the flanges of such structures while the shear capacity is determined solely by the corrugated web. If it is assumed that the corrugated web does not carry any axial stress from flexure, then the only stress which is applicable to the web is pure shear stress. Depending on the geometry of the corrugated web, as well as the end fixities, the behaviour will either be governed by shear buckling or steel yielding while for most practical range of dimensions failure occurs via a combination of the

Stellenbosch University https://scholar.sun.ac.za

two. Figure 2-4 shows the notation used to describe the corrugation profile for the web.

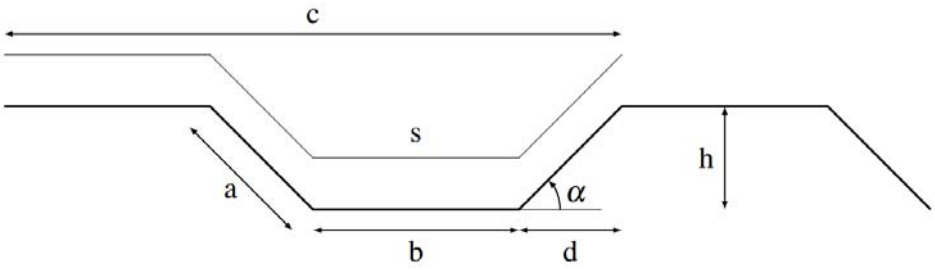

Figure 2-4: corrugation profile for trapezoidal section.

Failure of the web can either occur via local or global buckling. Local buckling of the corrugated web takes place when one or more steel panels situated between two folds undergo an instability. The corrugated web acts as a series of flat panels where each panel is supported along its long vertical edge by adjacent panels while the shorter edge is supported by the flange of the girder. Galambos (1988) derived equations to compute the elastic buckling shear stress based on isotropic plates. Equation 2.9 is used to compute the elastic critical shear stress, $\tau_{cr,l}$, for local buckling.

$$\tau_{cr,l} = k_s \frac{\pi^2 E}{12(1-\upsilon^2)} \left(\frac{t_w}{b}\right)^2 \qquad 2.9$$

where:

t_w	=	web plate thickness
b	=	panel width
E	=	Young's modulus
υ	=	Poisson's ratio
k_s	=	local shear buckling coefficient

The shear buckling coefficient is determined according to Equation 2.10 or 2.11. Equation 2.10 is used when the support condition between the flange and the web (shorter edge) approximates that of a simply supported connection. When the shorter flange and web are clamped, Equation 2.11 should be used.

$$k_s = 5.34 + 4\left(\frac{b}{h_w}\right)^2 \qquad 2.10$$

$$k_s = 5.34 + 2.31\left(\frac{b}{h_w}\right) - 3.44\left(\frac{b}{h_w}\right)^2 + 8.39\left(\frac{b}{h_w}\right)^3 \qquad 2.11$$

where:

h_w	=	height of web

The global buckling mode is characterised by diagonal buckling over several corrugation

Stellenbosch University https://scholar.sun.ac.za

panels. According to Elgaaly, (1998), if the dimension of the fold width is large, local buckling occurs while global buckling occurs for smaller fold widths. Galambos (1988) proposed the following equation for calculating the critical shear stress, $\tau_{cr,g}$, for global buckling of corrugated webs based on stability equations for orthotropic plates.

$$\tau_{cr,g} = k_g \frac{(D_y {D_x}^3)^{1/4}}{{h_w}^2 t_w} \tag{2.12}$$

where:

k_g = global shear buckling coefficient

$D_{x/y}$ = flexural stiffness per unit corrugation in the respective direction

Opposed to the shear buckling coefficient for local buckling, the global shear buckling coefficient is only dependent on the web top and bottom constraints. According to Galambos (1988), the global shear buckling coefficient has a value of 36 for steel girders (pinned) while a value of 68.4 is to be adopted for composite girders (fixed). Equation 2.13 and 2.14 are used to compute the flexural stiffness per unit corrugation in the *x* and *y* directions, respectively.

$$D_x = \frac{EI_x}{c} = \frac{E}{b+d}\left(\frac{bt_w[d\ tan\alpha]^2}{4} + \frac{t_w[d\ tan\alpha]^3}{12sin\alpha}\right) \tag{2.13}$$

$$D_y = \left(\frac{c}{s}\right)\left(\frac{E{t_w}^3}{12}\right) = \left(\frac{b+d}{b+d/cos\alpha}\right)\left(\frac{E{t_w}^3}{12}\right) \tag{2.14}$$

where:

I_x = moment of inertia of one wave

It is possible for the corrugated sheet to fail via shear yielding. The shear stress causing the corrugated web to yield is determined according to the von Mises yield criterion as highlighted in Equation 2.15.

$$\tau_y = \frac{f_y}{\sqrt{3}} \tag{2.15}$$

where:

f_y = uniaxial yield strength of the corrugated web

Similarly to the analytical method described in the previous subsection where an equation was proposed taking into account both yielding of the material and buckling, EL-Metwally and Loov (1999) and Sayed-Ahmed *et al.* (2003) developed an interaction equation which takes into account shear yielding as well as local and global buckling. Equation 2.16 is used to calculate the interactive failure stress $\tau_{cr,i}$ where n is shown by the authors to have a value of 3 for both trapezoidal and zigzag profiles.

Stellenbosch University https://scholar.sun.ac.za

$$\left(\frac{1}{\tau_{cr,i}}\right)^n = \left(\frac{1}{\tau_{cr,l}}\right)^n + \left(\frac{1}{\tau_{cr,g}}\right)^n + \left(\frac{1}{\tau_y}\right)^n \quad 2.16$$

2.4.2 Stiffness

As a light steel structure, the use of containers for building structures is becoming increasingly popular. One of the main advantages of these types of structures is that they can be combined into a variety of forms and shapes depending on the architectural requirements. Unfortunately, the modifications often deviate from the original design and currently there are limited guidelines for safely using these containers for building applications (Giriunas *et al.*, 2012). One of the main concerns with regard to modifying these modular units is the affect it has on the stiffness of the side and end walls.

Zha and Zuo (2016) performed theoretical and experimental studies on the in-plane stiffness of the side and end wall assemblies of modular buildings. The study shows that the stiffness of a side wall is provided predominantly by shear strength, while bending and tension also increase the stiffness slightly. Based on energy methods, an analytical solution was developed to determine the stiffness of a corrugated sheet both parallel and perpendicular to the corrugated direction. Zha and Zuo (2016b) used the analytical solution from Zha and Zuo (2016) to investigate the in-plane stiffness of the container structure when openings such as windows and doors are present. As expected, the stiffness of the container module decreases with an increase in hole area, while stiffening members around the extruded areas were shown to increase the stiffness significantly.

Further studies have been conducted by Yu and Chen (2018) to investigate the structural rigidity of corrugated plate side walls and the effect it has on structural design, particularly with regard to wind and earthquake loads. Further details on the study performed by Yu and Chen (2018) are discussed in Section 3.4.1.

In terms of lateral loads applied to modular structures where rigidity is of primary concern, the presence of corrugated sheeting greatly improves both the lateral resistance and the global rigidity of the modular structure. The lack of knowledge regarding the strengthening effect of corrugated steel shear walls means that designers tend to ignore the rigidity contribution which can ultimately lead to damage risk in modular structures. As discussed above, several studies have investigated the lateral stiffness of corrugated panels in modular buildings. One aspect which is still uncertain is the strengthening effect the corrugated sheeting has on the capacity of load bearing elements such as columns.

2.4.3 Energy methods for structural analysis

In the case of statically indeterminate structures, it is necessary to know the displacements either throughout the structure or at several discrete points. When the displacements at only a few locations are needed, energy methods become useful. The stiffness, whether it being axial, bending, shear or even torsion become relatively easy to compute when energy methods are

Stellenbosch University https://scholar.sun.ac.za

introduced. Two of the most common energy methods used are the principle of superposition and strain energy.

The principle of superposition is often overlooked but it forms the central concept in the analysis of structures where a linear relationship exists between external forces and displacements. The principle of superposition states that the deflection at a given point in a structure due to multiple loads may be determined as the summation of the displacements caused by the individual loads (Hibbeler, 2018).

When a structural member with a certain stiffness deforms, it stores a type of energy which is referred to as strain energy. The principle of virtual work can be defined as the product of the distance a particle moves during virtual displacement by the component in the direction of the displacement of a force acting on the particle. When an elastic body undergoes deformation, the virtual work done by the internal forces is equal to the corresponding increment in strain energy. One of the simplest examples of illustrating the concept of strain energy is to consider an elastic spring with load applied axially. When the load is applied slowly, the spring deflects by a certain distance. The work which the load performs on the spring can be calculated if the load displacement relationship is known. The area enclosed by the force-displacement curve is equal to the total work done by the applied load. If it is assumed that the energy is conserved, then the total work done by the applied load is equal to the energy stored in the structure also commonly referred to as internal or strain energy. The strain energy for the spring is computed according to Equation 2.17.

$$U = \frac{1}{2}Pu \tag{2.17}$$

where:

U	=	strain energy
P	=	Force
u	=	Displacement

A more appropriate way of defining strain energy is by relating the internal work done by stress resultants causing corresponding deformations (Hibbeler, 2018). Consider the infinitesimal element in Figure 2-5 with normal and shear stresses as indicated. If we consider the material to be isotropic and consider the symmetry of the stress and strain tensors, condensed stress and strain vectors can be derived for the general three-dimensional case as seen in Equation 2.18. Accompanying the normal and shear stresses are normal and shear strains. The strain energy of the infinitesimal element can be computed according to the integral in Equation 2.19.

Stellenbosch University https://scholar.sun.ac.za

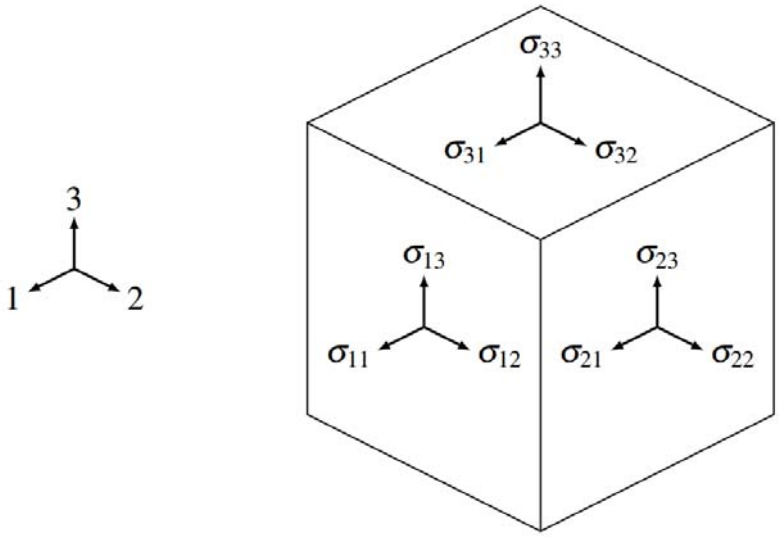

Figure 2-5: Infinitesimal volume element with normal and shear stresses recreated from (De Koker, 2021).

$$\{\sigma\} = \begin{Bmatrix} \sigma_{11} \\ \sigma_{22} \\ \sigma_{33} \\ \sigma_{23} \\ \sigma_{13} \\ \sigma_{12} \end{Bmatrix} \qquad \{\varepsilon\} = \begin{Bmatrix} \varepsilon_{11} \\ \varepsilon_{22} \\ \varepsilon_{33} \\ 2\varepsilon_{23} \\ 2\varepsilon_{13} \\ 2\varepsilon_{12} \end{Bmatrix} \tag{2.18}$$

$$U = \frac{1}{2}\int_{v} \sigma^{T} \varepsilon \, dv \tag{2.19}$$

As previously mentioned, a structural member such as a beam can be subjected to several forces or moments. If a corrugated plate is considered to be a structural element subjected to the shear force distribution as highlighted in Figure 2-6, then internal stresses develop which resist the external forces (Hibbeler, 2017). The strain energy stored in the plate can be calculated if these internal stresses and deflections at certain points are known. If we consider the corrugated beam below subjected to pure shear, the uniform shear stress can be calculated according to Equation 2.20.

Stellenbosch University https://scholar.sun.ac.za

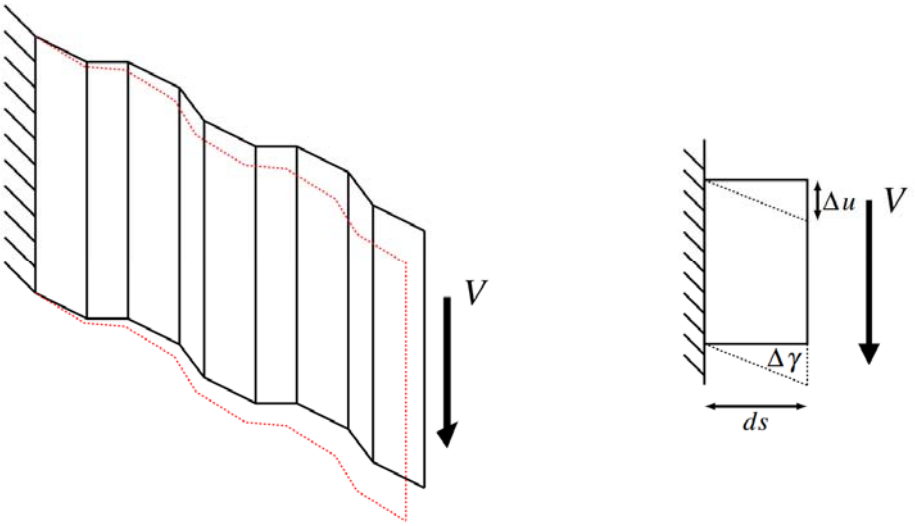

Figure 2-6: corrugated plate modelled as a structural beam.

$$\tau = k_f \frac{V}{A} \tag{2.20}$$

where:

τ	=	shear stress
k_f	=	form factor dependent on cross sectional shape
V	=	shear force
A	=	cross sectional area

The shear strain $\Delta\gamma$ can be computed if the deflections are known for a given segmental length ds and consequently it is related to the shear stress according to Equation 2.21. The total deformation of the corrugated panel due to pure shear is then calculated by the integral shown in Equation 2.22. Combining Equation 2.22 and the theory behind the discussion of Equation 2.17, the energy integral for pure shear is ultimately given by Equation 2.23.

$$\Delta\gamma = \frac{\tau}{G} = k\frac{V}{AG} \tag{2.21}$$

$$u = \int_0^L k\frac{V}{AG}ds \tag{2.22}$$

$$U = \frac{1}{2}Vu = \int_0^L k\frac{V^2}{2AG}ds \tag{2.23}$$

where:

G	=	shear modulus
l	=	length of the beam/corrugated panel

Stellenbosch University https://scholar.sun.ac.za

2.5 Fire safety

From a structural engineering point of view, the elevated temperature performance of any building is an important aspect to consider, limiting loss of lives as well as damage to adjacent buildings. Even though the probability of a fire arising within a building is dependent on various factors, in general it is considered an extreme event. The detrimental consequences of an uncontrolled fire are significant and cannot be neglected. (Buchanan and Abu, 2017).

In the case of an unwanted fire, the primary goals are to limit fatalities, property loss as well as environmental damage. More recently life safety has taken preference over property loss and environmental damage even though the balance between these objectives depends on the type of building as well as the occupants. In terms of life safety it is important to ensure that occupants are warned as soon as possible when a fire is detected and that suitable escape paths are designed to ensure that people are not affected by smoke while utilizing these paths (Delcourt and Garis, 2014).

To meet the above-mentioned fire safety objectives, either active or passive fire protection systems are installed. Automatic protection refers to either an action performed by a human being or an automatic device such as a sprinkler which is activated during the event of a fire (Drysdale, 2011). Passive protection is implemented in the construction of the building and therefore does not require specific operation. One of the most common examples of passive fire protection is the coating of structural elements, such as steel columns and beams, in intumescent coating.

2.6 Structural fire engineering

Over the past few decades, the design of structures in fire has become a crucial part when designing steel buildings. Historically, traditional fire resistance has been achieved by designing steel structures at room temperature and simply applying passive protection measures such as wrapping the steel elements in insulation material. Structural fire engineering is a relatively new discipline which promotes new approaches towards developing fire resistance. Structural fire engineering is an overlapping of structural engineering and fire engineering to ensure that a better understanding of structural behaviour in a fire is achieved. The structural fire engineering community is in favour of supporting a generalised performance-based design approach which is divided into three steps as highlighted in Figure 2-7 (Australian Steel Institute, 2005), which is specifically applied to steelwork.

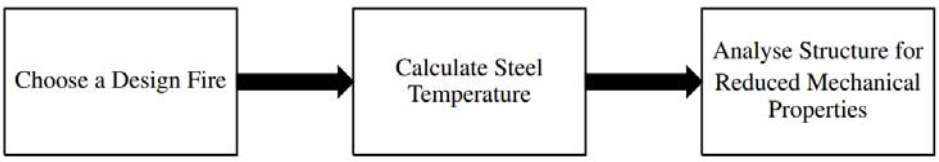

Figure 2-7: Structural Fire Engineering Approach adapted from Australian Steel Institute (2005).

The first step involves choosing a design fire so that a relationship can be developed between

Stellenbosch University https://scholar.sun.ac.za

temperature or heat flux in relation to time. The relationship will be influenced by the characteristics of the fuel load and the geometry of the room or compartment under consideration. Once the gas temperature is known, the temperature of the structural members and components can be obtained by performing a heat transfer analysis. The final step is to calculate the response of the structural system by including the effect of reduced temperature dependent mechanical properties.

2.6.1 Fire resistance and severity

Drysdale (2011) defines fire resistance as the ability of an element of a building to continue performing its function as a barrier or structural component during the event of a fire. According to Buchanan and Abu (2017), fire resistance is defined as the duration to which an element can satisfy certain criteria when exposed to the standard fire curve. When designing a structure for fire safety, it is important that the fire resistance of the structure is greater than the fire severity.

The destructive potential of a fire or the measure of forces and temperatures which could lead to collapse is what is referred to as fire severity. Fire severity is usually defined in terms of the period of exposure to the standard fire where the impact caused by a complete burnout of a real fire is associated with an equivalent time exposure to the standard fire curve resulting in the same impact. The practicality of this equivalent time concept is that it allows designers to compare the severity of real fires to published fire resistance ratings.

Depending on the type of member and its functionality, specific criteria need to be satisfied in the event of a fire. The Eurocode, and many other international standards, classify fire resistance according to three main criteria: stability, integrity and insulation. Load bearing elements such as columns need to satisfy the stability criteria by maintaining a high enough resistance to prevent failure and ultimately global collapse of a structure during the event of a fire. Separating members such as walls and partitions need to prevent flames and hot gases from penetrating through to adjacent compartments to minimise fire spread. The temperature on the unexposed surface of separating members needs to be kept low enough to prevent spontaneous ignition of members in close contact with the separating member. Special care is needed especially when electrical services are present in concealed spaces or ceiling partitions. It is therefore important that these types of members satisfy the insulation requirement where most codes specify an average temperature of 140 ℃ above ambient and a maximum overall temperature of 180 ℃ on the unexposed surface of such members (SABS, 2005).

2.6.2 Standard fire curve

The standard fire curve, also commonly referred to as the ISO 834 curve, is a furnace based time temperature relationship developed for determining fire resistance of structural elements (ISO, 1999). As mentioned in the previous section, the standard fire curve is a useful means for comparing fire resistances between structural elements.

One of the main disadvantages with respect to the standard fire is that it seldomly represents a

Stellenbosch University https://scholar.sun.ac.za

time temperature relationship for a real fire (Bisby *et al.*, 2013). The furnace-based fire model does not capture the behaviour of a real fire which is largely dependent on ventilation openings and fuel loads within the compartment. Initially the rate at which the standard fire temperature increases is rapid before it gradually reduces, but never to such an extent where a cooling phase is experienced. Equation 2.24 describes the time-temperature relationship for the standard fire curve.

$$T_g = 20 + 345log_{10}(8t + 1) \qquad 2.24$$

where:

T_g	=	gas temperature (°C)
t	=	time (minutes)

Buchanan & Abu (2017) describe two other fire curves often used in practice, namely the external fire curve and the hydrocarbon fire curve. While the external fire curve is less intense, as seen in Figure 2-8 and mainly used for members exposed to external fires, the hydrocarbon is clearly the most severe and replicates fires in structures that store petrochemical products.

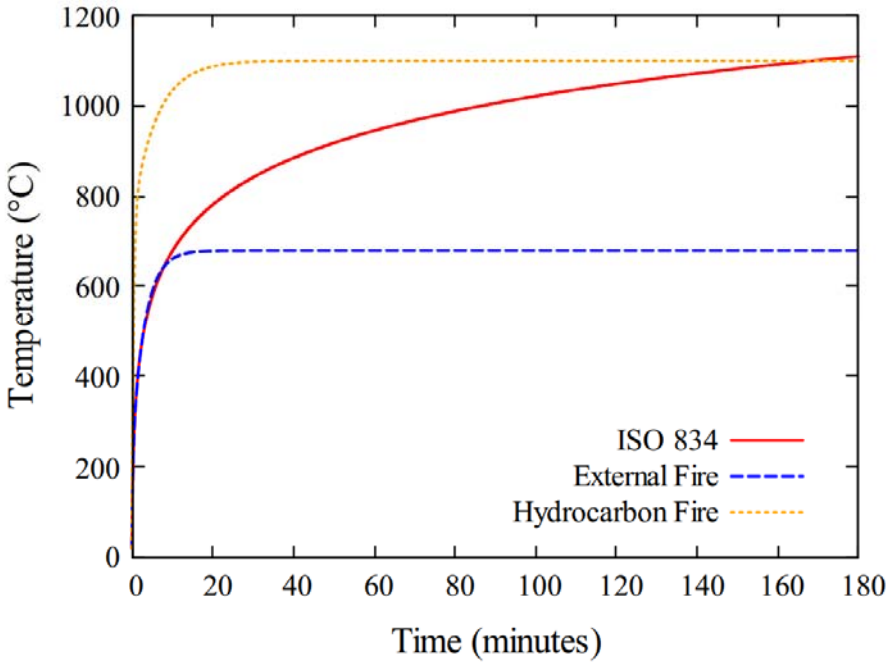

Figure 2-8: Published curves recreated from Buchanan & Abu (2017)

2.7 Heat transfer

A sound understanding of heat transfer is important when considering fire behaviour. The three mechanisms of heat transfer, namely conduction, convection and radiation, can occur via steady or transient state heat flow. Steady state refers to the case where the amount of heat entering the system is equal to that leaving the system. The equilibrium state is reached when the temperature at any point is constant. In transient heat transfer, the temperature difference

Stellenbosch University https://scholar.sun.ac.za

across the section keeps changing with time and as a result the heat entering the system is not equal to the heat leaving the system (Narang, 2005). The sections to follow provide a brief description on the fundamentals of the three modes of heat transfer as well as important considerations.

2.7.1 Conduction

For solid material such as steel or concrete, conduction is described as the transfer of heat because of induced vibration of the atoms and molecules while convection dominates heat transfer in fluids and gases. Conduction is described as the transfer of heat in solid materials such as steel or concrete. In general, materials which are good electrical conductors are also good conductors of heat due to the interaction between free electrons. The ignition of solid surfaces is dependent on the conduction of that material while conduction also plays a role in the fire resistance of structural members (Buchanan and Abu, 2017).

Thermal inertia is an important property derived which describes the degree of slowness with which the temperature of a body approaches that of its surroundings. For a constant fuel load, lining materials with low thermal inertia will result in higher temperatures experienced within a room. Even though most fire engineering related problems involve transient heat transfer, it is still important to understand steady state heat transfer as it represents the limiting condition for a given system once equilibrium is reached (Drysdale, 2011).

To perform conductive heat transfer calculations, the density, specific heat, and conductivity of the material is needed. Specific heat is defined as the amount of heat needed to raise the temperature of a unit mass of material by one degree Celsius. Thermal conductivity is the amount of heat transferred through a unit thickness of material per temperature difference. These properties will be discussed in relation to structural steelwork below.

The differential equation for steady state conduction is shown below. Because the steady state condition is reached, the calculation is independent of the specific heat of the material. The conductivity of a material may also vary with temperature as seen later.

$$\dot{q}'' = -k dT/\mathrm{d}x \qquad 2.25$$

where:

$\dot{q}''$	=	heat flux due to conduction
k	=	conductivity of material
T	=	temperature
x	=	Distance

To model transient heat flow, the amount of heat required to change the temperature of the material must be included. The thermal diffusivity can be thought of as the rate of heat transfer through a medium and is calculated according to Equation 2.26. As the thermal diffusivity is related to transient heat flow, it is unsurprising to see the specific heat listed in Equation 2.26. Equation 2.27 represents transient heat transfer for a one-dimensional case where materials

Stellenbosch University https://scholar.sun.ac.za

with a high thermal diffusivity transfer heat at a higher rate than materials with a low thermal diffusivity.

$$\alpha = k/\rho c_p \tag{2.26}$$

$$\frac{\partial^2 T}{\partial x^2} = \frac{1}{\alpha}\frac{\partial T}{\partial t} \tag{2.27}$$

where:

α	=	thermal diffusivity
c_p	=	specific heat
t	=	Time

2.7.2 Convection

Drysdale (2011) defines convection as the transfer of heat via the motion of a fluid or gas. The motion of the fluid usually arises from temperature gradients in the fluid which develop buoyancy driven flows known as free or natural convection. It is important to realise that there is a difference between free and forced convection even though the former is more applicable to fire scenarios. Forced convection involves fluids which are forced to move by a device such as a pump or fan to increase the heat transfer. Convective heat is important to consider in the upward transport of smoke to a ceiling of a compartment or out the window of a building. Convective heat transfer is directly proportional to the change in temperature between the surface of the solid and the fluid as seen in Equation 2.28.

One of the challenges regarding the calculation of convective heat transfer is choosing an appropriate value for the convective heat transfer coefficient. The convective heat transfer coefficient is dependent on fluid properties, flow parameters as well as the geometry of the surface. Various authors suggest relating the convective heat transfer coefficient to certain dimensionless groups which account for both the physical properties and flow velocity of the fluid (Drysdale, 2011).

$$\dot{q}'' = h_c \Delta T \tag{2.28}$$

where:

$\dot{q}''$	=	heat flux due to convection
h_c	=	convective heat transfer coefficient
ΔT	=	temperature difference

The value of the heat transfer coefficient for a given surface is generally dependent on whether it is an open surface or a closed cavity as this affects certain dimensionless properties related to fluids. Generally, the convective heat transfer coefficient increases for a given increase in the Reynolds number because higher velocities lead to an increase in turbulence. For this

Stellenbosch University https://scholar.sun.ac.za

reason, the convective heat transfer coefficient is typically higher for exposed surfaces even though it constantly changes as gas velocities vary. For the standard ISO 834 fire, EN 1991-1-2 (2002) recommends a convective heat transfer coefficient of $25\ \mathrm{W/m^2K}$ for the exposed side while lower values of $4 - 9\ \mathrm{W/m^2K}$ are suggested for the unexposed face.

2.7.3 Radiation

The final type of heat transfer is described by electromagnetic waves that travel through a vacuum or liquid. Radiation is extremely important as it is the main transfer mechanism of energy from the flames and smoke to other fuel loads within the building, as well as from the burning compartment to adjacent buildings. Not only do flames radiate heat but heated substances also play an important role in fire development. Heated substances will radiate heat to the surroundings while walls and other surfaces will radiate heat back to hot object. This phenomenon is what is referred to as radiative feedback or self-radiation and should be considered to accurately predict the heat flux due to radiation. The resultant heat flux for a given surface is determined according to Equation 2.29 where the negative sign indicates heat flow from hot to cold. The resultant emissivity as a result of self-radiation is calculated by Equation 2.30 (Sadiq *et al.*, 2013).

$$\dot{q}'' = -\varphi\varepsilon\sigma\left(T_e{}^4 - T_r{}^4\right) \tag{2.29}$$

$$\varepsilon = \frac{1}{\frac{1}{\varepsilon_e} + \frac{1}{\varepsilon_r} - 1} \tag{2.30}$$

where:

$\dot{q}''$	=	heat flux due to radiation
φ	=	configuration factor
ε_e	=	emissivity of the emitting surface
ε_r	=	emissivity of the receiving surface
σ	=	Stefan Boltzmann constant ($5.67.10^{-8}\ \mathrm{W/m^2K^4}$)
T_e	=	absolute temperature of the emitting surface (K)
T_r	=	absolute temperature of the receiving surface (K)

The emissivity of the emitting surface indicates how efficient it is as a radiator and has a value ranging between zero and one. The emissivity of a surface is not always constant, and this is especially the case for materials having a coating such as galvanized steel. During the event of a fire, the value of emissivity typically ranges between 0.7 and 1.0. The configuration factor is a function of the orientation of the emitting and receiving surfaces with respect to one another. The integral in Equation 2.31 is used to compute the configuration factor for an incident point based on the relative orientation and distance between the receiver and emitter. Franssen and Vila Real (2012) provide an equation to compute the configuration factor based on the geometric lengths between the receiving and emitting surface.

Stellenbosch University https://scholar.sun.ac.za

$$\varphi = \int_{A_1} \frac{cos\theta_1 cos\theta_2}{\pi r^2} dA_1 \quad 2.31$$

$$\varphi = \frac{|AC + BD - AD - BC|}{2|CD|} \quad 2.32$$

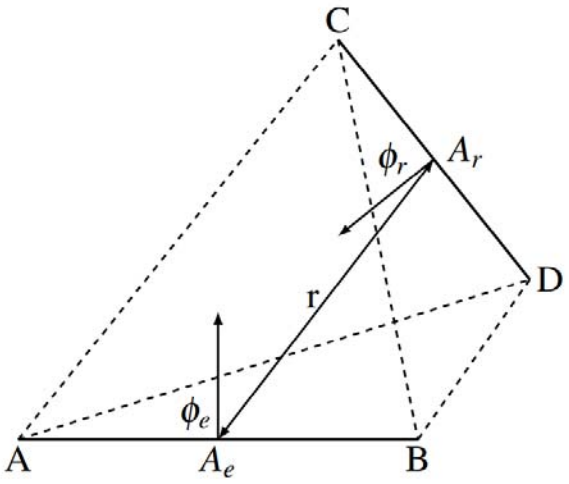

Figure 2-9: Radiative heat transfer between two infinitesimal surface areas (recreated from Franssen & Vila Real (2012))

2.8 Behaviour of steel structures in fire

Even though structural steel is strong and durable at ambient conditions, members often perform poorly in fire compared to concrete and timber structures due to thinner sections and higher conductivity. Even though steel has a relatively low specific heat, the relative magnitudes of the conductivity and density of steel in relation to other materials result in a high thermal inertia. Mechanical properties such as yield strength and Young's modulus reduce drastically at elevated temperatures. The temperature at which steel elements start losing strength is dependent on the grade of steel, but steel temperatures of around 600 ℃ usually correspond to around a 50% reduction in yield stress with an even greater reduction in Young's modulus observed. Structural elements such as columns and beams, which are susceptible to such increases in temperature, need to be evaluated to ensure the material has retained enough strength to prevent structural collapse. The rate at which steel temperatures increase is highly dependent on the severity of the fire and the amount of applied fire protection (Buchanan and Abu, 2017).

The thermal properties of steel such as conductivity and specific heat are also affected at elevated temperatures. Gross *et al.* (2010) recommends a performance-based fire engineering approach so that a broad range of realistic design parameters are included. The sections to follow provide a brief discussion on how the mechanical and thermal properties of steel are affected at elevated temperatures.

Stellenbosch University https://scholar.sun.ac.za

2.8.1 Mechanical properties of steel

In Section 2.2.2 the mechanical properties of steel at ambient temperatures were briefly introduced. The well-defined yield strength of steel at ambient conditions means that steel structures can be designed with higher certainty. To design steel structures in fire, it is necessary to know the yield strength, but unfortunately it is not as well defined at elevated temperatures. According to Kirby and Preston (1988) the effective yield strength of steel should be taken as the 1% proof strength at elevated temperatures. The structural Eurocode for steel EN 1993-1-2 (2005) has a detailed expression for computing the stress-strain relationship at elevated temperatures for carbon steels.

The less well-defined yield strength at elevated temperatures has led to considerable scatter in deriving equations for determining a suitable value. Several design codes have developed relationships for determining the reduction in yield strength for structural, reinforcing and prestressing steel. According to EN 1993-1-2 (2005), the reduction factor for yield strength of steel can be computed according to Equation 2.33, although reduction factors are also provided in a tabular format.

$$k_{y,T} = (0.9674\{1 + \exp\,[(T - 482)]/39.19\})^{-1/3.833} \qquad 2.33$$

where:

$k_{y,T}$	=	reduction factor for yield strength
T	=	steel temperature (°C)

Based on previous discussions, it is known that the buckling capacity of structural members, such as columns, is highly dependent on the Young's modulus of the material. Various material models also exist for modifying the Young's modulus of members. Figure 2-10 below shows the reduction factors for yield strength and the Young's modulus for steel according to EN

Stellenbosch University https://scholar.sun.ac.za

1993-1-2 (2005).

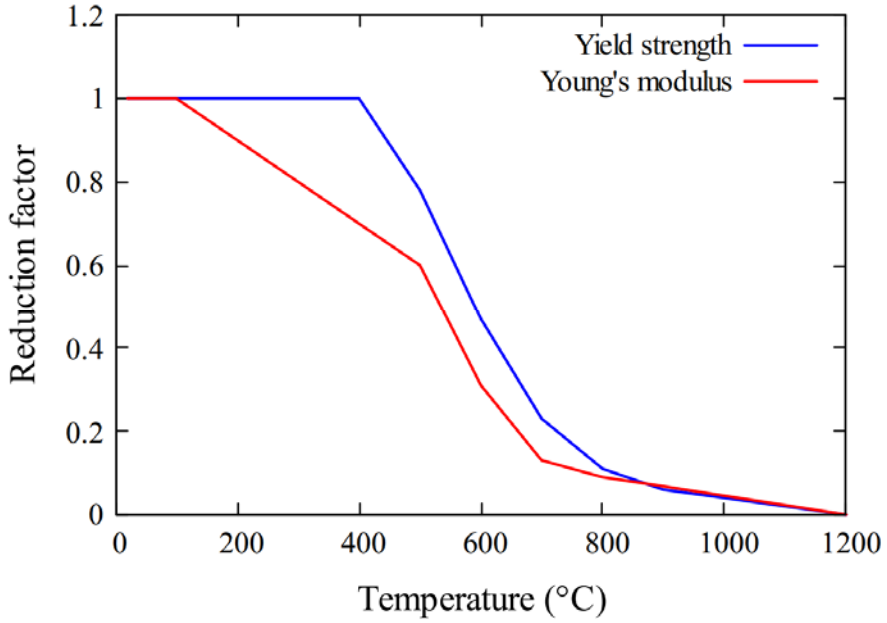

Figure 2-10: Reduction factors for yield strength and Young's modulus of steel recreated from EN 1993-1-2 (2005).

The degree to which thermal strain develops in a structural member when heated depends on the constraint provided. For simple structural fire engineering calculations, EN 1993-1-2 (2005) recommends a linear relationship for the thermal expansion of steel as shown in Equation 2.35. A more detailed relationship for the thermal elongation of steel is given by the piecewise solution in Equation 2.36 as depicted in Figure 2-12 (ECCS TC3, 2001).

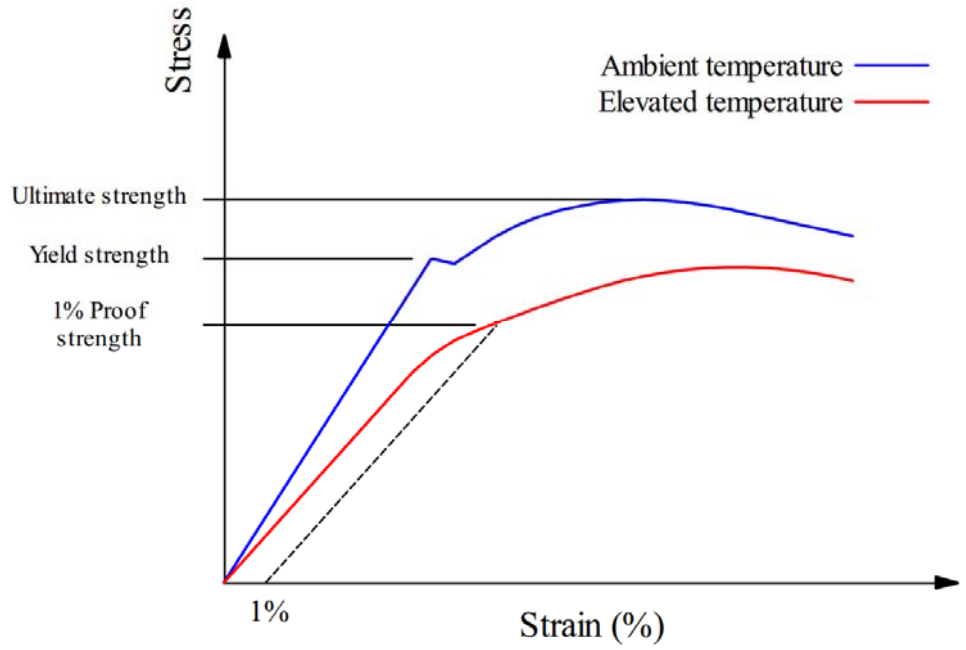

Figure 2-11: Comparison between constitutive relationships for steel at ambient and elevated temperature

Stellenbosch University https://scholar.sun.ac.za

Thermal restraint forces can either be beneficial or detrimental within steel structures. If steel columns are restrained from elongating due to an increase in temperature, the reaction forces on either side of the column increase. The increase in reaction forces can lead to excessive deflections and accelerate the buckling phenomena (Buchanan and Abu, 2017).

$$\Delta l/l = 14 \times 10^{-6}(T - 20) \qquad 2.35$$

$$\Delta l/l = \begin{cases} -2.416 \times 10^{-4} + 1.2 \times 10^{-5}T + 0.4 \times 10^{-8}T^2 & 20°C \leq T \leq 750°C \\ 11 \times 10^{-3} & 750°C < T \leq 860°C \\ -6.2 \times 10^{-3} + 2 \times 10^{-5}T & 860°C < T \leq 1200°C \end{cases} \qquad 2.36$$

where:

T	=	temperature of the steel
$\Delta l/l$	=	elongation of the member due to temperature change

Thermal strain should be considered for complex structural systems, especially where members are restrained by other parts of the structure leading to thermally induced forces, as mentioned above. The total strain for a steel member exposed to fire can be calculated according to Equation 2.37. Various formulations also include transient strain and creep strain in the formulation, although the Eurocode guidelines adopted in this work implicitly account for them. Creep strains refers to long term deformation of materials under constant load, while transient strain is only applicable to concrete structures due to the expansion of the cement paste when it is heated for the first time under load.

$$\varepsilon_{total} = \varepsilon_{\sigma} + \varepsilon_{th} \qquad 2.37$$

where:

ε_{σ}	=	stress related strain
ε_{th}	=	thermal strain

Stellenbosch University https://scholar.sun.ac.za

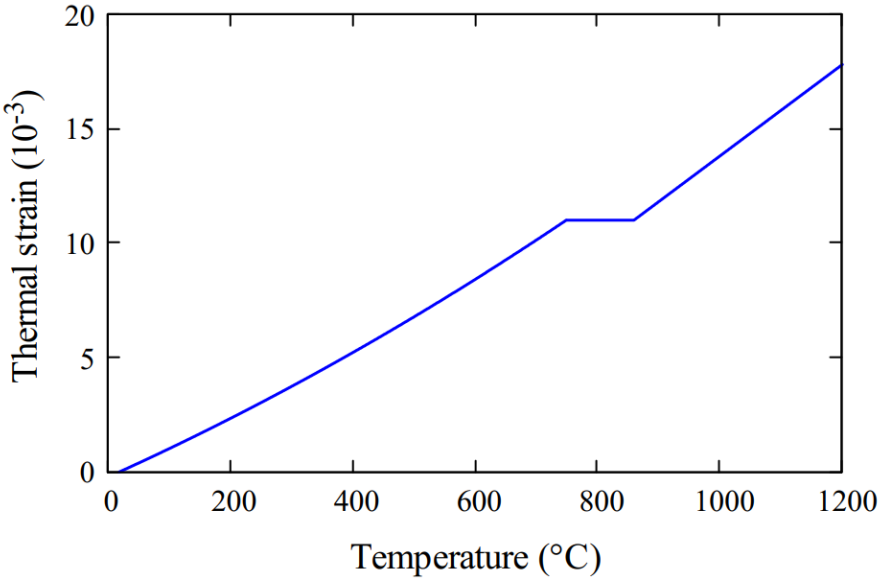

Figure 2-12: Thermal strain as a function of temperature.

When an axially loaded member which is uniformly heated is subjected to high temperatures the thermal expansion and axial force generated will depend on the stiffness of the surrounding structure. If the stiffness provided by the surrounding structure can be replaced with a spring stiffness, then the total strain induced in a column can be calculated according to fundamental structural mechanics. Equation 2.38 represents the total elongation in a column due to elevated temperature.

$$\Delta_{TOTAL} = \Delta_{THERM} - \Delta_{REST} - \Delta_{DET} \quad 2.38$$

with:

$$\Delta_{THERM} = \alpha_{exp} \Delta T L \quad 2.39$$

$$\Delta_{REST} = \frac{P_r L}{A E_T} \quad 2.40$$

$$\Delta_{DET} = \frac{PL}{AE_T} - \frac{PL}{AE} \quad 2.41$$

where:

Δ_{THERM}	=	thermal elongation
Δ_{REST}	=	elongation due to axial restraint forces
Δ_{DET}	=	shortening of column due to applied loads and deterioration of material property at elevated temperature.
α_{exp}	=	coefficient of thermal expansion
L	=	column length

Stellenbosch University https://scholar.sun.ac.za

E_T	=	Young's modulus at temperature T
P	=	imposed load
A	=	area of cross section
P_r	=	axial restraint force generated at elevated temperature

Ali *et al.* (1997) derived an equation for calculating the axial force generated in an axially restraint column subject to high temperatures based on the principles behind Equations 2.38 to 2.41. The proposed equation is shown below.

$$P_r = \alpha_K K_c(T) L \cdot f_1 \cdot f_2 \tag{2.42}$$

with:

$$\alpha_K = \frac{K_s}{K_c(T)} \tag{2.43}$$

$$f_1 = \alpha \Delta T - \frac{P}{A}\left(\frac{E - E_T}{E \cdot E_T}\right) \tag{2.44}$$

$$f_2 = \frac{AE_T}{AE_T + \alpha_K K_c(T) L} \tag{2.45}$$

where:

K_s	=	equivalent stiffness of surrounding elements
$K_c(T)$	=	stiffness of column at temperature T

2.8.2 Thermal properties

When a steel structure is exposed to a fire, the magnitude of various thermal properties change over the duration of the fire. Heat from the fire within the compartment is transferred to the structural elements mainly via convection and radiation. The density of steel remains constant even at high temperatures, and a value of 7850 $\mathrm{kg/m^3}$ is listed in the Eurocodes.

The specific heat of steel can be expressed by the piece-wise function described in Equation 2.46, while a constant value of 600 J/kgK is often used throughout for simple designs. Figure 2-13 depicts the relationship where the spike observed at around 735 ℃ is because of a change in the crystalline structure of steel.

$$c_p = \begin{cases} 425 + 0.773T - 1.69 \times 10^{-3}T^2 + 2.22 \times 10^{-6}T^3 & 20℃ \leq T < 600℃ \\ 666 + 13002/(738 - T) & 600℃ \leq T < 735℃ \\ 545 + 17820/(T - 731) & 735℃ \leq T < 900℃ \\ 650 & 900℃ \leq T \leq 1200℃ \end{cases} \tag{2.46}$$

Stellenbosch University https://scholar.sun.ac.za

The value of thermal conductivity for steel decreases linearly according to Equation 2.47 up until 800 °C before remaining constant. The relationship for thermal conductivity is illustrated in Figure 2-14.

$$k = \begin{cases} 54 - 0.0333T & 20°C \leq T \leq 800°C \\ 27.3 & 800°C < T \leq 1200°C \end{cases} \quad 2.47$$

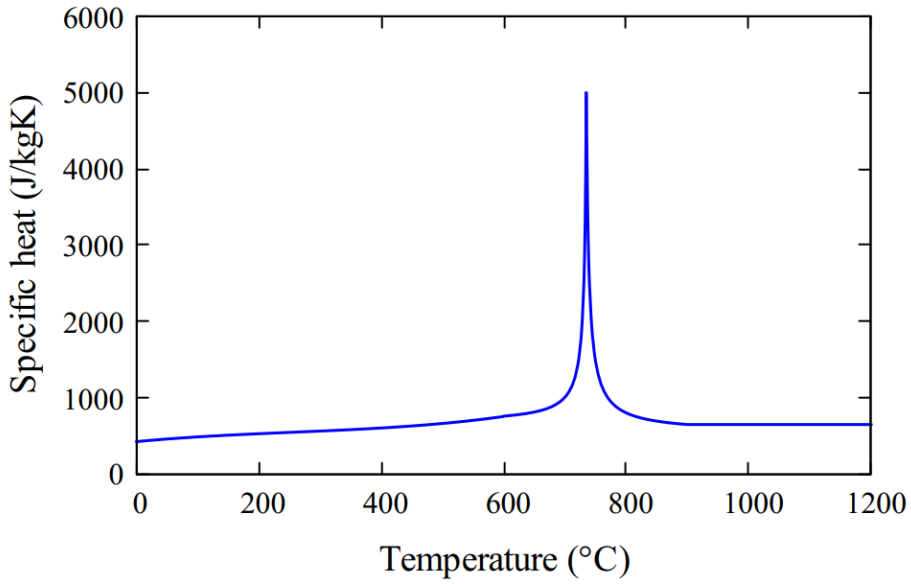

Figure 2-13: Specific heat of steel.

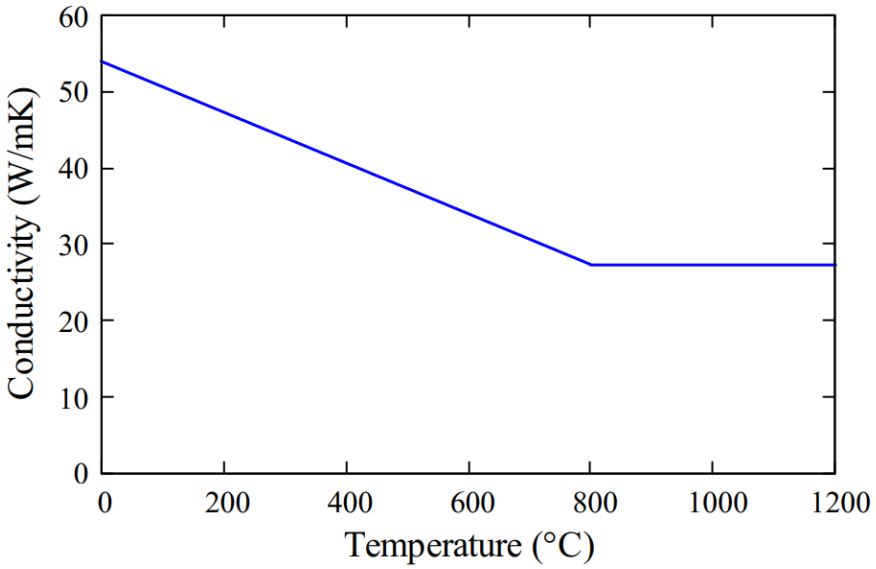

Figure 2-14: Thermal conductivity of steel.

2.8.3 Temperature gradients

Thermal gradients can develop when steel structures are exposed to fire. The temperature dependent mechanical properties as discussed previously influence the behaviour of many steel elements. The flexural buckling behaviour of columns is particularly a concern as the principles

Stellenbosch University https://scholar.sun.ac.za

behind the Euler buckling theory are no longer valid at elevated temperatures (Delgado Ojeda *et al.*, 2016). The violation of the Euler buckling is due to the curved stress-strain relationship at elevated temperatures as opposed to the well-defined yield plateau as highlighted in Figure 2-11.

Several studies on the flexural behaviour of columns at elevated temperatures have been conducted in the past which form the basis of the design guidelines listed in EN 1993-1-2 (2005). According to research conducted by Becker (2002), the temperature across a member or structure is never uniform in a real fire situation. The study concluded that the column capacity is slightly conservative if a uniform temperature equal to the maximum temperature within the column is used when calculating reduced steel properties. Several aspects affect the buckling behaviour of steel columns at elevated temperatures.

The variation of temperature throughout the cross section leads to a non-uniform distribution of elasticity and proof stress which poses challenges regarding the critical loads for both elastic and inelastic buckling. Due to the variation in stiffness, the elastic neutral axis shifts towards the cooler part of the cross section causing a moment because of eccentricity. The shifting of the neutral axis ultimately means that higher stresses will often occur in the hotter portion while stresses are relieved in the cooler part, although this is a function of geometry and load conditions.

Thermal bowing is another phenomena that occurs because of temperature gradients (Usmani *et al.*, 2001). The fire exposed side of steel columns heat up faster than the unexposed side which causes bending towards the fire. Thermal bowing is often considered as a form of geometrical imperfection and can also be modelled as an additional bending moment. The induced moment due to thermal bowing leads to tensile stresses in the fire exposed side of the column while compressive stresses occur in the unexposed side. Figure 2-15 shows the thermal behaviour of a pin connected column.

Shifting of the elastic neutral axis and thermal bowing counteract one another, where the former depends on the section geometry while the latter generally increases with slenderness. Many studies performed on the buckling capacity of steel columns at elevated temperatures only consider thermal bowing. According to Delgado Ojeda *et al.* (2016), thermal bowing and shifting of the neutral axis need to be considered to ensure that the buckling capacity is not under-predicted. Equations for determining the buckling capacity at elevated temperatures have been derived for simple cross sections accounting for the aspects discussed above. Many design codes ignore the shifting of the neutral axis and state that the reduced material properties should be determined based on the maximum temperature of the cross section (Agarwal *et al.*, 2014).

Stellenbosch University https://scholar.sun.ac.za

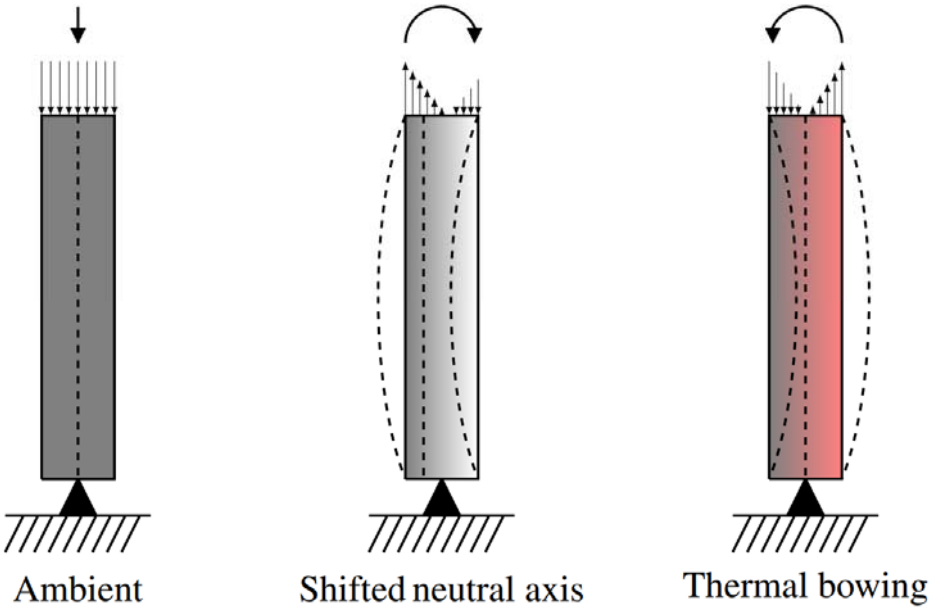

Figure 2-15: Stress distribution due to thermally induced forces and moments.

2.9 Finite element modelling

One of the most powerful tools used in structural engineering is computer based-numerical methods such as the finite element method. Most structural and thermal behaviour can be described by partial differential equations (PDEs). The finite element method is described as a set of numerical techniques which have been developed over the years to solve such PDEs (Harish, 2020). The analytical methods and derivations previously discussed are relatively easy to use and for simple problems they require less computational time. For complex problems, the use of advanced modelling is often needed especially when the assumptions behind analytical formulations have been violated.

The advantage of performing a finite element analysis, as opposed to a computational fluid dynamic (CFD) analysis, is that any given physical phenomenon can be modelled where the latter is mainly used for problems involving fluids. The finite element analyses performed in this thesis will be performed entirely with the aid of ABAQUS/CAE 2020 (Dassault-Systemes, 2020). Particularly for structural and heat transfer analysis, ABAQUS is acknowledged for its powerful capabilities and therefore it is the preferred finite element analysis package (Marx, 2018). ABAQUS can be used to perform several types of analyses such as thermal heat transfer, mechanical, decoupled thermo-mechanical as well as coupled thermo-mechanical (Dassault-Systemes, 2020).

Both the mesh size and type of element play a pivotal role when it comes to the accuracy of a finite element model. Based on the literature, the use of shell elements is the most widely used element for modelling thin-walled structures. A column can be defined as a thin-walled structure when the thickness of the flanges and web are significantly smaller than the corresponding width and height of the section. A study performed by Dinis and Camotim (2006) showed that the use of a shell finite element analysis provided accurate results for the

Stellenbosch University https://scholar.sun.ac.za

local and post buckling behaviour of cold formed steel thin-walled members.

According to Dassault-Systemes (2020), shell elements in ABAQUS can be modelled either by conventional shell elements or continuum shell elements. Conventional shell elements define the geometry of a body at a reference surface while continuum shell elements discretise an entire three-dimensional body. According to Hurley *et al.* (2016), the accuracy of numerical calculations performed by these packages is not only dependent on the algorithms within the package. Other factors which play a role in the reliability and accuracy of these packages is the validity of the finite element model as well as the material input parameters. The process of creating a finite element model involves several steps. The flow diagram shown in Figure 2-16 provides the main steps for developing a finite element model (Bathe, 1996).

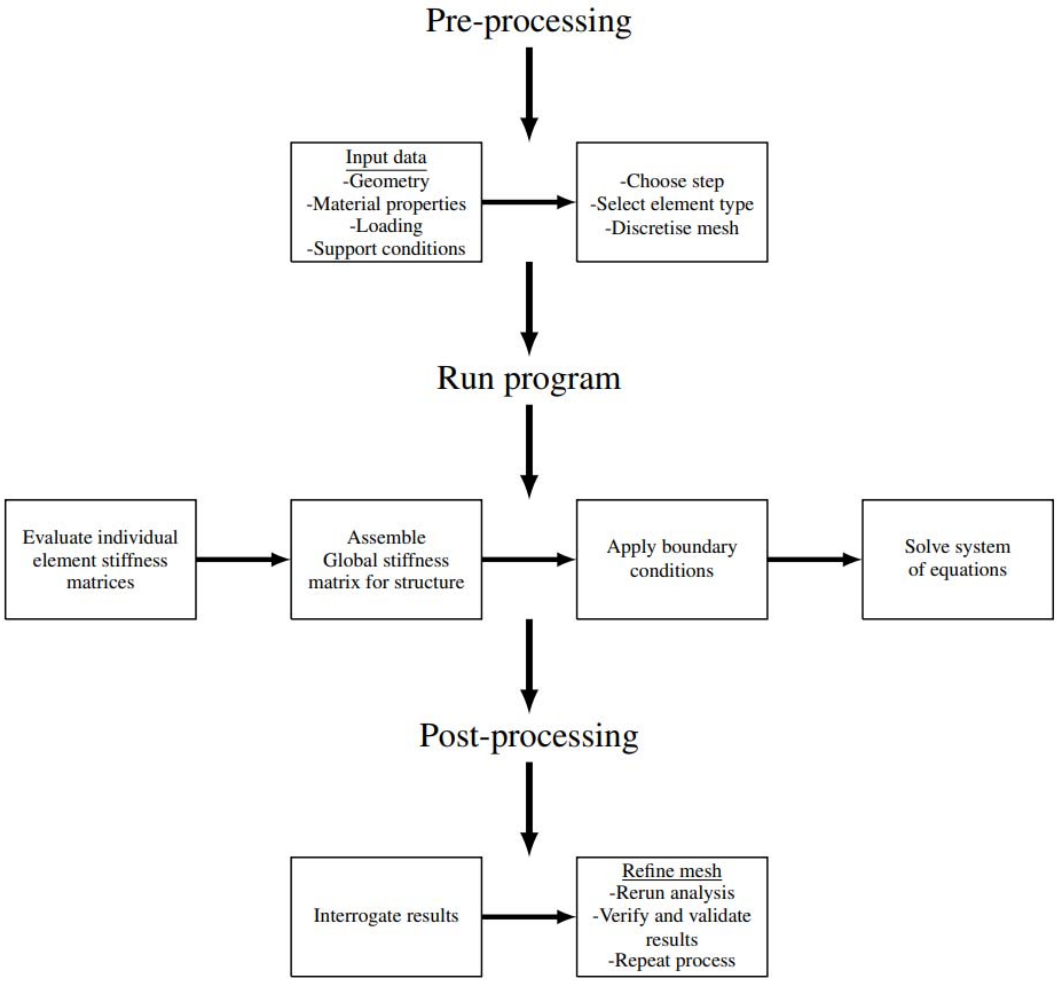

Figure 2-16: Finite element modelling procedure.

One of the most frequently used steps in ABAQUS is the static general step which is typically used for static stress analysis. A static general step can be linear or nonlinear and time dependent material effects are ignored even though rate dependent plasticity of the material is considered. In addition to the material and boundary nonlinearities as mentioned for the heat transfer step, nonlinearities may also arise due to large-displacement effects. Two methods are provided for a nonlinear static stress analysis. The first method considers a prescribed loading

Stellenbosch University https://scholar.sun.ac.za

history while the second method is designed for unstable problems where buckling or collapse is possible. The following section briefly describes the Riks method which is used to investigate unstable collapse and post buckling behaviour (Hibbitt, 1984).

2.9.1 Riks method

During buckling or collapse behaviour, the load displacement response sometimes shows a negative stiffness. To compensate for this, the structure must release strain energy to remain in equilibrium. There are several ways in which this type of behaviour can be modelled in ABAQUS where a load-deflection (Riks) analysis is often preferred. The modified Riks method, as defined by Dassault-Systemes (2020), is an algorithm that allows for effective nonlinear static equilibrium solutions. The Riks method can include both material and boundary nonlinearity, while a linear analysis, such as eigenvalue buckling, tends to precede a Riks analysis to capture structural collapse.

The Riks method solves for the loads and displacements simultaneously while using the load magnitude as an additional unknown. An additional parameter, namely the arc length, is used to measure the progress of the solution. ABAQUS uses the arc length along the static equilibrium path in the load-displacement space to determine a solution while the solutions are independent of whether the response is stable or not. The Newton-Raphson method is implemented to solve the necessary nonlinear equilibrium equations. Any loads that exist at the beginning of the step and are not redefined are treated as dead loads with a constant magnitude. The prescribed loads are ramped up until the user specified reference load is reached. The equation below shows the algorithm implemented by ABAQUS to calculate the load for the current increment during the step.

$$P_{total} = P_0 + \lambda(P_{ref} - P_0) \tag{2.48}$$

where:

P_{total}	=	current incremental load
P_0	=	dead load
λ_{LPF}	=	load proportionality factor
P_{ref}	=	reference load

The main purpose of the Riks analysis is to obtain an answer for an individual equilibrium path in space defined by nodal variables and loading parameters. Further information regarding the Riks method can be found in the ABAQUS user manual (Dassault-Systemes, 2020).

Stellenbosch University https://scholar.sun.ac.za

2.10 Overview of literature review

This chapter highlights important concepts and theory both in the field of general structural engineering and structural fire engineering. The basic mechanical behaviour of steel is introduced to aid the reader in understanding further discussions relating to the behaviour of compression elements of the 20 ft ISO standard shipping container as introduced in Chapter 1.

Both linear and nonlinear elastic material properties are discussed in terms of buckling while geometric and material imperfections of compression elements are also emphasised. The behaviour of corrugated plates in shear buckling is introduced in conjunction with energy methods used in the structural engineering profession. Analytical methods for predicting the buckling behaviour for both columns and corrugated plates are also discussed.

The chapter proceeds by describing the behaviour of steel at elevated temperatures. A brief overview on fire safety and structural fire engineering is provided followed by the three modes of heat transfer and the parameters associated with each. The behaviour of steel structures in fire is highlighted by discussing important considerations such as temperature gradients before the chapter concluded with a discussion on the finite element method.

Stellenbosch University https://scholar.sun.ac.za

3 Discussion of shipping container buildings and modifications

3.1 Introduction

It is well known that the primary use of shipping containers over the past 70 years has been to transport large quantities of commodities across the globe. The intermodal nature of these modular units means that goods are transported quicker and more economically, while no additional protection is necessary.

In the last 20 years, several different uses for these shipping containers have been implemented, with the most noticeable one being the conversion of these units into habitable structures. The geometry and ease of modifying these modular units means that architects can design aesthetically pleasing structures, both single and multistorey, as seen in Figure 3-1. With a growing demand in modular construction, a concern regarding the structural resistance at both ambient and elevated temperatures of these structures has risen.

Figure 3-1: Shipping container home (Home Containers, 2019).

There is negligible data regarding the fire performance of containers at elevated temperature. The United States Coast Guard performed large scale tests to investigate the possibility of fire spread from one shipping container to another (Eberly, 1977). The on-deck storage of cargo is a unique situation where the probability of a given container containing large quantities of combustible materials is high, meaning that an understanding of possible fire spread was needed for both an internal and external fire. The results showed that ignition within the sealed container led to minimal damage and no fire spread to adjacent containers was observed. If a container stack is exposed to an external fire source it is possible that structural failure and collapse could well occur, resulting in radiant heat fluxes causing flame spread to adjacent

Stellenbosch University https://scholar.sun.ac.za

containers (Eberly, 1977). Even though the sealed shipping containers do not pose a great fire hazard from a structural fire engineering perspective, the behaviour of modified shipping container buildings at both ambient and elevated temperatures need further investigation.

The following sections discuss load paths for the 20 ft ISO shipping container and considerations for a weakened structure are also introduced.

3.2 Geometry and load paths

From a structural engineering point of view two of the most important aspects to consider with regard to structural behaviour are load paths as well as boundary conditions and understand how they influence overall structural behaviour. The International Organization for Standardization (ISO) has created a set of documents which dictate shipping container specifications, structural strengths as well as the application thereof. Shipping containers come in three sizes namely 10, 20 and 40 ft. As previously mentioned, this thesis will only consider the 20 ft ISO shipping container with dimensions as listed in Table 3-1. Table 3-2 provides load specifications for the 20 ft ISO shipping container according to ISO 668 (1995). The high compressive capacity of 4117 kN for a single container should be noted.

Table 3-1: Dimensions of container (Singamas, 2018)

Type of dimension	Magnitude (mm)
Length (external)	6058
Length (internal)	5898
Width (external)	2438
Width (internal)	2352
Height (external)	2591
Height (internal)	2393

Table 3-2: Load capacities for 20ft shipping container (ISO 668, 1995)

Allowable weight (kN)	Empty weight (kN)	Maximum compressive force (kN)
299	48.8	4117

The container consists of a steel frame enclosed by 2 mm thick corrugated sheeting which is welded to the frame. The base of the container frame consists of bottom side and end beams (primary beams) as well as several cross beams (secondary beams). The spacing of the secondary beams vary slightly throughout the span of the floor system while the average spacing is approximately 300 mm. The floor of the container consists of plywood having a thickness of 28 mm which is compositely connected to the secondary beams via zinc plated steel screws. The secondary beams consist of pressed channel sections which are located beneath the plywood floor. The rear end of the container consists of a frame and a corrugated sheet which are welded together as a sub assembly. The rear frame consists of two corner

Stellenbosch University https://scholar.sun.ac.za

columns as well as a top and bottom end beam which are connected by loading blocks via welding. The front frame consists of two corner columns, a door header and sill which are once again connected via the loading blocks. The two side wall assemblies consist of corrugated sheeting with top and bottom side beams which connect the front and rear frames. The roof also consists of a corrugated sheet which is welded to the rear, front and side assemblies. Figure 3-2 shows the main structural components of a standard 20 ft shipping container.

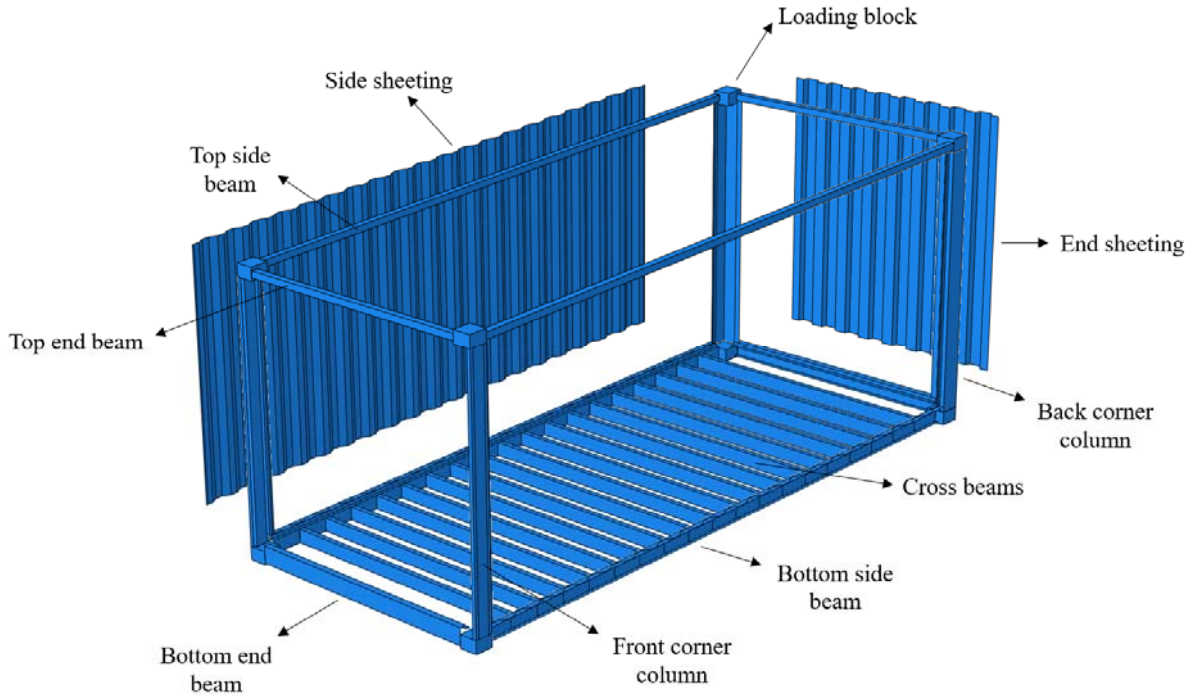

Figure 3-2: Exploded view showing salient structural components for the 20 ft ISO shipping container.

In a typical stacked configuration, the loads within each shipping container are carried by the composite floor system. From the composite floor system, the loads are further distributed to the primary bottom side and end beams and ultimately to the load bearing corner columns. As previously mentioned, the ceiling is supported by the top beams. The corrugated ceiling on its own is relatively light, with a primary function of adding rigidity to the top beams by providing out of plane stiffness, while from a practical point of view it prevents water ingress. It is evident that both the top and bottom beams brace the frame. The axial stiffness of the floor and ceiling configurations play a key role as they prevent lateral movement of the loading blocks which reduces the effective length of the column.

It is evident that containers were originally designed to bear loads on the corner posts and therefore both the front and back corner columns play an important structural role as compression elements. S Jones Containers (2021) emphasises the fact that corner columns should protrude slightly above the roof to prevent stresses occurring in areas which oppose the original design and present structural issues. The back corner column is made of 6 mm thick section steel while two ø14 brackets are welded equidistantly along the length of the column. The front corner column consists of an inner part of channel shaped hot-rolled section steel and an outer part of steel pressing. The thickness across the front corner column section varies,

Stellenbosch University https://scholar.sun.ac.za

where the thickness of the web of the inner channel is 11 mm as opposed to 6 mm for the remainder of the section. The cross-sectional geometry of the structural elements of the 20 ft ISO shipping container are depicted in Table 3-3. Appendix A provides the section properties for the beams and columns as listed in the first two rows of Table 3-3.

Table 3-3: Salient structural components for the ISO 20ft shipping container.

Back corner column	Front corner column	Bottom side beam
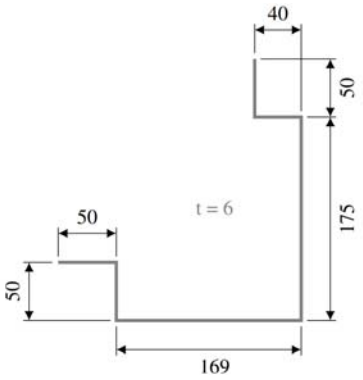	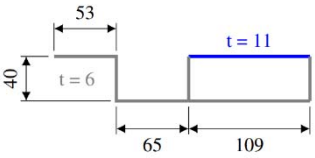	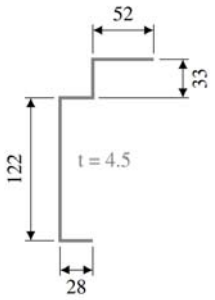
Bottom end beam	**Top side and end beam**	**Cross beam**
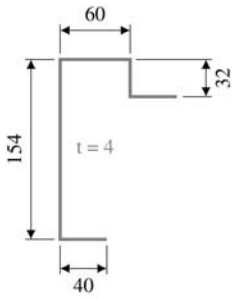	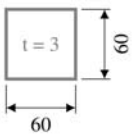	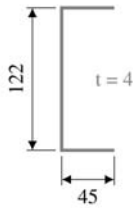
Side wall	**End wall**	**Loading block**
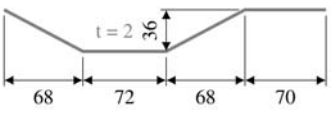	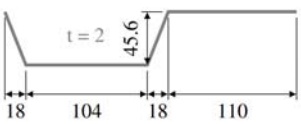	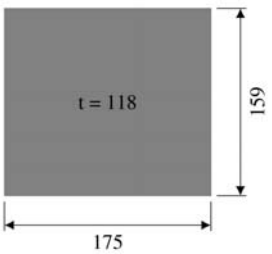

Stellenbosch University https://scholar.sun.ac.za

3.3 Considerations for a weakened structure

In contrast to a shipping container serving its original purpose where the unit is essentially closed on all six sides, from Figure 3-1 it is evident that when modified, large portions of the corrugated sheeting are removed, and in some instances the sheeting of one or more sides are entirely removed. Another interesting observation is the stacking nature of these modular units when used in multistorey construction. As previously mentioned, shipping containers have been designed to bear vertical loads on the columns, while the primary beams add rigidity to each individual container. Architecturally driven container buildings seldomly consider the modified structural resistance because of a change in load paths opposing the original design. From a structural engineering perspective, the difference between a simple structure and a complex multistorey container building is highlighted in Figure 3-3.

(a) **(b)**

Figure 3-3: (a) simple container building (Lallanilla, 2019), *(b) complex container building* (Howard, 2017)

When stacked vertically on top of one another, a 20 ft ISO shipping container has a payload capacity of 30 tons each and the recommended upper limit for the number of fully loaded containers stacked and connected on top of one another is 9 (Wankhede, 2021). This gives a total load of around 2650 kN, meaning that the maximum compressive capacity of 4117 kN listed above is approximately 1.6 times higher, which is a suitable imposed load partial factor (SABS, 2011b).

As mentioned in the beginning of this section, several questions regarding the construction of these modular structures as well as the modifications performed on the individual container units need to be answered. When these shipping containers are used to construct habitable structures, doors and windows are created by cutting openings out of the corrugated sheeting. The ease at which sheeting can be removed from these shipping containers allows clients to specify complex architectural designs and, in some instances, all the sheeting of one or more of the walls is removed. By using shipping containers as residential homes, the imposed load is considerably smaller as opposed to it being used as a mode of transport. For a residential or office occupancy with an imposed load of 3.0 kPa, the total required capacity is 90.4 kN which is significantly less than its 299 kN capacity, as will be discussed in Section 6.4.2. Even though this is the case, the possibility of over-modifying the structure and reducing the structural integrity of the container, needs further investigation. If the removal of sheeting reduces the strength of a container considerably, steel beams would need to be welded in place to improve

Stellenbosch University https://scholar.sun.ac.za

the strength which leads to additional costs.

The load bearing nature of shipping containers mean that they have been specifically designed to be stacked with the columns on top of one another. Many multistorey shipping container structures are being built with containers stacked perpendicularly on top of one another as seen in Figure 3-1 and Figure 3-3. Figure 3-4 highlights the difference in load path between shipping containers stacked on their corners and perpendicular to one another. The top side and end beams of a shipping container are designed primarily to support the lightweight roof and brace the structure as previously mentioned. When one shipping container has been stacked perpendicularly on top of another container, the load from the above shipping container is supported either partially or entirely by the top primary beams of the container below before being transferred to the outer columns. This means that certain elements of the container are now carrying more load than was anticipated based on the original design and functionality. Depending on the magnitude of the load coming from above, the corrugated side wall assembly could undergo buckling while failure of the top beam might occur.

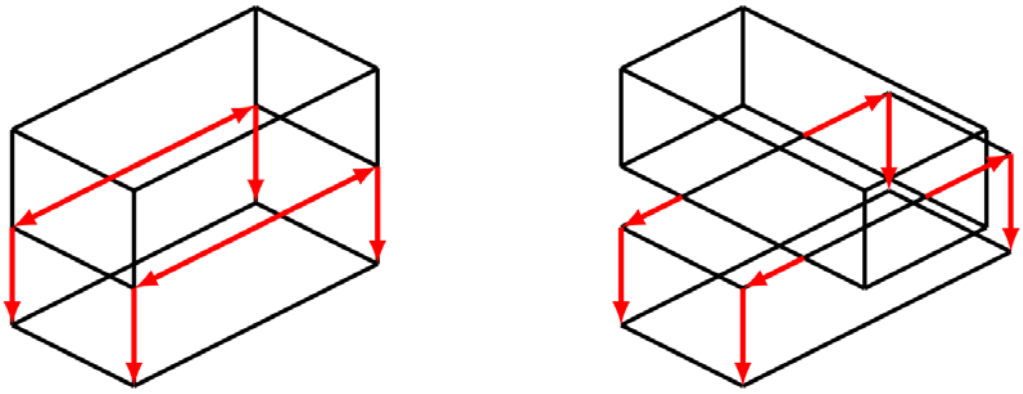

Figure 3-4: Load paths for different stacked configurations.

From a structural fire engineering perspective, the type of fire within a modified shipping container needs further investigation. The study performed by the United States Coast Guard, as discussed at the beginning of this section, leads to a fire which is considered relatively safe while the addition of ventilation to a weakened structure could make the structure particularly vulnerable to the extreme event of a fire.

When steel structures are exposed to a fire, the steel temperature increases at a high rate. Various passive fire protection measures have been implemented in the past such as board systems, spray-on systems and intumescent paint (Buchanan and Abu, 2017). Board systems with a wide range of material properties serve as an effective means of insulating shipping containers as discussed in the coming sections. Calcium silicate and gypsum boards are two of the most common board systems used due to the good insulating properties. In general, the boards are either glued or screwed to a metal frame which is then fastened to the steel elements.

Stellenbosch University https://scholar.sun.ac.za

3.4 Previous studies and preliminary verification

Before proceeding with the finite element models in the chapters to follow, three studies are briefly looked at while a preliminary verification study on the most important modelling techniques applicable to this thesis are performed. These studies focus on:

(1) Determination of the lateral stiffness of the corrugated side walls.

(2) Plate girder web buckling to understand wall structural resistance

(3) Thermal modelling of shipping containers to obtain insulation fire resistance ratings.

3.4.1 Verification Study 1 - Lateral stiffness of corrugated side wall (Yu and Chen, 2018)

Due to the lack of design guidance and understanding of modular construction, these structures are often modelled as simple frame units with negligible lateral stiffness. The lack of design guidance about modular construction has led designers to ignore the strengthening effect of the sidewalls with respect to practical structural design.

The study performed by Yu and Chen (2018) investigated the lateral rigidity of container modules with specific focus on the strengthening effect of the corrugated sidewall. The rigidity of the corrugated sidewall was computed via both an analytical and numerical approach, while the results of the latter were verified by simulating experimental tests performed by Ding *et al.* 2017. Several assumptions were made by Yu and Chen (2018) while developing the analytical formulations. The computed lateral stiffness was simplified and included into a multistorey modular apartment to assess the structural behaviour against laterally induced forces, such as wind and earthquakes.

3.4.1.1 Analytical method

To determine the lateral stiffness of the corrugated sheets analytically, energy methods as outlined in Chapter 2 were used. Yu and Chen (2018) followed an elastic design approach thereby only considering the elastic stiffness of the corrugated sheets. The lateral pushing trend from the upper modular unit in a stacked configuration was assumed to be evenly transferred to the loading block of the unit below. Figure 3-5 shows the deformation transfer between vertically stacked containers and the corresponding shear forces acting on the corrugated panel.

Stellenbosch University https://scholar.sun.ac.za

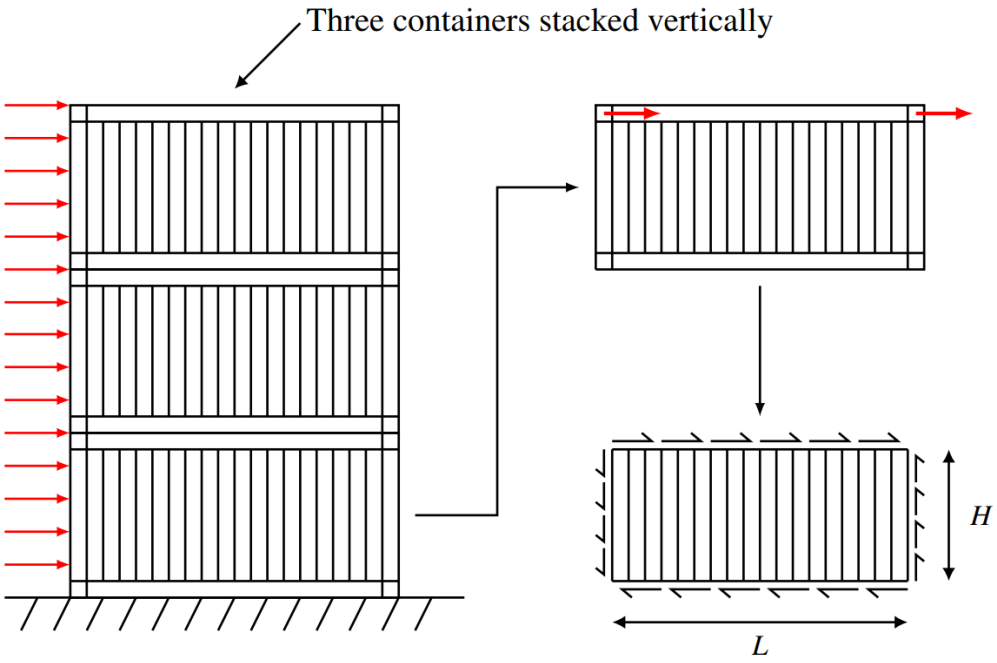

Figure 3-5: Shear distribution acting along the corrugated sidewall due to lateral loading on stacked configuration.

Yu and Chen (2018) argue that lateral deformations of a shipping container sidewall are mainly due to pure shear deformation and the distortion twist effect of the corrugated construction. According to ECCS (1995) the steel frame surrounding the corrugated sheeting prevents any nonlinear warping and out of plane bending from taking place. Typically modular units are built up from box sections which will provide certain restraint to free distortion of the corrugated sheet when shear is present. Yu and Chen (2018) conservatively accounted for the warp distortion twist by assuming a linear model as depicted in Figure 3-6.

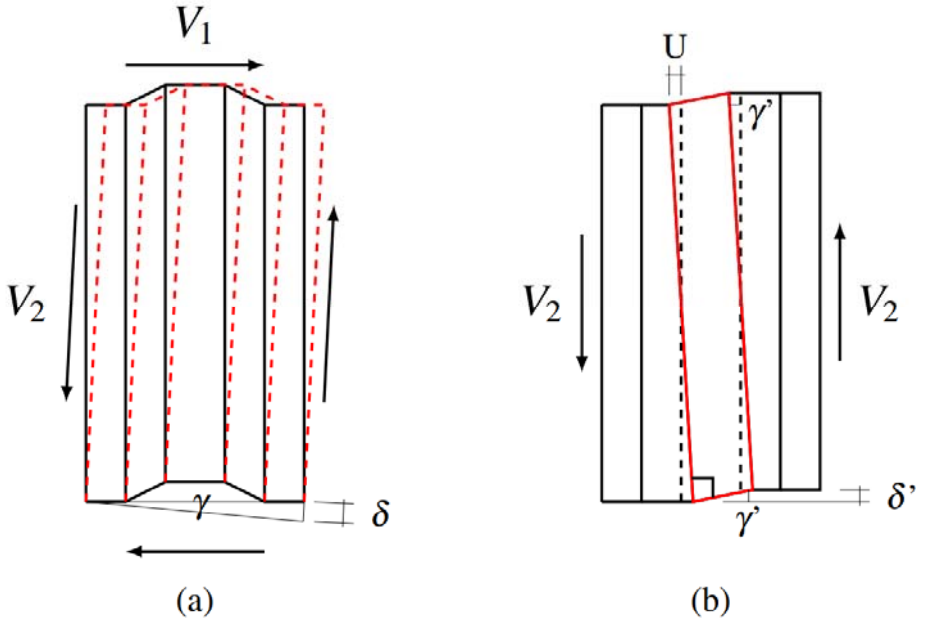

Figure 3-6: (a) Pure shear deformation, (b) distortion twist deformation, recreated from Yu and Chen (2018).

Stellenbosch University https://scholar.sun.ac.za

The shear strain energy due to pure shear was computed according to energy theory by applying Castigliano's theory (Beer *et al.*, 2014). As highlighted in Equation 3.1, Castigliano stated that when a body is elastically deflected, the deflection at any point and in any direction is equal to the partial derivative of strain energy with respect to the load located at that point and acting in the respective direction.

$$\Delta = \frac{\partial U}{\partial Q} \tag{3.1}$$

where:

Δ	=	deflection
U	=	energy
Q	=	force

Applying the principle above in conjunction with Equation 2.23, the displacement deformation and shear strain of the corrugated wall can be computed according to Equation 3.2. The section dimensions as used by the original author in developing Equation 3.2 are shown in Figure 3-7

$$\gamma = \frac{\delta}{d} = \frac{4(b_L + b_S + b_T)(1+\nu)}{dELt_w} V_1 \tag{3.2}$$

where:

δ	=	displacement deformation due to pure shear
ν	=	Poisson's ratio
E	=	Young's modulus
t_w	=	thickness of corrugated wall panel

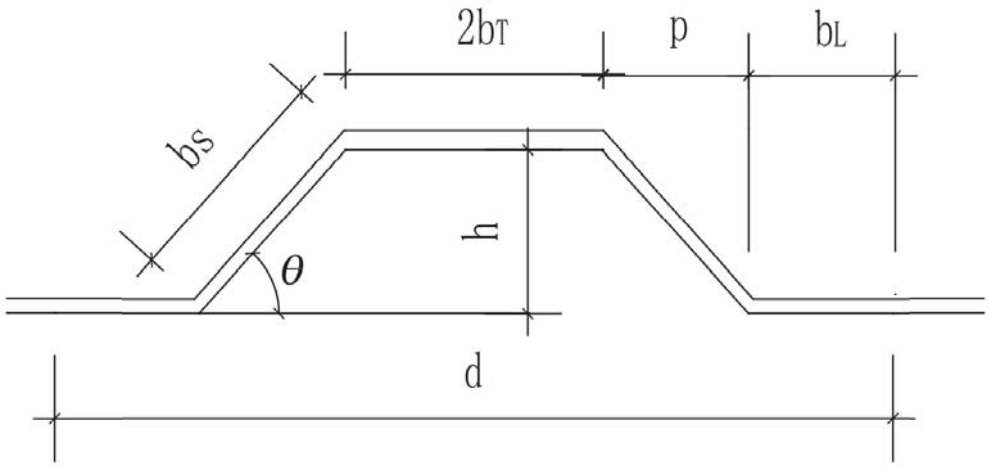

Figure 3-7: Section dimensions for a single wave of the corrugated panel(Yu and Chen, 2018).

The internal strain energy that results from linear warp distortion was also computed according to the energy integral. Remembering that the internal strain energy is equal to the work performed by the shear force, the strain due to linear warp distortion was derived to yield Equation 3.3. To compute the lateral displacement U as depicted in Figure 3-6 (b), the unit

Stellenbosch University https://scholar.sun.ac.za

load, which is similar to the principle of virtual work method, was implemented by modelling a single wave of the corrugated sheeting as a portal frame with a shear traction corresponding to V_1 acting along the to top edge of the wall. The coefficient α is because of the bending moment multiplication which follows from the unit load method and only depends on the geometry of the panel configuration. It should be noted that only the most important equations are listed here, comprehensive derivations for both Equations 3.2 and 3.3 are provided by Yu and Chen (2018).

$$\gamma' = \frac{\delta'}{d} = \frac{288\alpha b_T(1-\nu^2)}{dEt^3H^2L}V_1 \tag{3.3}$$

$$\alpha = \frac{4{b_L}^3h^2(2b_T+p)}{3d^2} - \frac{ph^2}{3d^2sin(\Theta)}(dpb_L - 2dpb_T + db_Lb_T - 2d{b_T}^2 \\ -2p^2b_L + 4p^2b_T - 6p{b_L}^2 + 2pb_Lb_T + 8p{b_T}^2 - 12{b_L}^2b_{T+} + 12b_L{b_T}^2) \tag{3.4}$$

Using Equation 3.2 and 3.3 to compute the strain due to pure shear deformation and linear warp distortion, the total shear stiffness K_p of a corrugated sheet with a known geometry can be computed simply according to Equation 3.5.

$$K_p = \frac{V_1}{H(\gamma+\gamma')} \tag{3.5}$$

3.4.1.2 Numerical method

As previously mentioned, the aim of the study by Yu and Chen (2018) was to investigate the influence of lateral rigidity in container-like modules and incorporate this into a multistorey modular structure. Numerical models were developed in ABAQUS to determine the lateral stiffness of the individual corrugated wall which was then incorporated into a modular apartment building using the MIDAS software program. Figure 3-8 shows a schematic of the modular side wall, while the equivalent cross bracing system used for the MIDAS model is also shown.

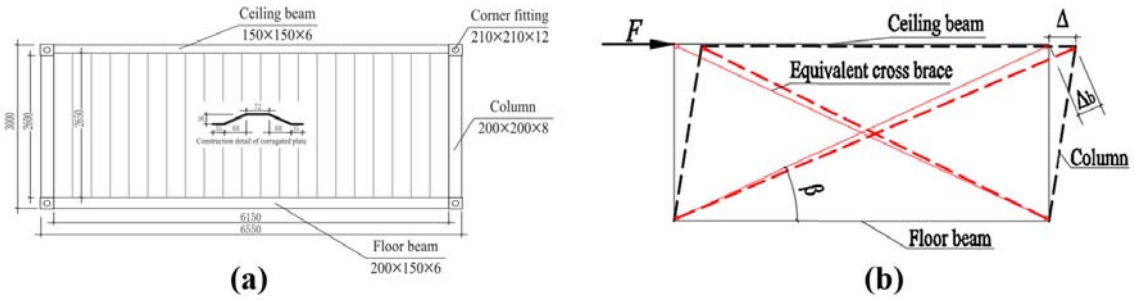

Figure 3-8: (a) Schematic of side wall under consideration, (b) design model for equivalent bracing system (Yu and Chen, 2018).

The model consisted of four-node shell elements (S4R), while the mechanical behaviour of the steel was simplified to that of an elastoplastic material. In terms of connecting the corrugated

Stellenbosch University https://scholar.sun.ac.za

sheeting to the surrounding beams and columns, tie constraints were used to replicate the welded sections. The bottom column ends were restrained against both rotation and displacement while the bottom side beam was restrained against in-plane lateral displacement due to the rigid floor system of the unit. The top corner ends were fixed to the bottom of the container above and therefore rotations were not permitted. As opposed to applying a lateral force to the model, it was decided to rather apply a unit displacement load thereby reducing the complexity in calculating the lateral stiffness of the corrugated sheet. In general, the ceiling of such a modular unit consists of a strong steel frame although some modular steel buildings incorporate a lightweight steel joist ceiling system. For a strong steel frame, high in-plane lateral stiffness is present and therefore the displacement load was applied to both top loading blocks and beams.

To validate the numerical procedures and models developed later in this thesis, the model of Yu and Chen (2018) was recreated in ABAQUS based on the model description above. To compute the elastic lateral stiffness of the corrugated sheeting, it is only necessary to include the Young's modulus and Poisson's ratio which have values of 190 GPa and 0.3 respectively, based on Q345 steel. Unfortunately only the most important numerical steps are highlighted by Yu and Chen (2018) and no information regarding mesh sizes used in their models is provided. Due to the relatively complex three-dimensional assembly of the modular side wall, the parts were meshed independently by seeding the edges of the individual parts to ensure that the nodes coincide with one another. This is particularly important for the shear load transfer between the top beam and the corrugated wall. It was found that a mesh of four to five elements per fold length resulted in mesh convergence while a finer mesh led to increased computational time with no added benefit in terms of accuracy. Figure 3-9 shows the discretised mesh of the model developed to validate the work performed by Yu and Chen (2018).

Both the strong (i.e. full corrugated steel roof) and weak (lightweight joists) ceiling models were created where the load was applied as a unit displacement and boundary conditions were applied as discussed previously. In contrast to a buckling analysis where multiple displacement solutions are possible for a given load, it is assumed that static equilibrium is reached, and therefore a static general step was chosen to obtain the elastic stiffness of the corrugated sheet.

Stellenbosch University https://scholar.sun.ac.za

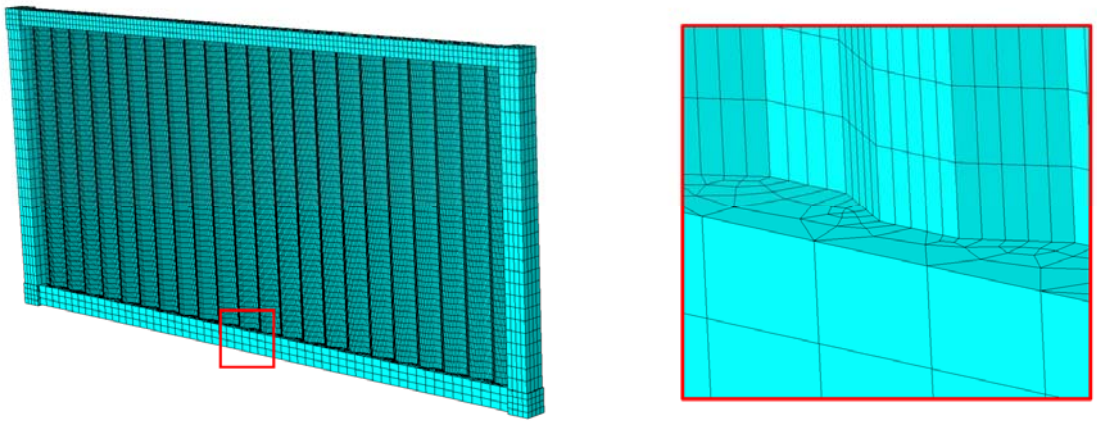

Figure 3-9: Mesh used to recreate the modular side wall (Yu and Chen, 2018).

The von Mises stress contours for the replicated models are shown in Figure 3-10. The stress contours agree well with the models developed by Yu and Chen (2018). To compute the lateral stiffness of the corrugated sheet, a nodal set consisting of twenty nodes along the interface between the top beam and corrugated sheet was generated. One advantage of using shell elements for this specific analysis is that ABAQUS provides several different section forces which are useful for post processing of results. The average shear membrane force per unit width (SF3) was computed for the nodal set before multiplying this value by the length of the corrugated sheet to obtain the shear force (V_1) acting between the beam and corrugated sheet.

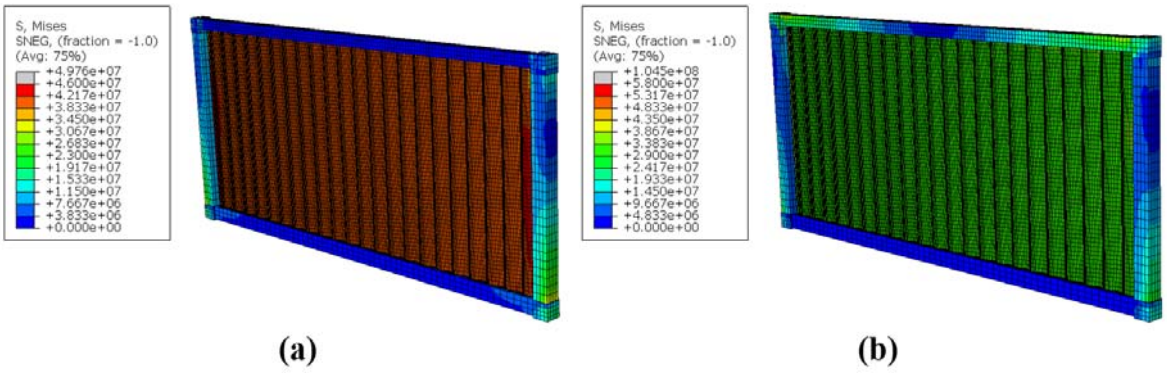

Figure 3-10: (a) Von Mises stress contours for strong ceiling and (b) weak ceiling modules.

The lateral stiffness of the side wall assemblies computed based on the replicated models is compared to the results of Yu and Chen (2018) in Table 3-4. The results of the lateral stiffness computed in the verification study, i.e. Yu and Chen, is slightly higher than the values reported in this work. The reason for this can be attributed to the fact that the bending stiffness of the columns have been neglected in the replicated models. To compute the global rigidity of the modular side wall assembly, the bending stiffness of both columns should be computed according to Equation 3.6. According to Yu and Chen, the lateral rigidity of both columns used in the container module are 8.5 kN/mm. Taking into consideration the bending stiffness of the modular columns, the results are within 4% of those presented by Yu and Chen (2018). The theoretical stiffness of the corrugated side wall as depicted in Figure 3-8 (a) was computed via Equations 3.2 to 3.5 and had a value of 285 kN/mm which is comparable to the numerical

Stellenbosch University https://scholar.sun.ac.za

results for the strong ceiling case.

Even though several assumptions were made with regard to the numerical models developed in this thesis, the results are in good agreement with those presented by Yu and Chen (2018). This verification highlights the fact that a realistic finite element model can be developed and analysed in ABAQUS if a sound understanding of boundary conditions and load transfer is applied.

$$K_B = \frac{48EI_c}{l^3} \tag{3.6}$$

where:

K_B	=	bending stiffness
E	=	Young's modulus
I_c	=	moment of inertia of column
l	=	length of column

Table 3-4: Comparison between the verification study Yu and Chen (2018) and the author's FEM results.

Model	Yu and Chen results (kN/mm)	Author's results sheeting only (kN/mm)	Author's results sheeting and columns (kN/mm)
Strong ceiling	294.4	276.2	284.7
Weak ceiling	221.4	210.6	219.1

3.4.2 Verification Study 2 - Plate girder web buckling (Sayed-Ahmed et al., 2003)

Sayed-Ahmed *et al.* (2003) investigated the buckling behaviour of corrugated steel web girders according to numerical methods as well as the analytical methods as outlined in Section 2.4.1. The aim of this study was to predict the buckling behaviour of steel and composite beams with corrugated steel webs. The original authors only investigated the linear elastic buckling behaviour via numerical models developed in ANSYS.

The purpose of the verification study investigated in this thesis is not only to replicate the results of the original authors but to develop further understanding of modelling both linear and nonlinear elastic buckling in ABAQUS. As discussed in the literature review, the buckling behaviour of corrugated webs is not uniquely governed by the web height to thickness ratio. Sayed-Ahmed *et al.* (2003) found that the buckling behaviour was highly dependent on the panel width and therefore the critical shear stress was plotted as a function of the panel width. The numerical models of the steel beams with corrugated webs were modelled using 8-node iso-parametric shell elements. The model consisted of 20 mm thick steel flanges and stiffeners connected to a corrugated web with a constant web height to thickness ratio of 250. Figure 3-11 (a) depicts a schematic of the numerical model implemented by the original authors in their study. Five different panel widths were considered ranging from 20-400 mm. The results of

Stellenbosch University https://scholar.sun.ac.za

the linear elastic buckling analysis, as shown in Figure 3-11, (b) agree well with the theoretical formulations developed for global and local buckling. The results show that the type of buckling is highly dependent on the panel width where global buckling is the dominating mode of failure for smaller panel widths. For intermediate panel width sizes, a discrepancy is present between the interactive formulation and the elastic local and global buckling equations. This stresses the importance of accounting for web yielding which can influence the buckling behaviour.

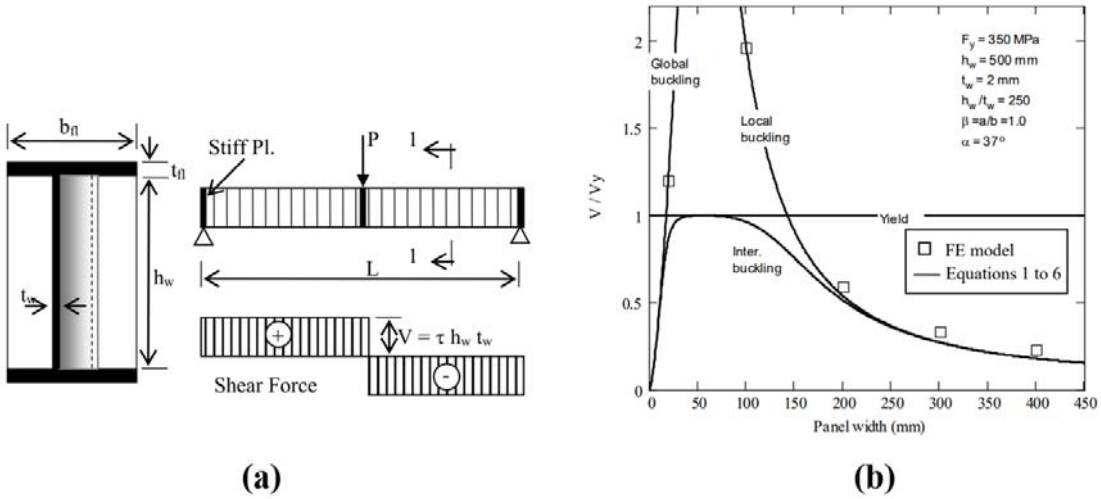

Figure 3-11: (a) Loading configuration considered for the numerical model, (b) results for numerical and analytical model considered (Sayed-Ahmed et al., 2003).

To replicate the results of the verification study, two three-dimensional models were created in ABAQUS with panel widths of 100 and 200 mm, like those proposed by the original authors. The flanges, stiffeners and web were defined similarly by using shell elements while the individual parts were connected in the assembly module via tie constraints. A similar mesh was assigned to the finite element models by seeding the edges by number.

The steel had a Young's modulus of 200 GPa and a Poisson's ratio of 0.3 respectively. When defining the buckle step, the linear perturbation procedure was the preferred procedure as it allows for an eigenvalue buckling analysis to be performed. According to Dassault-Systemes (2020), a unit load should be applied when an eigenvalue buckling analysis is performed in ABAQUS. In terms of boundary conditions, the bottom ends of the beam were pin connected while the top and bottom flanges were restrained from lateral movement thereby inducing web buckling as opposed to lateral torsional buckling of the beam.

Figure 3-12 shows the deformed shape of the critical eigenvalue mode as well as the magnitude of the critical load (N) for panel widths of 100 and 200 mm respectively. The shear force initiated at buckling was determined by assuming a simply supported beam model as shown in Figure 3-11 (a). The critical shear stress was then approximated by assuming a uniform shear stress distribution along the entire web with a known cross-sectional area. The graph displayed in Figure 3-13 shows the results of the numerical and analytical models. Since only the Young's modulus was included in the material property definition, the theoretical equations for the

Stellenbosch University https://scholar.sun.ac.za

critical elastic buckling stress are in good agreement with the numerical results. Even though the results are promising, there is a clear discrepancy present for the 100 mm panel width as the critical buckling stress according to the interaction equation is equal to half of that predicted by the local buckling equation.

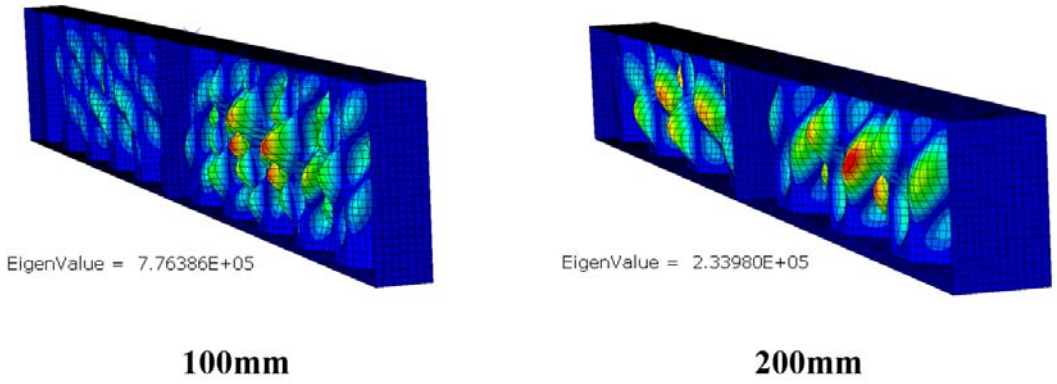

Figure 3-12: Deflected shapes for the critical eigen modes and critical load (N).

To investigate the true buckling behaviour of the 100 mm panel width, it was decided to modify the material properties by including the yield and ultimate strength of the steel which had values of 350 and 450 MPa respectively. The step used to analyse the nonlinear elastic buckling behaviour was the Riks method as outlined in Section 2.9.1.

Even though the interaction equation considers material yielding, material and geometric nonlinearity are not accounted for. In Section 2.3.2 it was mentioned that the buckling capacity is dependent on the geometric and mechanical imperfections of steel. Guidelines are provided by the European standards for modelling equivalent initial geometric imperfections in the form of an initial curvature or out of straightness. To remain consistent with the theoretical derivations, it was decided to omit the inclusion of imperfections in the numerical model. The deflected shape of the Riks analysis model for the plate girder with a 100 mm panel width is depicted in Figure 3-14. The load proportionality factor had a value of 0.48 which corresponds to a critical shear stress to yield stress ratio of 0.91 as seen in Figure 3-13. In comparison to the deflected shapes characterised by local buckling as seen in Figure 3-12, steel yielding is evident in Figure 3-14.

Stellenbosch University https://scholar.sun.ac.za

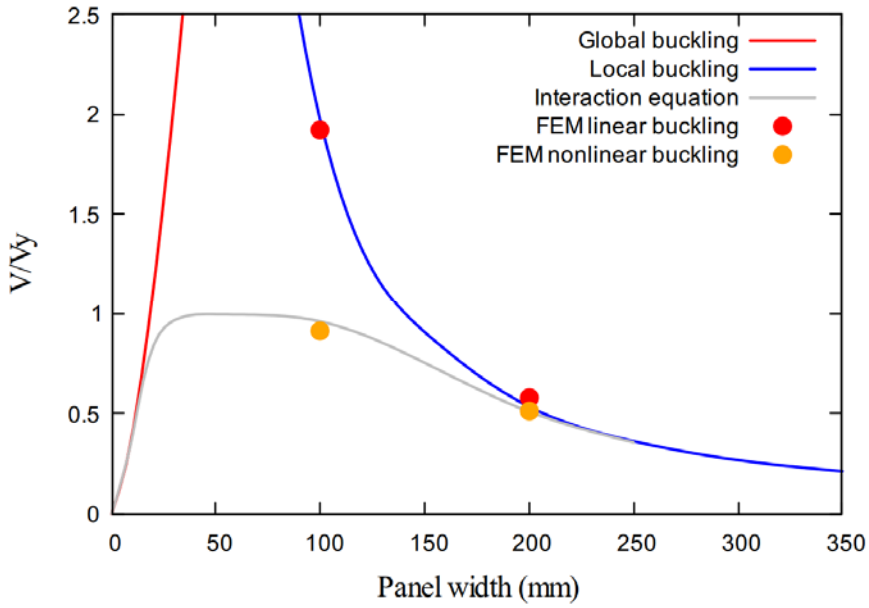

Figure 3-13: Numerical and analytical results based on the replicated models.

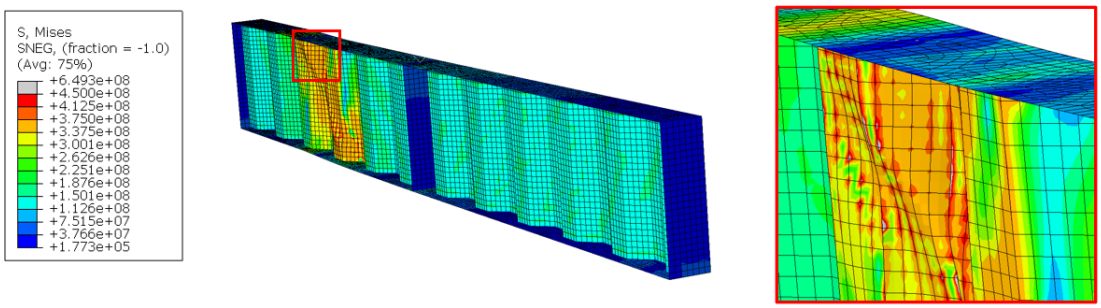

Figure 3-14: Von mises stress contours on the deflected shape for the nonlinear elastic buckling model

Even though the results from the Riks analyses are in good agreement with the theoretical equation developed for interactive shear buckling. The deflected shape depicted in Figure 3-14 is similar to that of a bearing failure as opposed to shear yielding. This verification confirms the capabilities of performing both linear and nonlinear elastic buckling analyses using ABAQUS.

3.4.3 Verification Study 3 - Shuttleworth et al. (2020)

Currently limited research is available in terms of the resistance of shipping container structures in fire. The study performed by Shuttleworth *et al.* (2020) investigated the fire resistance of passively protected shipping container walls with specific focus on insulation.

The primary objective of this study was to develop insulation time reference curves for specifying passive fire protection in accordance with the ISO 834 standard fire curve. This involved using ABAQUS to perform multiple transient heat transfer analyses for a wide spectrum of thermal material properties and side panel configurations.

Stellenbosch University https://scholar.sun.ac.za

3.4.3.1 Methodology

The shipping container thermal properties were taken in accordance with weathering steel as defined in EN 1993-1-2 (2005). Refractive boards generally consist of light weight bulk and refractive materials such as magnesium oxide (MgO), gypsum, vermiculite or calcium-silicate (CaSi). The thermal diffusivity of these refractive materials lies between $2.0 - 3.7 \times 10^{-7}\ \mathrm{m^2/s}$ and therefore a range of $0.5 - 5.0 \times 10^{-7}\ \mathrm{m^2/s}$ was considered. The thermal conductivity was computed by rearranging Equation 2.26 and assuming a volumetric heat capacity of $8.16 \times 10^5\ \mathrm{J/m^3K}$. The thermal conductivity values ranged from $0.041 - 0.408\ \mathrm{W/mK}$ which is typical for fibre insulating board through to gypsum.

As previously mentioned, different refractive board configurations were considered. Refractive board thicknesses of 10 mm were considered either only on the exposed or both exposed and unexposed sides, while multiple layers of the refractive board were also considered. Table 3-5 lists the refractive board thicknesses considered for the different side panel configurations investigated while Figure 3-15 shows a schematic for one of the configurations.

Table 3-5: Refractive panel configurations considered for the heat transfer analysis.

Side panel board configuration	
Exposed refractive board width (mm)	Unexposed refractive board width (mm)
10	10
20	20
30	30
10	20
20	10
10	-
20	-
30	-

Each configuration was created in ABAQUS by the original authors, and the time-dependent behaviour was computed according to Equation 2.27 while all three modes of heat transfer were accounted for in the models. Conductive heat transfer occurred through all the solid components namely container wall, brackets and refractive boards. One useful feature of performing a heat transfer analysis in ABAQUS is that both external and cavity radiation can be included in the model. Convective heat transfer was accounted for onto and off the outer surfaces and within the cavities by using convective heat transfer coefficients as specified by EN 1993-1-2 (2005). The eight side panel configurations as listed in Table 3-5 were considered independently for the range of thermal diffusivities and the insulation fire rating times were determined once the average temperature on the unexposed side increased by 140 ℃.

Stellenbosch University https://scholar.sun.ac.za

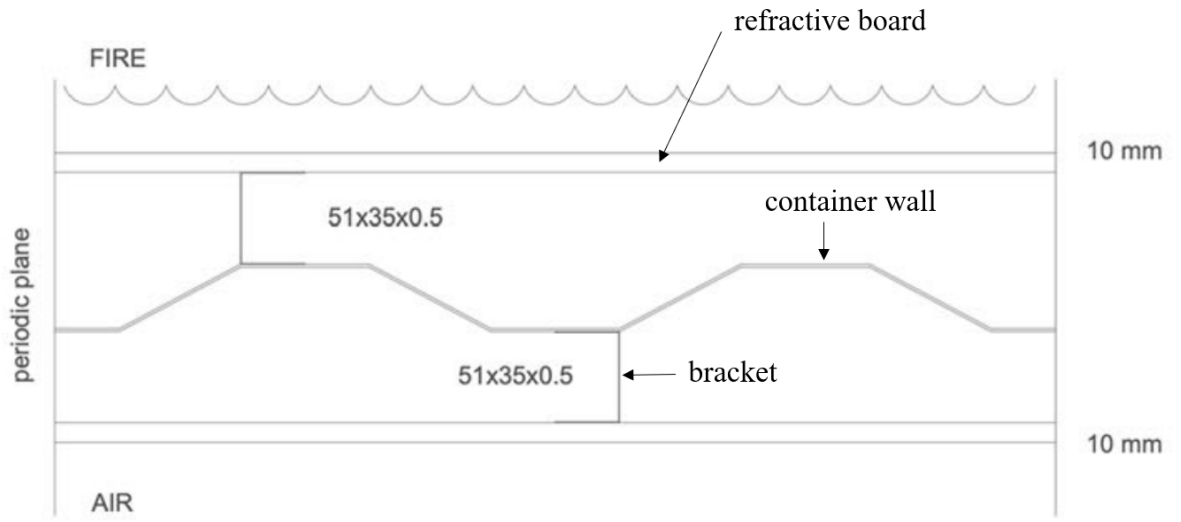

Figure 3-15: Side panel board configuration considering 10mm refractive boards on either side adapted from Shuttleworth et al. (2020).

3.4.3.2 Results

Figure 3-16 shows the temperature distribution for one of the configurations under consideration. The effectiveness of the passive fire protection is clearly visible as the temperature distribution on the unexposed face is reduced significantly.

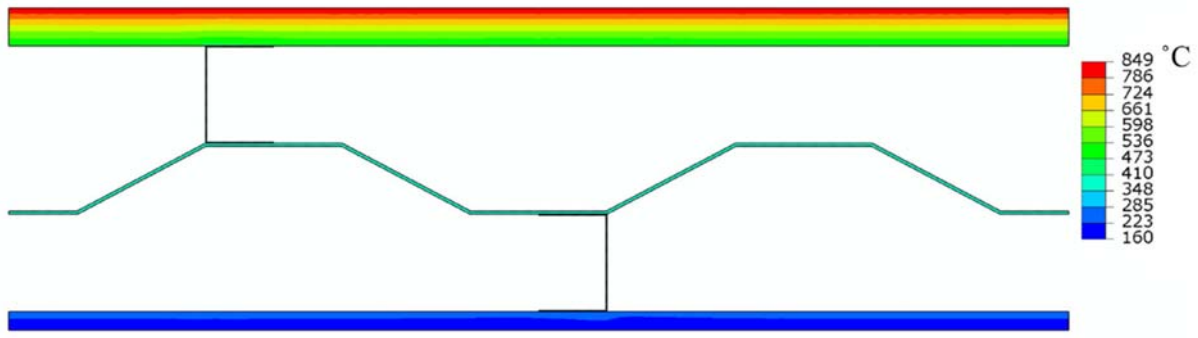

Figure 3-16: Temperature distribution after a 2 hour exposure to the standard fire curve for the configuration consisting of 20 (top) and 10mm (bottom) thick refractive boards having a thermal diffusivity of $4 \times 10^7 m^2/s$ *(Shuttleworth et al., 2020)*

All the models developed by Shuttleworth *et al.* (2020) were similar with respect to the mechanisms of heat transfer applicable, while only the thicknesses of the boards were varied. As a result, it was decided to only replicate one of the reference curves namely the single sided configuration with a 20 mm board thickness.

The reference curves for the single sided board configurations are shown in Figure 3-17. In general, the correlation between the results proposed by the original authors and the replicated model are in good agreement. The insulation time ratings for the replicated models are slightly higher than those proposed by the original authors for low thermal diffusivity values. Even though all of the necessary input parameters are provided by Shuttleworth *et al.* (2020), the

Stellenbosch University https://scholar.sun.ac.za

discrepancy in results is possibly due to the complexity involved in modelling the different modes of heat transfer and the application thereof. The convective heat transfer within the voids for the replicated models was defined based on a uniform sink temperature while it is possible that the original authors defined a sink amplitude instead based on preliminary model results. The reference curves developed are useful in the sense that they can be used to determine the insulation resistance requirement in accordance with the ISO 834 standard fire curve for a wide range of refractive board products on the market. From this study it can be concluded that numerical methods can be used to great effect to better understand the time dependent heat transfer behaviour of salient structural members of the ISO 20 ft shipping container.

Shuttleworth *et al.* (2020) states that steel temperatures of load bearing elements, such as the corner columns, can reach high temperatures if not adequately protected. Even though the capacity of the columns reduces drastically when temperatures exceed 600 °C, the design loads of typical homes or offices are significantly smaller in comparison to the intended design as discussed above. Further research is required to determine the effect that elevated temperatures have on the capacity of load bearing elements which need to satisfy the stability criteria.

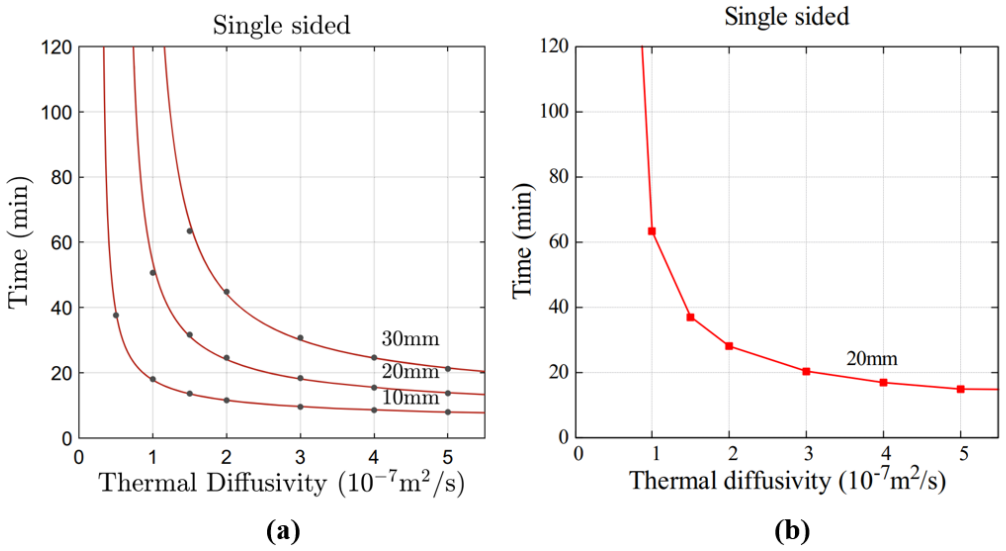

Figure 3-17: (a) Reference curves developed by Shuttleworth et al. (2020), (b) replicated model for a single sided 20mm thick board.

3.5 Conclusions

In this chapter, the 20 ft ISO shipping container was introduced. The geometry of the container was listed as well as the salient features of the shipping container while load transfer according to the original design was discussed. Two modes of weakening were identified for a modified shipping container to be used as a habitable structure. The first mode considers the removal of the corrugated wall which could not only affect the lateral resistance of the shipping container but also the load bearing capacity of the main load bearing elements namely the corner columns. The second mode considers shipping containers stacked perpendicularly on top of one another which results in elements such as the top beams and corrugated wall to carry more load than anticipated based on the original design.

Stellenbosch University https://scholar.sun.ac.za

The results of three verification studies were replicated to determine the suitability of using ABAQUS to further investigate the modes of weakening highlighted previously.

The first study considered the computation of the lateral stiffness of corrugated walls via numerical and analytical methods (Yu and Chen, 2018). The numerical results of the replicated models were within 4% of those proposed by the original authors while the analytical results were also in good agreement.

The second study investigated the shear buckling behaviour of corrugated sidewalls for typical plate girders once again via numerical and analytical models (Sayed-Ahmed *et al.*, 2003). The results of the eigen value buckling analyses for the 100 and 200 mm panel widths coincided with the original authors results as well as the analytical equations for elastic global and local buckling as outlined in Chapter 2. The inclusion of material nonlinearity led to a reduction in capacity of more than 50% for the 100 mm panel width which agreed well with the interaction equation, while the dominant mode of failure for the 200 mm panel width was due to elastic local buckling.

The purpose of the final study was to determine the effectiveness of using ABAQUS to define heat transfer finite element models for structural systems applicable to this work. The study performed by Shuttleworth *et al.* (2020) investigated the insulation fire resistance ratings for passively protected shipping containers. A series of reference curves were developed by the original authors while only one of the configurations were replicated. In general, the results of the replicated model corresponded well with those proposed by the original authors, while the insulation time ratings for low thermal diffusivity values were higher for the replicated models. The discrepancy in results is deemed satisfactory due to the many considerations and complexities involved in modelling heat transfer while further experimental testing is required to validate the results. A thorough understanding of heat transfer modelling was gained, which included convective, conductive and radiative heat transfer parameters.

Stellenbosch University https://scholar.sun.ac.za

4 Finite element analysis at ambient temperature

4.1 Introduction

This Chapter provides a discussion on the development and results of finite element models developed in this thesis to investigate the behaviour of load bearing elements for the 20 ft ISO shipping container specifically at ambient conditions. The finite element models were developed based on the considerations of a weakened container module as outlined in Section 3.3, with modelling approaches as validated in Section 3.4. All models were developed using ABAQUS as discussed in Section 2.9. The following models are provided:

(1) Sensitivity analyses considering various parameters affecting the buckling capacity of the main load bearing elements namely the corner columns of the shipping container.

(2) Side and end wall models to determine the lateral stiffness of the corrugated walls. The stiffness is used to model the lateral restraint along the length of the column as provided by the corrugated side and end wall panels.

(3) Back and front corner column models are proposed based on the findings from the sensitivity analyses to ultimately investigate the change in capacity when the wall panels are present and excluded.

Results for columns with no side sheeting would be representative of a modified shipping container when the entire wall has been removed. In many instances only sections of the wall would be reduced, but assuming no wall contribution to stiffness provides a conservative estimate of capacity. Hence, the results provide an upper and lower bound capacity that engineers can use to assess the suitability of modified containers for applied loads.

The section to follow provides a description on how each finite element model was developed as well as the input parameters considered for the models. A sensitivity analysis is then performed to investigate several parameters which influence the buckling behaviour of the columns. The results of the sensitivity analysis are then used to develop final models to predict the load bearing capacity of the corner columns. Penultimately this chapter compares the results of the finite element models to theoretical principles outlined in previous chapters before concluding remarks are made.

4.2 Development of FE models and input parameters

Several finite element models were developed to investigate the load bearing capacity of the back and front corner columns while Chapter 5 investigates the behaviour of the corrugated wall in the case of a load applied not at the corner columns. Before the development of each finite element model is discussed in the sections below, the chosen material properties and the mechanical behaviour are discussed.

Stellenbosch University https://scholar.sun.ac.za

4.2.1 Material properties

For the finite element analysis to follow, it is important that the material input parameters correspond to the elements of the 20 ft ISO shipping container. According to Speed Spares (2019), all of the salient components as depicted in Table 3-3 consist of weathered steel, also commonly referred to as COR-TEN® steel. EN 10025-5:2019 states that the mechanical properties of COR-TEN steel is comparable to that of structural steel S355. The mechanical properties for the COR-TEN steel are displayed in Table 4-1 below.

Table 4-1: Mechanical properties of weathering steel (Speed Spares, 2019)

Property		
Young's modulus	200	GPa
Poisson's ratio	0.3	-
Yield point	345	MPa
Tensile strength (ultimate strength)	485	MPa
Elongation at ultimate strength	18	%

One advantage of defining a material in ABAQUS is that the stress-strain relationship can be defined to include the effect of elastic and plastic behaviour as needed. An approximation was made in terms of the mechanical behaviour of the material by assuming an idealized model in the form of a bilinear stress-strain relationship as depicted in Figure 4-1. The constitutive relationship for the material model is not drawn to scale so that the regions of elasticity and plasticity are clearly differentiable. Due to the ductile behaviour of steel, rupture beyond the ultimate strength point depicted in Figure 4-1 is not considered and therefore the constitutive relationship adopted in this study is deemed sufficient. For brittle materials, hardening in other regions might lead to higher overall structural resistance which requires cotinuum softening approaches, and reguarisation of continuum description of localisation.

One parameter which is needed for a nonlinear elastic buckling analysis is the plastic strain. The elongation at ultimate strength is used to define the hardening parameter of the plastic component used in the material model. Theoreticlly speaking, the elongation at the ultimate strength as listed in Table 4-1, consists of both elastic and plastic strain as determined during the tensile test. Even though the strain at onset of plastic behaviour is considered negligible relative to the total strain at ultimate strength, the plastic strain was computed by subtracting the elastic strain from the total strain as listed in Table 4-1.

The definiton of the material behaviour is highly dependent on the type of analysis performed. The development of the finite element models discussed in the coming sections state which material properties are included in the various models.

Stellenbosch University https://scholar.sun.ac.za

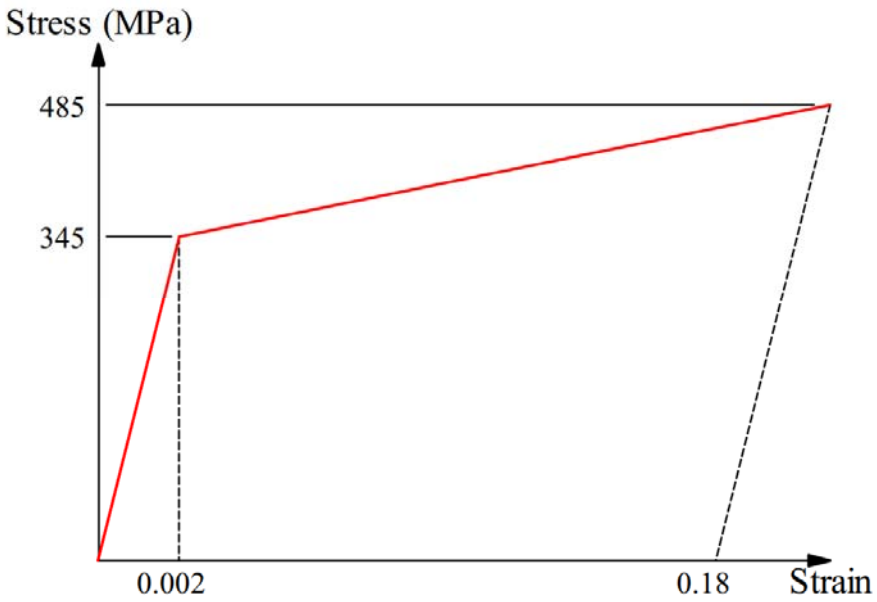

Figure 4-1: Idealized constitutive relationship for weathered steel described by a linear elastic and plastic hardening region (not to scale).

4.2.2 Side and end walls

As highlighted by Yu and Chen (2018) in their study on the rigidity of corrugated plate sidewalls, it is evident that these corrugated walls provide considerable lateral stiffness in modular buildings. The extent to which the side and end walls of the 20 ft ISO shipping container provide lateral restraint, and ultimately dictate the effective length of the corner columns, needs further investigation before proceeding with the modelling of the corner columns. Models have been developed, similarly to those described in Section 3.4.1, by using the geometry of the 20 ft ISO shipping container members as depicted in Table 3-3. Figure 4-2 depicts the geometry of the side wall assembly model as well as the axis system.

Only the elastic stiffness of the corrugated sheeting is considered and therefore shell elements were appropriate. The corrugated sheet, beams, columns and loading blocks were modelled in three-dimensional space using the conventional shell element (S4R). The S4R element has displacement and rotational degrees of freedom as opposed to the continuum shell elements which only have the latter. The material definition included the Young's modulus and Poisson's ratio as discussed in the previous section. The individual parts were connected via tie constraints to simulate the welds used during the manufacturing process of the 20 ft ISO shipping container. The tie constraints were assigned with caution in the assembly module to ensure that each node only belonged to one tie surface thereby avoiding termination during analysis.

Stellenbosch University https://scholar.sun.ac.za

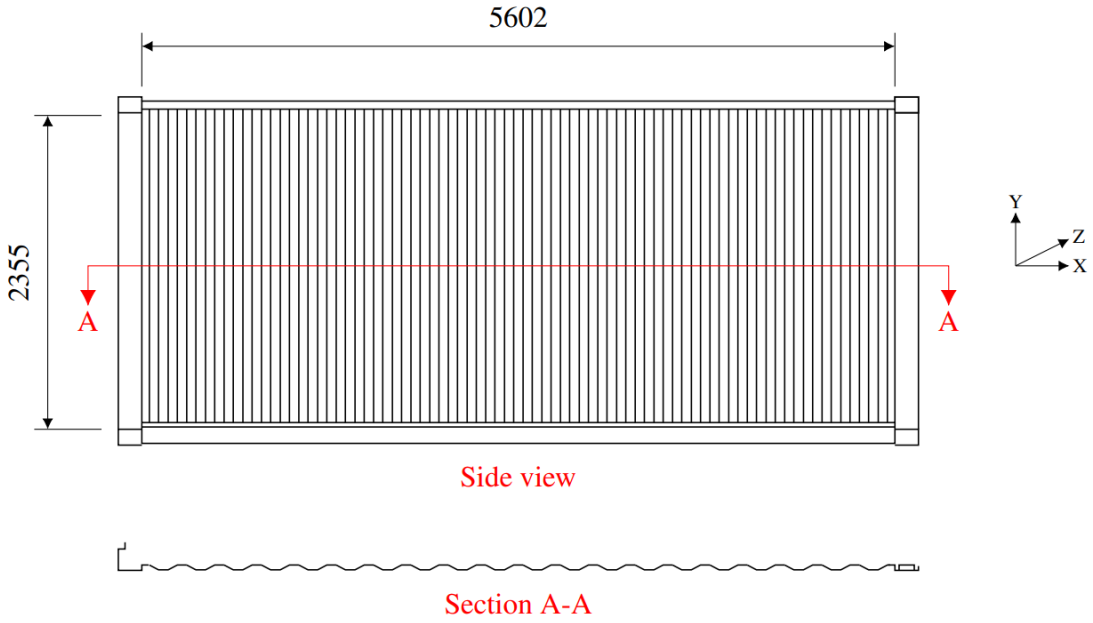

Figure 4-2: Schematic considered for the 20ft ISO shipping container side wall and axis orientation.

The connection between the base beams and the loading blocks are assumed to provide both displacement and rotational restraint while this was modelled accordingly for the sidewall model. The top loading blocks were rotationally restrained in all directions while only out of plane displacement was prevented in the Z-direction. The presence of the rigid floor system meant that displacements in the X and Y directions were restrained along the internal face of the bottom side beam of the wall assembly.

For computing the stiffness of the corrugated sidewall, an assumption regarding the stiffness of the ceiling was needed. For both the side and end wall models it was assumed that the ceiling provided rigidity to such an extent that the top loading blocks and top side beam would deflect as a unit. Based on this assumption, a unit displacement load was applied along the top face of both corner columns as well as the surface of the top beam where the ceiling is welded to.

Due to the relatively complex geometry of the side and end wall assemblies, it was decided to make all instances independent within the assembly module, thereby aiding the meshing process. The dimensions of the members used in the assembly make it challenging to determine the size of each element needed for a finite number of elements along each edge. Without exhaustively seeding the edges by size, it was decided to rather seed the edges of the members by number. As the shear membrane force along the interface between the top side beam and the corrugated web was needed, it was decided to use four and five elements along the flat and inclined folds of the corrugated sheet respectively. Figure 4-3 shows the mesh considered for the side wall numerical model.

Stellenbosch University https://scholar.sun.ac.za

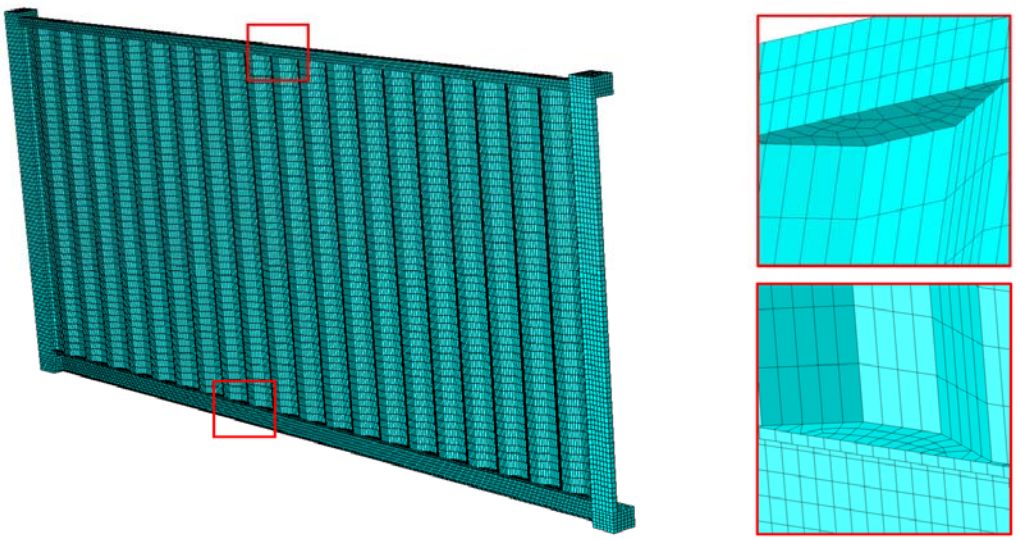

Figure 4-3: Meshing configuration for the side wall.

The type of analysis performed consisted of a static general analysis while geometrically nonlinear effects are automatically included in the analysis. The final step before running the analysis was to create a node set along the interface between the top beam and the corrugated web. The shear membrane force (SF3) of this set was extracted during the post analysis of the results to compute the total shear force acting along the top edge of the corrugated sheet. With both the lateral displacement and shear force known, the elastic lateral stiffness was computed easily.

4.2.3 Corner columns

Two scenarios were considered for each column, where the first model considered the presence of lateral restraint from the sheeting as calculated from the model described in Section 4.2.2, while the second model ignored the presence of the sheeting. To determine the buckling capacity of each scenario it was necessary to perform two analyses, namely a linear elastic buckling analysis followed by a nonlinear elastic buckling analysis. The linear elastic buckling analysis is necessary to determine the buckled shapes of the eigenmodes as well as the critical buckling load. The buckled shape is used as an input parameter for determining the initial geometric imperfections within the model. The nonlinear elastic buckling analysis was performed according to the static Riks method as discussed in Section 2.9.1 by including the geometric nonlinearity. For the linear elastic buckling analysis only the Young's modulus and Poisson's ratio were needed while the complete mechanical behaviour was included in the material definition for the Riks analysis. When defining a nonlinear elastic buckling analysis in ABAQUS, several parameters are needed for the Riks algorithm to be performed. The parameters used for the buckling analyses are listed in Table 4-2.

Stellenbosch University https://scholar.sun.ac.za

Table 4-2: Increment parameters used for Riks analysis.

Parameter	
Maximum number of load increments	100
Minimum increment size	1E-05
Maximum increment size	1E+05
Initial increment size	0.01

The geometric imperfection was incorporated in the model by considering out of straightness and calculated as L/1000, where L is the length of the column (EN 1993-1-5, 2006). EN 1993-1-1 (2005) also suggests that the lowest eigenmode should be scaled by 1/1000 times the member length. To perform the linear and nonlinear elastic buckling analysis, a series of steps were implemented as listed in Appendix B.

The finite element models developed for the back and front corner columns are based on the geometry and dimensions as outlined in Table 3-3. Three-dimensional shell elements (S4R) were chosen to model both columns. For the back corner column only one section was assigned corresponding to the thickness as listed in Table 3-3. The inner part of the front corner column consisted of a pressed channel section having a tapering cross-sectional thickness while the outer part had a constant thickness. A simplification was made by assigning an average thickness of 11 mm to the inner part while a constant thickness of 6 mm was assigned to the outer part.

The sections to follow address the importance of simulating boundary conditions for the buckling analyses. For both corner columns, a rigid body constraint is assigned to the top and bottom faces, thereby simulating the welded connection between the columns and loading blocks. For the back corner column, the presence of the continuously welded sheeting along the column edges was assumed to provide lateral restraint in the X and Z-directions respectively based on the axis convention shown in Figure 4-2. The lateral restraint provided in the Z-direction for the front corner column is slightly different to that of the back corner column due to the presence of the door leaf. The door leaf is attached to the front corner column via three hinges equidistantly spaced along the length of the column. Assuming the door leaves to be closed, the lateral restraint in the Z-direction is then defined at three discrete points as opposed to the full length of the column as is the case for the back corner column.

4.3 Sensitivity analysis

In ABAQUS, there are many different options available for developing a buckling analysis. This section provides a sensitivity analysis on the parameters considered to be relevant for the numerical modelling of the 20 ft ISO shipping container corner columns. The parameters to be discussed in this section are as follows:

1. Mesh configuration

Stellenbosch University https://scholar.sun.ac.za

2. Influence of rounds and fillets
3. Boundary conditions
4. Initial geometric imperfection
5. Number of springs (i.e. how many distinct points the lateral stiffness provided by sheeting is discretized into)

For each parameter investigated it is important that all other parameters and inputs are kept constant while only changing the parameter under consideration. After investigating the influence that these parameters have on the buckling analysis, a final numerical model is proposed for each column.

4.3.1 Mesh configuration

As outlined in Section 2.9, the mesh size and chosen element can influence the accuracy of a finite element analysis. Similarly, to the side and end walls models described in Section 4.2.2, the conventional shell element was used (S4R).

To evaluate the effect of the mesh size, four different mesh sizes were investigated, ranging from 6.25 to 50 mm as shown in Figure 4-4. Each model was meshed by assigning a global seed size to the entire instance. From a finite element modelling perspective, it is important that an optimum mesh size is chosen to ensure accurate results are generated without comprising the computational time. Due to the partition lines created for connecting the corner brackets to the back corner column, the aspect ratio for the coarsest mesh, i.e. 50 mm highlighted elongated elements as opposed to square elements as depicted in the finer meshes considered. It is well known that aspect ratios add additional inaccuracy and therefore other meshing/portioning techniques should be considered or a different choice of element size.

Both a linear and nonlinear elastic buckling analysis were performed while imperfections were included in the models according to EN 1993-1-5 (2006) as discussed previously. The ends of the columns were considered fixed for all models developed for the mesh configuration sensitivity analysis.

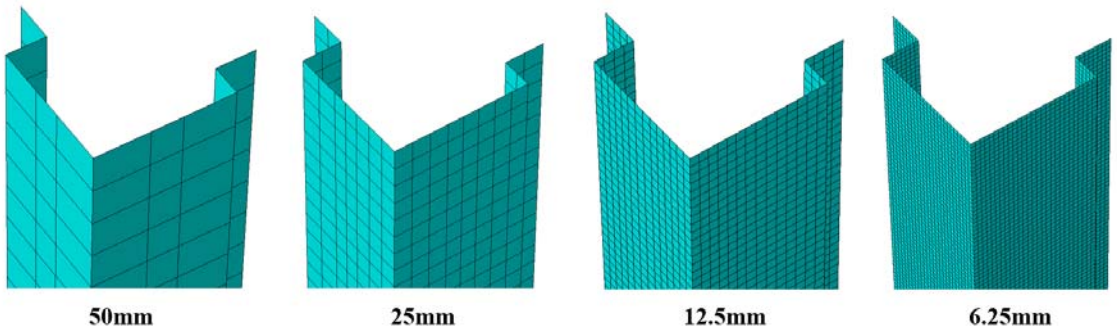

Figure 4-4: Mesh sizes considered for the back corner column.

From the results as depicted in Figure 4-5, it is evident that an increase in the number of

Stellenbosch University https://scholar.sun.ac.za

discretized elements results in convergence for the corner column capacities. The increase in capacity between an element size of 25 and 12.5 mm is less than 5% while an increase of less than 1% is observed between elements having a size of 12.5 and 6.25 mm. A significant increase in computational time occurred between the models consisting of 12.5 and 6.25 mm sized elements. For the eigenvalue buckling analysis, the computational time for the 25 and 12.5 mm sized elements were 15 and 30 seconds respectively while the model discretized into 6.25 mm sized elements took 130 seconds to complete.

Based on the analyses, it can be concluded that by discretising the models into elements with a size of 12.5 mm provides accurate results. The remainder of the sensitivity analysis will only consider meshes with element sizes of 12.5 mm.

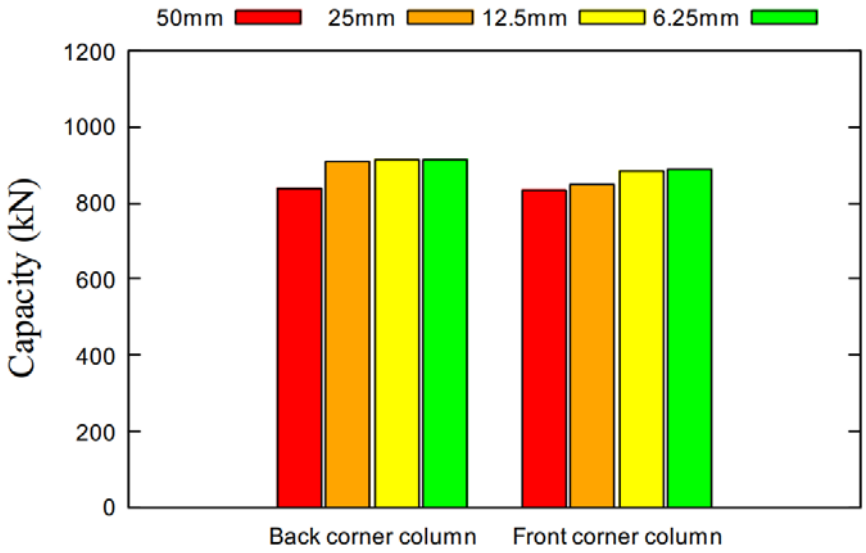

Figure 4-5: Capacities for different mesh sizes.

4.3.2 Influence of rounds and fillets

A study performed by Sadowski & Rotter (2013) investigated the global buckling behaviour of solid and shell elements used to model cylindrical tubes. One issue with shell elements is that the analysis becomes increasingly uncertain when the ratio between the radius of curvature and the thickness of the section become smaller. With respect to the back and front corner columns, a simplification was made in terms of the geometry where the rounds and fillets were neglected as depicted in Figure 4-6.

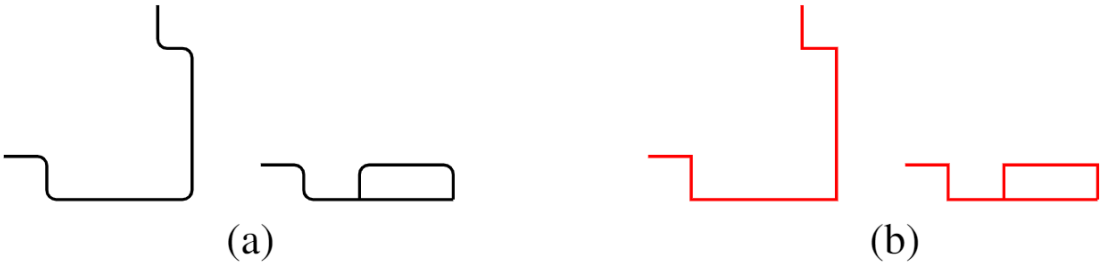

Figure 4-6: Cross-sections of corner columns showing the (a) real sections, and (b) simplified sections, with the

Stellenbosch University https://scholar.sun.ac.za

back corner and front corner columns on the left and right sides respectively.

Further studies have also shown that omission of rounds and fillets can influence the torsional resistance of channel sections by more than 10% (Seaburg and Carter, 2003). As a result of this, it is sometimes necessary to use solid elements instead of shell elements so that rounds and fillets can be modelled correctly.

To investigate the effect of the rounds and fillets on the buckling capacity of the columns, two models were created for each column based off the real and simplified geometries using conventional shell elements. Like the previous models, both columns were fixed at their ends while linear and nonlinear elastic buckling analyses were performed.

Figure 4-7 shows the results for the nonlinear elastic buckling analysis. The simplified sections correspond to a higher capacity than those including the rounding. The reason for this is mainly attributed to the fact that the simplified sections have a slightly higher torsional stiffness than the real sections. Another interesting observation is the higher discrepancy of the capacity between the real and simplified sections for the back corner column as opposed to the front corner column. For the back corner column, the capacity of the simplified section was 11% greater than the real geometry. For the front corner column, a difference of only 3% was observed between the different sections.

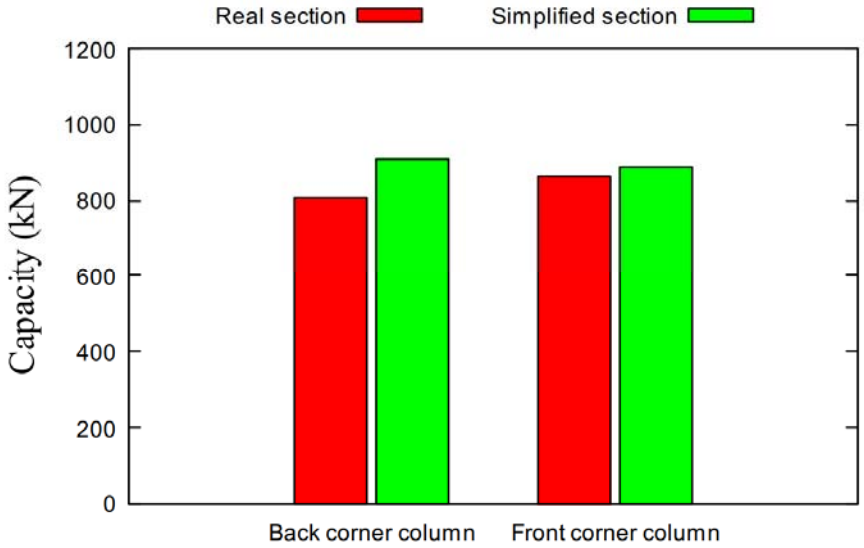

Figure 4-7: Capacities for the real and simplified sections.

Figure 4-8 shows the buckled shapes for the back and front corner columns during post analysis of the results. The deflected shape of the back corner column showed local buckling failure while global buckling about the weak axis was observed for the front corner column. Based on this observation, it is evident that rounds and fillets should be included in the geometry for the numerical modeling of columns prone to local buckling such as the back corner column of the 20 ft ISO shipping container.

Stellenbosch University https://scholar.sun.ac.za

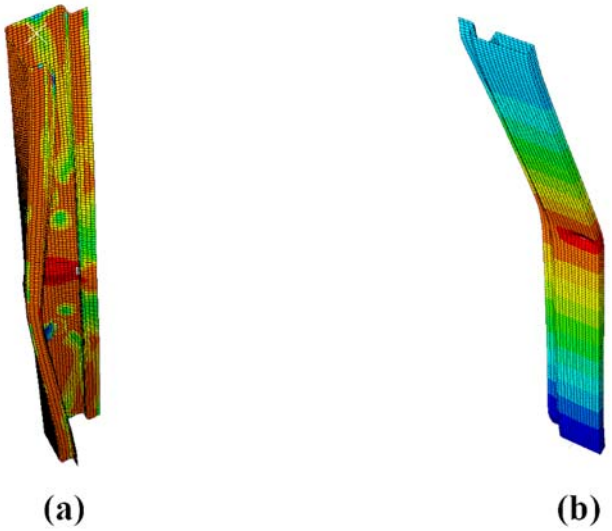

Figure 4-8: Buckled shapes for Riks analysis (a) back corner column and (b) front corner column.

4.3.3 Boundary conditions

Simulating boundary conditions for buckling behaviour is an important part of the analyses as it can have a significant impact on the buckling capacity of the columns. A study performed by Eröz *et al.* (2008) on the buckling behaviour of partially fixed base columns highlighted the fact that the assumption of fully fixed or pinned ends can lead to inaccurate results. Usually, the end conditions of the column are somewhere between these two extremes. The end conditions can be modelled with reasonable accuracy by using springs to model both the axial and rotational stiffness. For the top and bottom end conditions, the beams were fixed at the remote ends due to the welded connection between the loading block and the beam. Equations 4.1 and 4.2 are used to compute the axial and rotational stiffness of the top and bottom beams respectively.

$$K_A = AE/L \quad (4.1)$$

$$K_R = 4EI/L \quad (4.2)$$

where:

K_A	=	equivalent axial stiffness
K_R	=	equivalent rotational stiffness
E	=	Young's modulus
I	=	moment of inertia
L	=	length of beam

To study the effect of the boundary conditions on the capacity of the corner columns, three different cases were considered. The first set of models considered the ends of the columns to be fixed, thereby permitting no rotation or lateral displacement at the ends, while the second set of models only provided lateral restraint thereby simulating a perfectly pinned connection. The final set of models considered the ends of the columns to be somewhere between those of

Stellenbosch University https://scholar.sun.ac.za

fully fixed and pinned by modelling the axial and rotational stiffness provided by the beams as springs according to Equation 4.1 and 4.2. Figure 4-9 shows the results of the nonlinear elastic buckling analysis for the three end conditions considered.

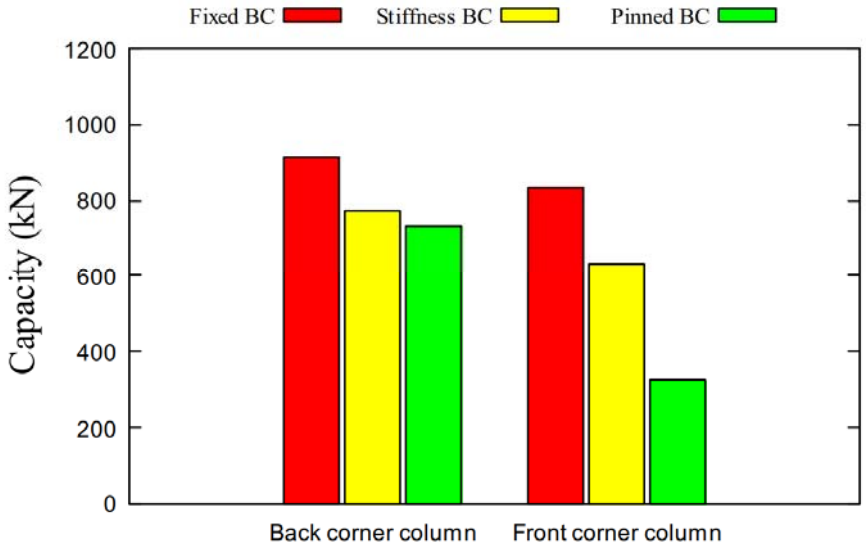

Figure 4-9: Predicted column capacities for the different boundary end conditions.

As expected, the capacity for both columns decrease as the rotational restraint at the ends decrease. The front corner column is particularly sensitive to the end conditions in comparison to the back corner column where a reduction of 61 and 20% occurred respectively, as the end conditions changed from fixed to pinned. In the previous discussion, it was stated that sections susceptible to local buckling should not be simplified in terms of geometry and that rounds and fillets should be included. Ismail and Hesham (2015) investigated local buckling of steel I-section beams and columns and found that the end conditions of the beams and columns do not influence local buckling behaviour. Based on the literature, global buckling behaviour was found to be dependent on the slenderness ratio of the column while local buckling depends on the ratio of flange and web heights to their corresponding section thicknesses.

The deflected shape and type of buckling as discussed in the previous section agree well with the trend in capacities as shown in Figure 4-9. Even though local buckling is independent on the global boundary conditions, the capacity of the back corner column still decreases with a reduction in rotational restraint. A possible reason for this is the occurrence of an interactive buckling failure somewhere between global and local buckling meaning that the back corner column will be slightly sensitive with respect to the end conditions.

The capacities determined based on the axial and rotational stiffnesses are conservative. The rotational stiffness provided by the top and bottom beams were determined solely on the cross-sectional geometry of the beams while it could be argued that the rigid floor system provides additional restraint. Similarly, the in plane rotational stiffness of the top beams were assumed to be unaffected by the presence of the corrugated ceiling. The numerical models developed up until now have not included lateral restraint from the side and end walls which could possibly increase the capacity of the columns. The extent to which the side and end walls provide lateral

Stellenbosch University https://scholar.sun.ac.za

restraint is one of the main objectives of this thesis and is discussed further in the coming sections.

4.3.4 Initial geometric imperfection

The concept of geometric and mechanical imperfections for steel columns was introduced in Section 2.3.2. The approach outlined in EN 1993-1-1 (2005) was applied in the previous numerical models as discussed in Section 4.3.1-4.3.3 by using 1/1000 times the member length for sinusoidal imperfections.

The inclusion of mechanical imperfections, namely residual stresses in numerical models, is still a topic of research due to a lack of reliable data. As a result, residual stresses are often neglected altogether within finite element models. Schafer and Peköz (1996) suggest modifying the stress-strain relationship of a material in an attempt to model the effect of residual stresses. The Eurocode states that residual stresses may be accounted for by including a stress pattern from the fabrication process with amplitudes equivalent to the mean values (Nemer and Papp, 2021). Unfortunately, due to the welded nature of the corner columns, it is near impossible to consider different patterns of welded residual stresses. Subsequently examining existing data, and the lack thereof, it is evident that there is a difficulty in understanding the magnitude and distribution of residual stresses and therefore only geometric imperfections are considered further in this study. The aim of the numerical models described below are to investigate the sensitivity of the magnitude of the imperfection and the mode of buckling or shape of the imperfection according to the traditional approach as applied in this work.

A series of numerical models were developed for both corner columns using different values of initial central deflection. The basic problem assumed a value of L/1000 while three additional values were chosen, namely L/∞ (i.e. 0mm), L/500 and L/250. In addition to varying the magnitude of the imperfection, the capacities were also determined for the 1st, 2nd, and 3rd eigen modes for a constant imperfection thereby resulting in twelve numerical models developed for each column. The end conditions for all columns were once again considered to be fully fixed.

The results for the back and front corner columns are shown in Figure 4-10 and Figure 4-11 respectively. The results of the numerical models are in good agreement with the imperfection model proposed by EN 1993-1-1 (2005). For both the back and front corner columns, the most conservative capacity is determined based on the lowest bifurcation mode. As expected, a reduction in capacity occurs for an increase in the magnitude of the imperfection. If an imperfection of L/250 is considered in conjunction with the deflected shape of the first eigen mode, the capacity of the back and front corner columns reduces by 30 and 37% respectively relative to a perfectly straight column. Even though an imperfection equal to L/250 times the member length results in the most unfavourable capacity, Nseir *et al.* (2016) suggests that such high imperfections are unrealistic and too severe to be adopted in finite element models. The imperfection model proposed by the Eurocode is considered sufficient for the work to follow.

Stellenbosch University https://scholar.sun.ac.za

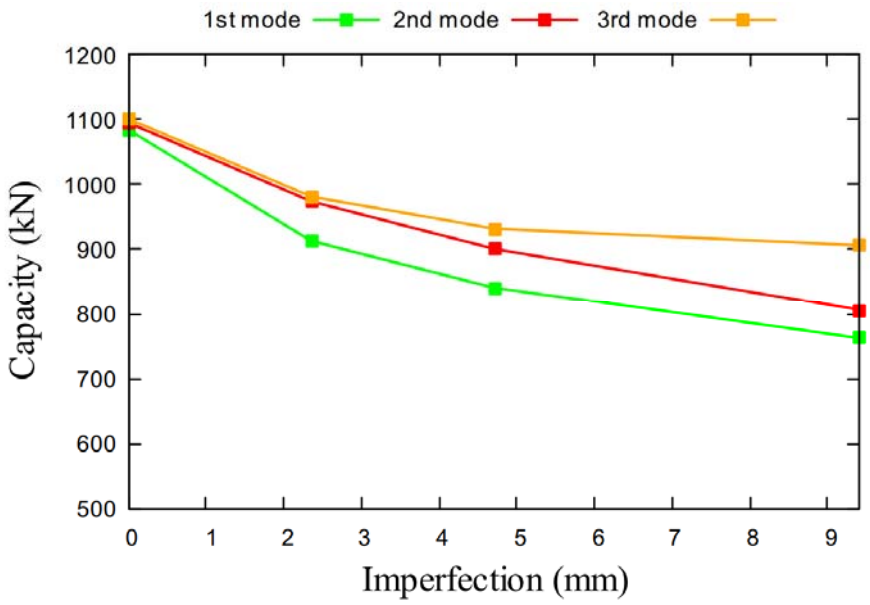

Figure 4-10: Variation in capacity for the back corner column due to geometric imperfections.

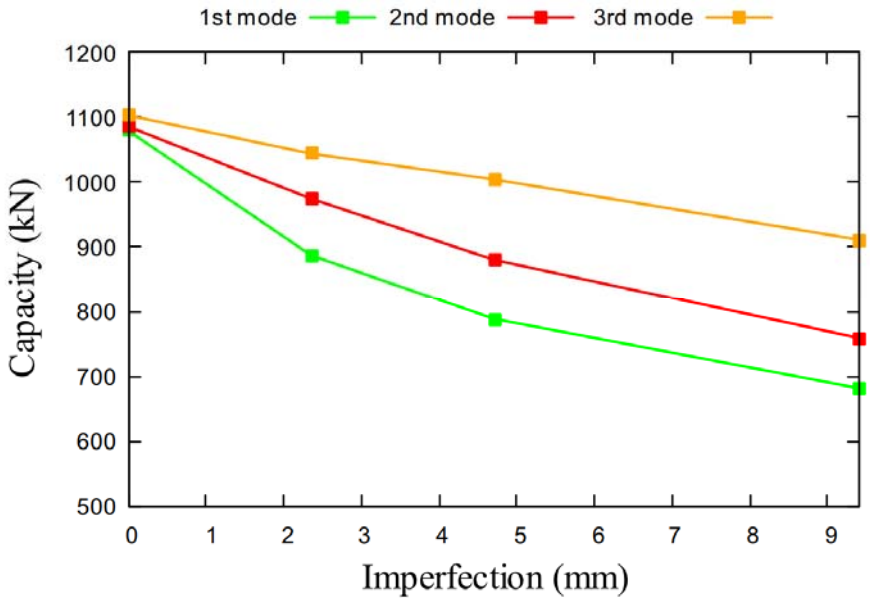

Figure 4-11: Variation in capacity for the front corner column due to geometric imperfections.

4.3.5 Number of springs

Section 4.2.2 described the numerical models developed to determine the lateral stiffness of the side and end walls of the 20 ft ISO shipping container. To simulate the lateral restraint of the side and end walls on the corner columns, it is necessary to incorporate this stiffness into the buckling analyses.

As seen in Section 4.3.3, ABAQUS allows for both axial and rotational stiffness to be modelled for idealised structural components. When defining a spring in ABAQUS, a discrete point needs to be selected while the option for selecting an edge of a face is vacant. This poses a certain challenge with regard to the finite element modelling as the corrugated side and end

Stellenbosch University https://scholar.sun.ac.za

walls are welded continuously along the entire length of the columns. At best it was decided to model the lateral stiffness of the corrugated sheet via a series of springs defined at discrete points along the edges of the column. The purpose of the finite element models described below was to find a suitable number of springs to which the capacity of the columns converged.

A constant lateral stiffness of 100 kN/mm was considered for both the side and end walls. This value is in the same order of magnitude as those determined in the first verification study while the actual computed lateral stiffness of the corrugated wall is applied in the final models. This stiffness was divided by the number of springs chosen for the sensitivity analysis namely 2, 4, 10 and 20. Figure 4-12 below shows the spring interactions modelled in ABAQUS for the back corner column.

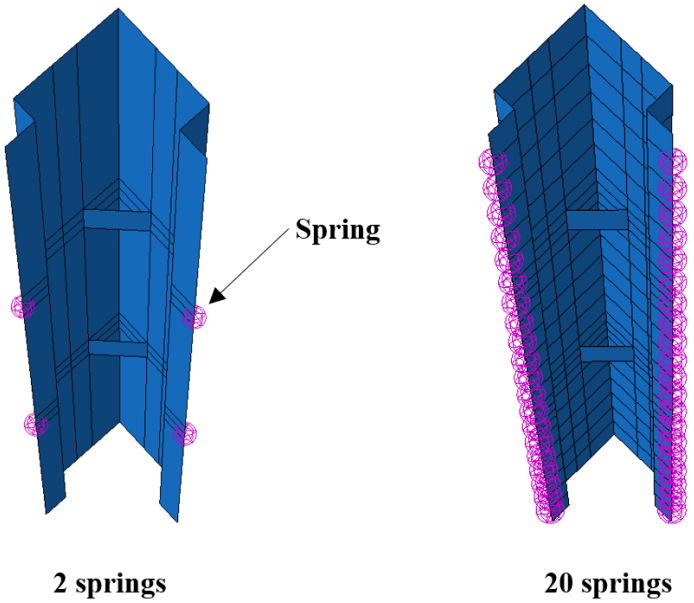

Figure 4-12: Spring interactions modelled to simulate the lateral stiffness of the corrugated wall sheeting.

The ends of the columns were once again considered to be fully fixed. Figure 4-13 shows the results for the analyses performed. The capacity of the back and front corner columns increased by 3 and 5% when the number of springs increased from 4 to 20. Even though negligible increase in capacity occurs between 10 and 20 springs, the possibility of local buckling in combination with plastic yielding between springs needs to be minimised. The computational time was found to be independent on the number of springs thereby providing the user a certain degree of freedom when deciding on the number of springs to be used in the models.

Stellenbosch University https://scholar.sun.ac.za

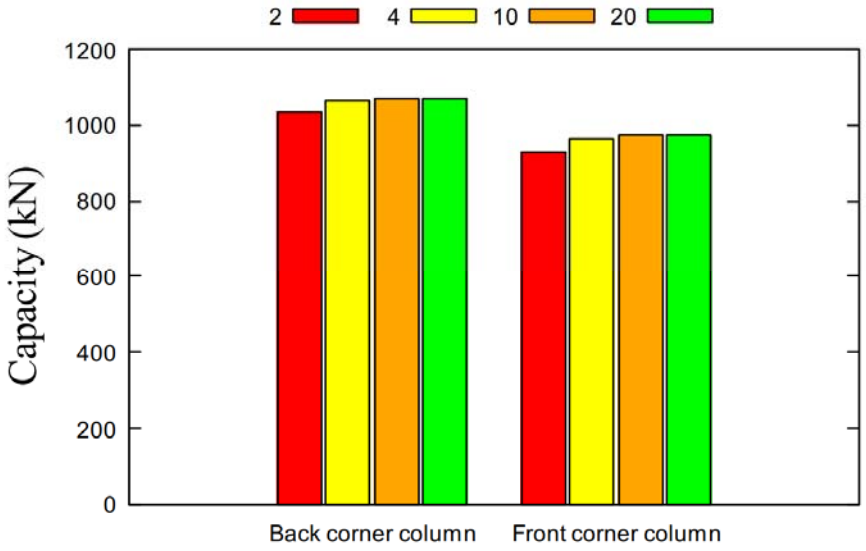

Figure 4-13: Capacities of the convergence study for simulating the continuous welded sheet along the length of the columns.

4.4 Finite element model results

Section 4.2 provided a discussion on the development of a numerical model to predict (a) the lateral stiffness of wall panels, and (b) the buckling capacity for the corner columns of the 20 ft ISO shipping container. In this section, the buckling capacity models based on the findings in Section 4.3 are proposed for the two scenarios as defined in Section 4.2.3, namely when the corrugated sheeting is present as well as the case when it is excluded.

The numerical results are compared to those proposed by analytical formulae as discussed in the literature and ISO 668 (1995) which specifies the performance requirements of shipping containers.

4.4.1 Calculation of wall stiffness

Discussions regarding the numerical procedure followed to perform the necessary buckling analyses have already been discussed in previous sections. The focus of this section is to describe the final models developed based on the findings from the sensitivity analysis. The lateral stiffness of the side and end walls computed from the numerical model, as described in Section 4.2.2, have values of 289 and 75 kN/mm respectively.

The lateral stiffness was computed according to the analytical method proposed by Yu and Chen (2018) by calculating the strain due pure shear deformation and the linear shear distortion twist as discussed in Section 3.4.1.1.

In general, the results between the numerical and analytical models as depicted in Figure 4-14 are in good agreement with one another. The analytical prediction for the lateral stiffness of the end wall is 20% lower than the numerical value while a decrease of only 2% is observed for the side wall. For the side wall, pure shear strain contributed to 81% of the total shear induced strain as opposed to 54% for the end wall. Based on these results, the conservative

Stellenbosch University https://scholar.sun.ac.za

value for lateral stiffness predicted according to the analytical model for the end wall shear stiffness is likely due to an overprediction of the shear strain because of the shear distortion affect.

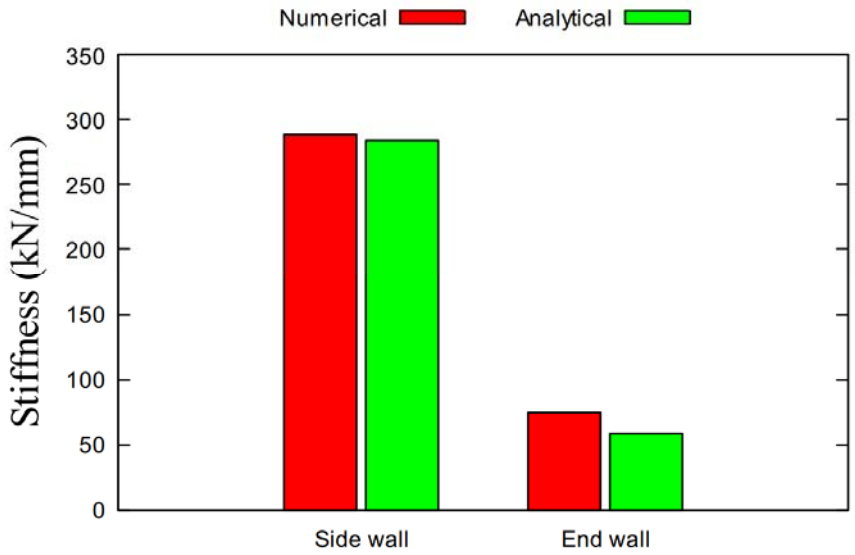

Figure 4-14: Numerical and analytical results for the lateral stiffness of the side and end walls.

4.4.2 Application of wall stiffness results to the column capacity models

Even though a discrepancy is present between the numerical and analytical results for the end wall panel, the theoretical formulae are still considered useful for computing the shear stiffness of corrugated wall panels subjected to lateral loads. The shear stiffness of the side and end walls, as computed from the numerical models, is incorporated into the models for compressive capacity by using 20 springs along the edges of the columns as discussed previously. Each corrugated panel is assumed to provide in plane lateral stiffness only and therefore rotational stiffness is neglected. As previously mentioned, the lateral stiffness of the end wall is not applicable to the front corner column due to the presence of the door leaf. The lateral restraint provided by the door leaf was modelled by creating 3 boundary conditions at the positions of the hinges where displacement in the Z-direction was fixed according to the axis system in Figure 4-2. The boundary conditions and interactions, i.e. springs considered for modelling the wall stiffness are depicted in Figure 4-15.

Stellenbosch University https://scholar.sun.ac.za

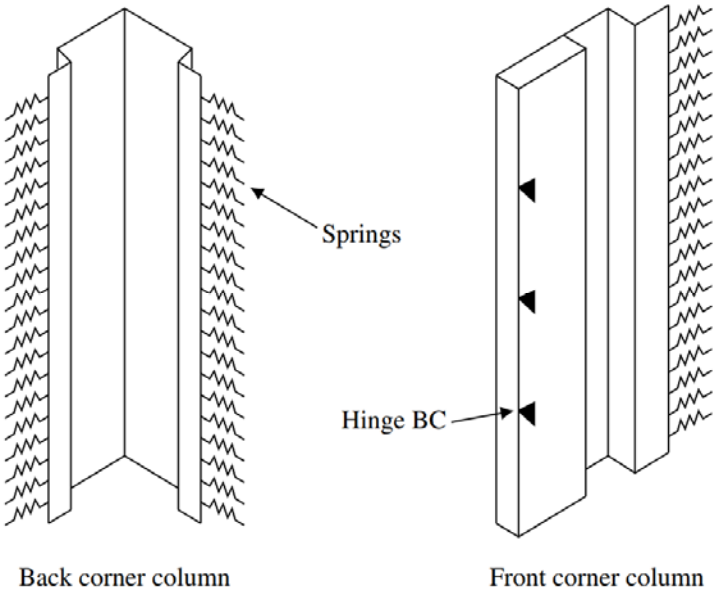

Figure 4-15: Boundary conditions and interactions considered for the proposed models.

Both corner columns were modelled by including the rounds and fillets to account for possible local buckling even though the front corner column was insensitive to this parameter. As discussed previously, a discretised mesh consisting of 12.5 mm sized elements provided accurate results and is therefore implemented in the proposed models. The boundary conditions for the proposed models include the axial and rotational stiffness of the top and bottom beams as discussed in Section 4.3.3 and are depicted in Figure 4-16. The models developed for the so-called weakened corner columns are the same as those described above except that the lateral stiffness provided by the wall panels were neglected.

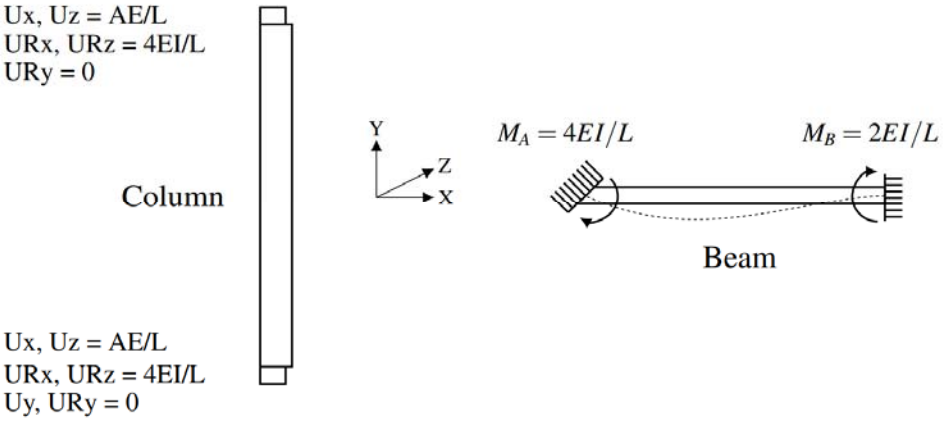

Figure 4-16: End boundary conditions considered for the proposed models.

4.4.3 Capacity of corner columns

The proposed model described in the preceding section was implemented according to the methodology outlined in Section 4.2.3 and Appendix B. Figure 4-17 shows the comparison between the capacities of the corner columns when the corrugated wall panels are included and excluded in the analysis. As introduced above, the case with no wall panel represents a

Stellenbosch University https://scholar.sun.ac.za

modified shipping container where the entire side wall has been removed.

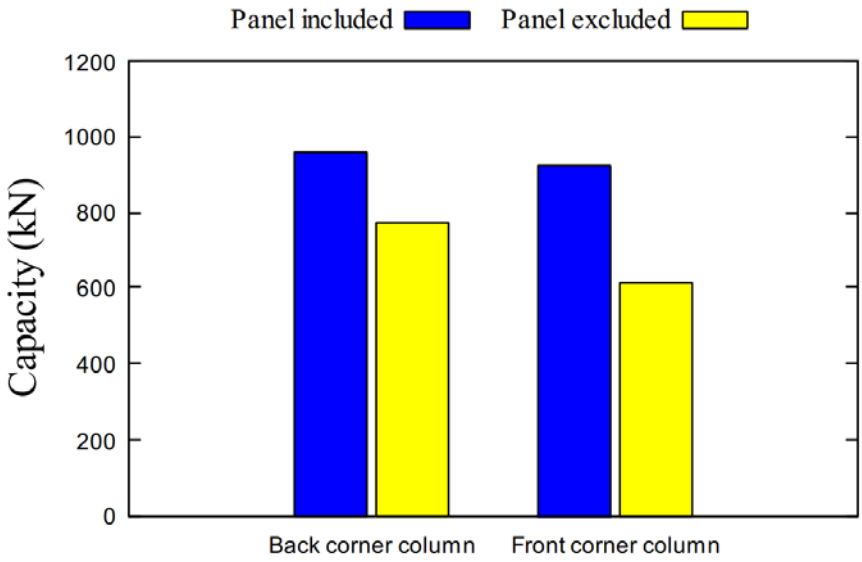

Figure 4-17: Column capacities for the proposed numerical models when the side wall panels are present or excluded.

For both the front and back corner columns, a reduction in capacity was observed when the lateral restraint from the side and end walls was removed. The capacity of the back corner column reduces from 958 to 772 kN corresponding to a 20% reduction, while the capacity of the front corner column reduced by 34% as the capacity dropped from 923 to 614 kN. The reduction in capacity highlights the fact that there is a degree of slenderness with respect to both columns and that the capacity is not merely governed by material yielding, as is the case for a perfect short column, as discussed in the literature. The relative reduction in capacities for the columns are different as the front corner column experiences a more significant drop in capacity. Based on the findings from the sensitivity analysis, it was concluded that the capacity of the front corner column is sensitive to the end conditions due to global buckling occurring about the weak axis. It is possible that global buckling behaviour is more sensitive to the restraint provided by the continuously welded sheet as opposed to local buckling which is less sensitive to the effective length of the column. This appears correct seeing that the back corner column is more susceptible to local buckling and therefore a less severe reduction in capacity occurred.

In Section 3.2, the maximum compressive force for a 20 ft ISO shipping container was listed as 4117 kN according to experimental testing done by ISO 668 (1995). Table 4-3 shows the capacities computed by summing the individual capacities of the corner column for the numerical results. The weight of one container is also listed which includes the own weight of the container as well as an imposed load of 3 kPa as discussed in Chapter 3. The compressive resistance is found to be 3762 kN for the case when the panels are included. Even though this value is 8.6% smaller than the capacity provided by ISO 668 (1995) it is still in good agreement with ISO standards. If lateral loads are ignored, the capacity of a shipping container when the corrugated wall panels are present and excluded are equivalent to 29 and 21 times the modified design load of an individual container unit based on load combinations according to EN

Stellenbosch University https://scholar.sun.ac.za

1990:2002+A1 (2011). Due to the significantly smaller imposed loads within a habitable container structure in relation to a unit containing cargo, the number of units which can be stacked on top of one another is significantly higher. The results give a good indication as to how high these modular structures can be built.

Table 4-3: Capacities according to standards and numerical models developed in this work.

ISO standard (kN)	Numerical - including wall panel (kN)	Numerical - excluding wall panel (kN)	Characteristic weight of one habitable container unit (kN)
4117	3762	2772	90.4

Furthermore, it is currently assumed that wall panels carry no vertical load, whereas in full-scale testing it is likely that the steel sheeting in the immediate vicinity of the columns will contribute to load capacity. Assuming the loads from above are evenly distributed to the four corner columns for a given container, it would seem reasonable that the capacity differential between the back and front corner columns is small. Based on the results depicted in Figure 4-17, it is evident that the capacities for the back and front corner columns are nearly identical for the case when the corrugated panel is included. A larger differential is present for the case when the corrugated panel is excluded due to the difference in buckling behaviour as discussed previously.

A comparison between the numerical and analytical results are shown in Figure 4-18. The theoretical buckling capacities were determined according to Equation 2.8 as discussed in the literature. The theoretical formula considers the effective length of a column which is typically dependent on the end conditions. To remain consistent with this, it was decided to only compare the analytically predicted values with the numerical models where the sheeting is excluded. The effective lengths of the columns were taken to be half of the overall length about all three axes due to the high axial and rotational stiffness provided by the floor and ceiling system. The analytical model predicts values like the numerical models, with results ranging between 8-13%. Geometrical imperfections are not accounted for in the theoretical formulae which could be a possible reason for the slightly higher analytical capacities predicted. The presence of the corrugated sheeting does influence the effective length of the column as highlighted in Figure 4-17 but suitable effective length factors are to be determined before the analytical formulation is used to predict the capacities of such columns.

Stellenbosch University https://scholar.sun.ac.za

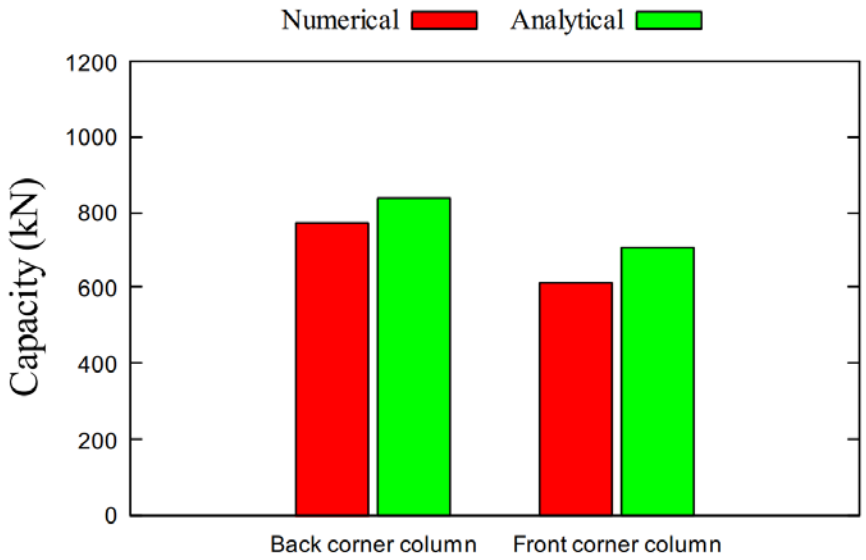

Figure 4-18: Numerical and analytical column capacities when side panels are excluded from analyses.

The maximum compressive force of the 20 ft ISO shipping container is 2772 kN according to the numerical models when the panels are excluded, in comparison to the analytical models with a capacity of 3092 kN. The former corresponds to a 26% reduction in load bearing capacity due to the removal of the side sheeting.

Initially this might seem like a drastic reduction in the load bearing capacity of the container unit. However, accompanying this reduction is a significantly smaller imposed load due to the change in purpose of the unit. The payload capacity for an unmodified 20 ft ISO shipping container is 299 kN according to ISO 668 (1995). It is reasonable to assume the payload capacity to be unaffected when the corrugated side and end walls of the container unit are removed as the load within the container is carried entirely by the rigid floor system as discussed in Section 3.2. According to the literature a maximum value of 14 kN/m^2 is often assumed for the floor load of a 20 ft ISO shipping container, however this value can vary (GDV, 2021). Even though the compressive capacities of the columns reduce when the corrugated walls are removed, the smaller imposed load more than compensates for this reduction in most instances.

4.5 Conclusions

Several models were developed in this section to investigate the influence that the corrugated side and end walls have on the buckling capacity of the corner columns. Initially a finite element model was developed to predict the lateral stiffness of the side and end walls which was then incorporated into numerical models for determining the buckling capacity of the columns. The results of the numerical models were verified by theoretical formulae as discussed in the literature.

The lateral stiffness of the side and end walls were determined by using ABAQUS, similarly to the models developed by Yu and Chen (2018), as discussed in Section 3.4.1. The lateral stiffness of the side wall as predicted from the numerical results were in good agreement with

Stellenbosch University https://scholar.sun.ac.za

the theoretically predicted values. A differential of 20% was observed between the stiffness predicted by the numerical and analytical models for the end wall. The reason for this variance is uncertain although the shear strain due to distortion for the end wall contributed significantly more to the total shear strain as opposed to the side wall according to the analytical results.

Before proposing numerical models for the corner columns, a sensitivity analysis was performed on parameters specifically applicable to the buckling analysis performed in ABAQUS. These parameters included mesh size, influence of corner rounds and fillets, boundary end conditions, initial geometric imperfection and the number of springs needed to simulate the presence of the continuously welded corrugated sheet. A mesh size of 12.5 mm led to converging results while local buckling behaviour was sensitive to the inclusion of the rounds and fillets. The capacity of the front corner column was sensitive to the end constraints as the capacity decreased significantly from fully fixed to pin ended conditions. The buckled shape of the front corner column showed dominant weak axis global buckling while the back corner column was not as susceptible to the boundary end conditions due to evident local buckling. Furthermore, the geometric imperfection model proposed by the Eurocode was considered sufficient based on the results of the sensitivity analysis.

The proposed numerical models were developed based on the findings from the sensitivity analysis. The buckling capacity of the back and front corner columns reduce by 24 and 50% respectively when the side and end walls of the container unit are removed. It can therefore be concluded that the corrugated side and end walls not only provide lateral rigidity as was shown by Yu and Chen (2018), but they also play a role in strengthening the load bearing elements. The numerical results of the weakened columns were in good agreement with the analytical formulation as outlined in the literature, while further research is needed to determine suitable effective lengths for columns supported along their entire edge.

The corrugated side and end walls of the shipping container not only provide significant resistance with regard to horizontal loading but also affect the load bearing capacity of the main load bearing elements namely the corner columns. It is crucial that bracing elements are installed when side and end walls are removed so that adequate lateral rigidity is still provided to resist horizontal loading. According to the results of the numerical models, the capacity of a 20 ft ISO shipping container when the sheeting is present and excluded respectively is equal to 29 and 21 times the modified design load for civilian use of an individual 20 ft unit. The results are promising and support the idea of using shipping container units for multistorey modular construction. Further understanding of such structures is necessary while the knowledge gained from this chapter will be used to investigate the performance of the corner columns at elevated temperatures in Chapter 6.

Stellenbosch University https://scholar.sun.ac.za

5 Finite element analysis for different load paths

5.1 Introduction

In Section 2.4, corrugated plates and their innovative use in structural engineering were introduced. Corrugated web plates used in steel shear walls provide a great deal of axial and out-of-plane stiffness along the direction parallel to the corrugations, while the out-of-plane stiffness in the direction perpendicular to the corrugations is negligible (Faegh and Fanaie, 2018). Corrugated webs do not carry significant longitudinal stresses, and therefore the bending moment can be assumed to be carried totally by the flanges while the web only resists shear stresses. One of the main advantages of using corrugated panels, as opposed to flat panels, is the increase in shear buckling strength. Even though various theoretical derivations exist for determining the shear buckling capacity of corrugated steel plates utilised in the webs of plate girders, the accuracy and reliability of these formulae are uncertain when used for corrugated steel plate shear walls. The verification study investigated in Section 3.4.2 showed that theoretical equations can be used to great effect if the buckling behaviour is governed by elastic local or global buckling. Further studies performed by Driver *et al.* (2006) highlight that theoretical equations overestimate the shear buckling capacity due to factors not captured in the formulation such as initial web imperfections.

As discussed previously, one of the concerns with regard to modular construction is the change in load paths due to different stacking configurations. The aim of this section is to predict the capacity of the corrugated side wall of the 20 ft ISO shipping container due to loads applied to the support beams of the containers rather than at the corner columns. This chapter includes a discussion on the development of the finite element models followed by the numerical and theoretical results. It is shown that there is significantly reduced capacity when loads are applied at the midspan of containers relative to the corners, although capacity will still typically be sufficient for low-rise buildings. Details are proposed for how structures could be strengthened should high loads need to be carried.

5.2 Development of finite element model

The discussion in Section 4.3 showed that the reliability and accuracy of a finite element model is largely dependent on the input parameters as defined by the user. The general input parameters applicable to the models developed in this section include element type, material properties, mesh configuration and boundary conditions. To capture the behaviour of the sidewall due to loading applied at the support beam, the assembly was modelled in three-dimensional space. The finite element analysis was performed by using four-node shell elements (S4R) as these were shown to yield accurate results based on previous results and it is also the default element to use for thin-walled structures. Each component of the sidewall assembly consisted of COR-TEN steel as discussed in Section 4.2.1. Based on the slenderness of the corrugated web, a linear elastic buckling analysis has been conducted, thereby assuming buckling to occur before yielding. Hence, only the Young's modulus and Poisson's ratio were included in the material property definition.

Stellenbosch University https://scholar.sun.ac.za

In Section 4.2.2 the development of the side and end wall assemblies were discussed to determine the lateral stiffness. Due to the similarity in terms of geometry between the models developed in Section 4.2.2 and the model currently being described, it was decided to use a similar mesh size. The shear buckling behaviour of the corrugated sidewall is highly dependent on the corrugated web and beams which resist shear and flexure respectively. The meshing configuration of these elements is therefore crucial to ensure accurate predictions of the sidewall behaviour under loading. The cross-section of the corrugated web was discretised into four and five elements for the flat and inclined folds respectively while the height of the panel consisted of fifty elements. To connect the top and bottom beams to the corrugated panel, it was necessary to sketch partitions on the faces of the beams corresponding to the geometry of the corrugated web. These partitions were meshed according to the corrugated panel to ensure that the nodes of the mesh coincide. Figure 5-1 depicts the loading, boundary conditions and mesh configuration considered for the model.

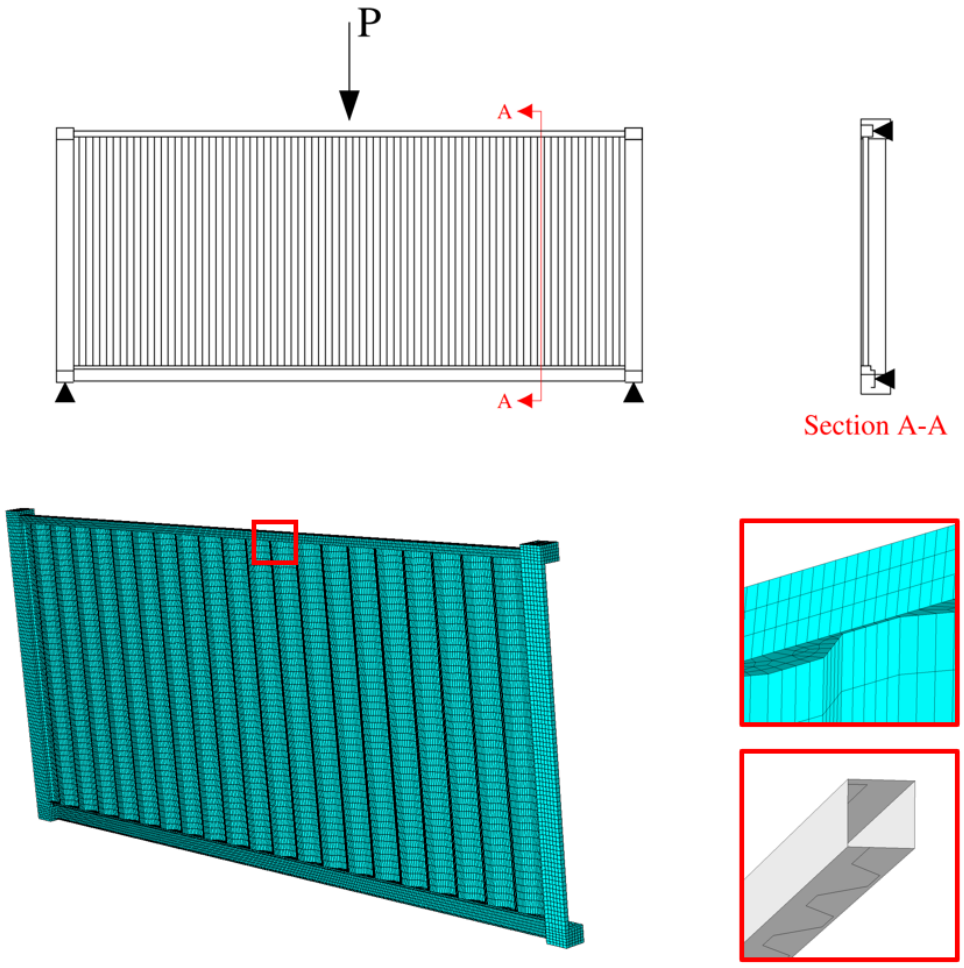

Figure 5-1: Loading, boundary conditions and mesh configuration considered for the sidewall model due to loading applied to the support beams.

From the finite element models developed in Chapter 4, it is evident that complex structural engineering problems can be dealt with if sound assumptions are made. By modelling only part of the structure and applying the influence of the rest of the structure as boundary conditions, accurate results can still be achieved with the merit of reduced computational time. Only the

Stellenbosch University https://scholar.sun.ac.za

side wall was created, while the displacement and rotational restraints provided by the rest of the structure were modelled as discussed below.

The sidewall assembly consists of four loading blocks, two beams, two columns and one corrugated panel as discussed previously. The individual components were connected to one another by defining tie constraints, thereby simulating the welded connections applicable to the sidewall. Rigid body constraints were further assigned to the bottom faces of the two lower loading blocks. The container unit is assumed to be either fixed to the ground or connected to a container unit below for the case of multistorey construction. The buckling capacity was found to be insensitive towards rotational restraint of the bottom loading blocks as fully fixed boundary conditions yielded similar results to that of pinned restraints. Out of plane displacement and rotation about the longitudinal axes of the beams were prevented due to the presence of the ceiling and rigid floor system and boundary conditions were applied accordingly along the faces of the top and bottom beams.

5.3 Results and comparison

The deflected shape of the linear elastic buckling analysis performed for the model described in the previous section is shown in Figure 5-2. The critical buckling load according to the numerical model is 317 kN. Based on the deflected shape, it is evident that the behaviour is different to that of shear buckling as was seen for the second verification study as discussed in Section 3.4.2. As a result of this, the analytical formulations presented in the literature for computing shear buckling capacity cannot be used to validate the numerical model. When a concentrated force is applied to the flange of a beam, a compressive stress is induced in the web. If plasticity is included in the model, the web may fail via yielding or crippling of the web, while the possibility of web buckling also needs to be considered. As the numerical model only considered elasticity in the material definition, it is not plausible to verify the capacity according to formulations derived for yielding or crippling of the web but to rather adopt the formulation derived for compressive resistance as discussed in Section 2.3.3.

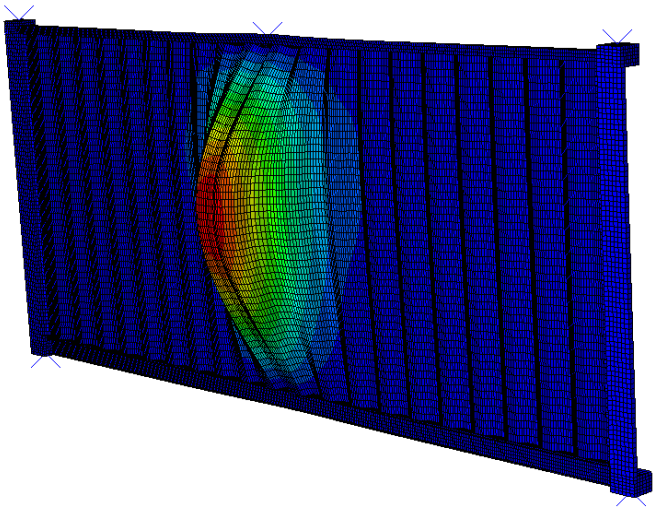

Figure 5-2: Deformed shape of the container side wall for the first eigen buckling mode.

Stellenbosch University https://scholar.sun.ac.za

To analytically verify the buckling capacity of the numerical model, it was necessary to determine an effective width of corrugation for the cross section based on the deflected shape. This is the same approach used in steel design codes (e.g. SANS 10162-1) for calculating the bearing capacity of a beam when subjected to a point load, and for the calculations below the equations provided in Section 2.3.3 were used. Three cross sectional geometries were considered with a corrugated pitch of 2, 4 and 6 as shown in Figure 5-3. The effective length factor was 0.75 for the height of the corrugated panel due to the rotational restraint provided to the top and bottom side beams, as also done in SANS 10162-1 for web capacity. Furthermore, the slenderness of the cross section was determined based on weak axis buckling as strong axis buckling and torsion are restrained by the web. The buckled shape agrees well with the assumption of weak axis buckling.

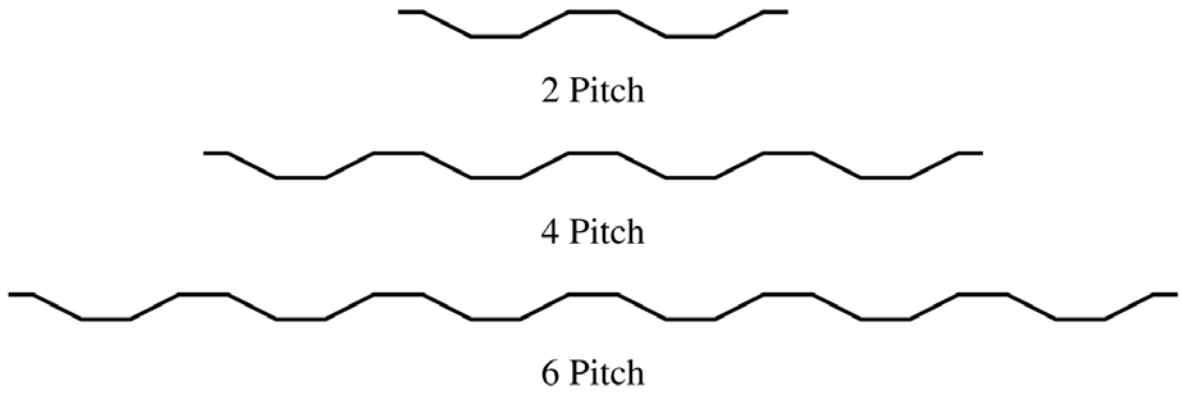

Figure 5-3: Different cross-sectional geometries considered for the analytical models.

Table 5-1 shows the numerical and analytical results for the model described earlier on in this chapter, while Figure 5-4 shows the relative width between the 4 and 6 pitch configurations and the buckled shape of the corrugated web. The theoretical capacity of the 6-pitch configuration is within 5% of the numerical value. Even though this is the case, the width of the buckled shape is in better agreement with the 4-pitch configuration. The effective length factor was solely based on the end conditions of the corrugated web, i.e. restraint provided by the top and bottom side beams. This is considered conservative, as each of the three pitch configurations considered are essentially supported along the entire height on either side by the adjacent panels for the given pitch configuration considered. For a flat panel, the direction of restraint provided should not affect weak axis buckling while it should be remembered that the corrugated panel provides a certain degree of out-of-plane stiffness along the direction parallel to the corrugation. As a result of this, the effective length of the pitch configurations considered are in fact conservative for the analytical models which explains why the numerical result for the 4-pitch configuration is higher than the analytical result.

Stellenbosch University https://scholar.sun.ac.za

Table 5-1: Analytical and numerical capacities for the side wall due to a load applied to the top side beam.

Model	P (kN)
Analytical (2 Pitch)	110.6
Analytical (4 Pitch)	221.2
Analytical (6 Pitch)	331.8
Numerical (linear elastic)	317.0
Numerical (nonlinear elastic)	171.7

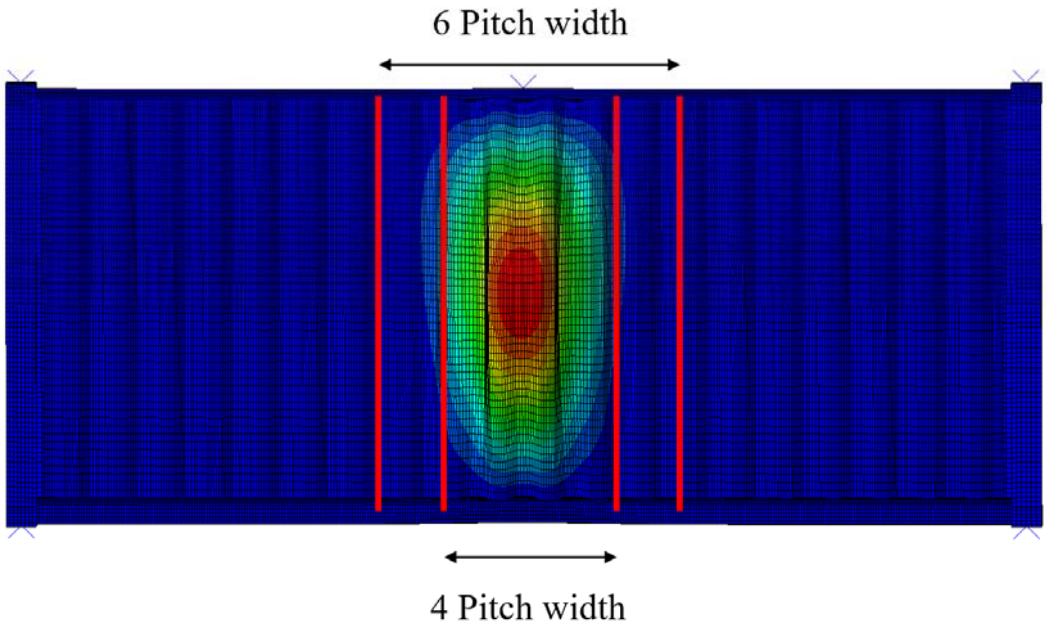

Figure 5-4: Width of 4 and 6 pitch configuration in relation to the deflected shape.

Initially it was assumed that an eigen-value buckling analysis would be sufficient to predict the capacity because of the slenderness of the corrugated panel, nevertheless, it was decided to investigate the nonlinear elastic buckling capacity as well. The model described in Section 5.2 was adjusted by including the effects of nonlinear elastic material behaviour so that a Riks analysis could be performed. The nonlinear elastic buckling analysis was performed as discussed in Appendix B. Due to the localised buckling, it was not suitable to use the first eigen mode to predict the geometrical imperfections of the corrugated web. As a result, it was decided to omit the inclusion of geometrical imperfections in this instance.

Figure 5-5 shows the deflected shape for the nonlinear elastic buckling analysis. The deflected shape is considerably different to that of the eigen-value buckling analysis. The load proportionality factor had a value of 0.54 which corresponds to a capacity of 171.7 kN when plasticity is included in the material definition. The load proportionality factor is low considering the high slenderness of the corrugated web as elastic buckling was expected to govern the capacity of the sidewall assembly. Further investigation of the deflected shape highlights failure of the top side beam which explains why the load proportionality factor is low. As the top side beam fails, it is unable to transfer the loading to the corrugated panel and

Stellenbosch University https://scholar.sun.ac.za

induces buckling as shown in Figure 5-5. The elastic buckling capacity of the side wall assembly due to a monolithic load applied is equivalent to 33-34% of the corner column capacity when the corrugated sheeting is present as discussed in Section 4.4.3. When plasticity is accounted for, the capacity of the side wall is only equal to 18-19% of the load bearing capacity of one of the corner columns. Even though this is the case, the elastic buckling capacity is still considered to be high due to the significantly smaller imposed loads associated with a habitable container unit. Further testing and research are needed to validate the capacity predicted by the nonlinear elastic buckling analysis.

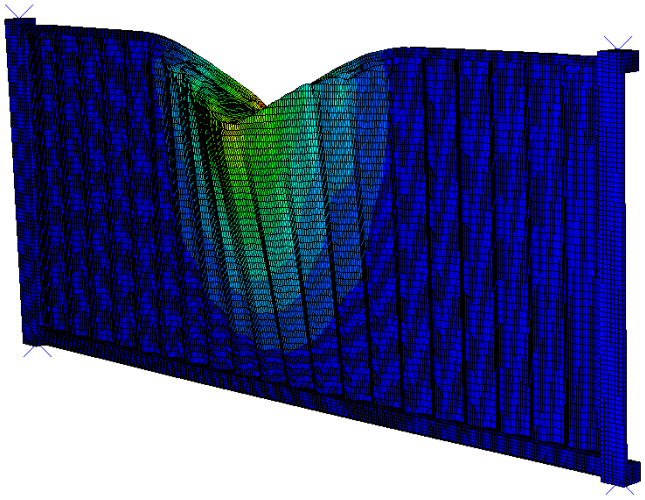

Figure 5-5: Nonlinear elastic buckling analysis for the sidewall due to monolithic loading applied to the top beam.

Several studies have been performed to investigate the sensitivity of geometric properties on the buckling capacity of plate girders and corrugated steel shear walls. The stiffness of boundary members such as columns and beams have been shown to influence the ultimate bearing capacity significantly where an increase in stiffness of these members leads to an enhanced capacity of the corrugated panel (Hosseinpour *et al.*, 2015). Further studies performed by Subramanian and White (2017) highlighted that the magnitude of the plate buckling coefficients are overestimated for smaller flanges.

There are several ways in which shear walls can be strengthened to enhance the buckling capacity. By increasing the thickness of the corrugated panel up until the point where the plate no longer buckles before yielding can increase the buckling capacity significantly. Although this method has been implemented successfully in the past especially in seismic regions, it is uneconomic especially for shipping containers which have defined geometries (Gil and Lee, 2005). Even though corrugated panels provide a certain level of out of plane stiffness, additional stiffeners can be welded in place while the boundary members as previously discussed can be increased in size to ultimately enhance the shear buckling capacity of the sidewall.

The following sections introduce an updated numerical model where pure shear buckling behaviour is induced in the corrugated sidewall assembly by addition of stiffer elements.

Stellenbosch University https://scholar.sun.ac.za

5.4 Adjusted numerical model

As mentioned in Section 5.3, the capacity of the sidewall configuration based on the eigen value buckling analysis is still considered high in the context of the applied loads associated with modular buildings (i.e. it would be able to support a multi-storey arrangement of containers). However, the uncertainty with regard to the results of the nonlinear elastic buckling analysis, it was decided to propose a method for strengthening the sidewall to carry more load. Hence, this also allows the work to investigate what load could potentially be supported by a modified shipping container, even when loads are not carried at the corners. Stiffener plates were added at the positions where bearing failure can be expected to occur, namely below the position of loading and at the supports, i.e. position of the columns. Figure 5-6 depicts the adjusted numerical model. The meshing configuration and boundary conditions as discussed for the previous model remain unchanged. A series of models were developed by changing the thickness of the flange and stiffener plates in the section properties. The width of the flange was kept constant at 300 mm for all models considered. The thickness of the flanges was altered from 10 to 40 mm by keeping the thickness of the stiffeners constant at 20 mm. Similarly, the stiffener thickness was varied from 10 to 40 mm for a constant flange thickness of 20 mm.

The advantage of using shell elements for this model is once again emphasised by the fact that the section thickness only needs to be altered as opposed to redefining the cross section of the plate as would be the case for solid elements.

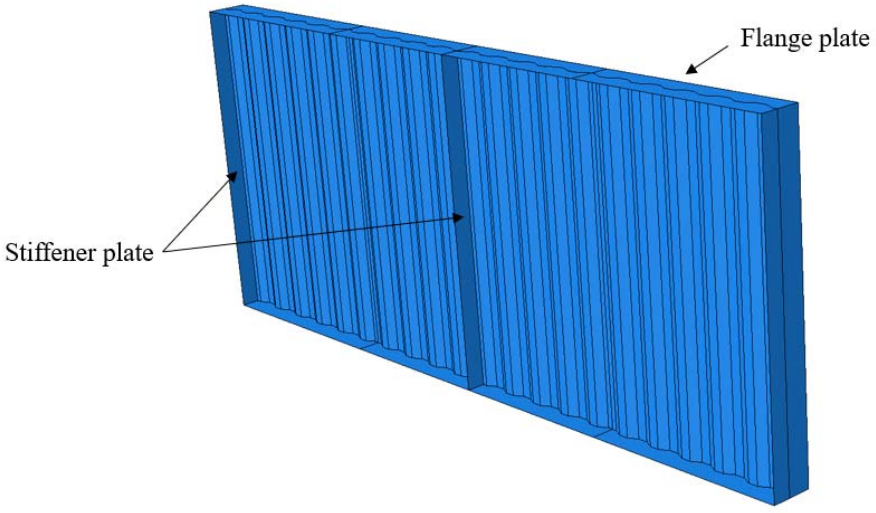

Figure 5-6: Adjusted numerical model.

The results of the eigen value buckling analysis for the models described above are listed in Table 5-2 while Figure 5-7. depicts the deflected shape of the first eigen mode for a flange and stiffener thickness of 20 mm. Based on the deflected shape, the strengthening method proposed, leads to a failure mode comparable to shear buckling as highlighted in the second verification study by Sayed-Ahmed *et al.* (2003). An increase in flange thickness results in a higher critical

Stellenbosch University https://scholar.sun.ac.za

buckling load. An increase of 70% was observed for the critical Euler buckling capacity when the flange thickness increased from 10 to 40 mm. The critical buckling load was less sensitive to the thickness of the stiffener as an increase of less than 1% occurred when the thickness was altered from 10 to 40 mm. From these results it is evident that an increase in flange thickness leads to an increase in the critical buckling capacity. Even though negligible increase in the critical buckling load was observed for an increase in stiffener thickness, it is possible that the critical buckling load had already converged for the lower bound stiffener thickness considered.

Table 5-2: Eigenvalue buckling analysis for sidewall.

Flange thickness (mm)	Stiffener thickness (mm)	Critical buckling load (kN)
Unstiffened wall		317
10	20	1099
20	-	1559
30	-	1780
40	-	1864
20	10	1555
-	20	1559
-	30	1560
-	40	1561

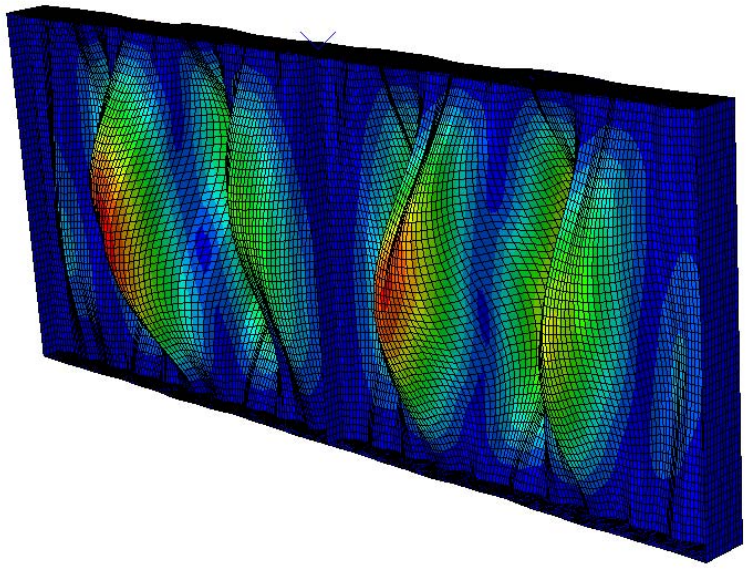

Figure 5-7: Deflected shape of the first eigen mode with a flange and stiffener thickness of 20mm.

The theoretical shear buckling capacities were computed for the given side wall configuration according to the formulae outlined in Section 2.4.1 based on the area of the corrugated web and are listed in Table 5-3. The local buckling coefficient was calculated by assuming the corrugated web and beams to be fully clamped due to the rotational restraint provided while

Stellenbosch University https://scholar.sun.ac.za

the global shear buckling coefficient was taken as 68.4 as discussed in the literature. The critical buckling loads recorded in Table 5-2 are comparable to the theoretical buckling load predicted for global buckling as listed in Table 5-3. Diagonal buckling of multiple fold widths is apparent which agrees well with the definition of global shear buckling. Even though the shear buckling capacities according to the numerical models are in a similar range to the theoretically predicted value for global shear buckling, there is still a great deal of variability in the numerical results. This highlights the fact that the shear buckling capacity is highly sensitive to the thicknesses of the stiffeners and flanges. The global shear buckling coefficient only accounts for the restraint between the web and the flanges and does not consider the effect of the stiffness provided by the flanges.

Table 5-3: Theoretical shear buckling capacities

Type of buckling stress	Stress (MPa)	P (kN)	Equation
Local critical shear stress	6980	70000	2.9
Global critical shear stress	109.4	1020	2.12
Shear yield stress	202.1	1885	2.15
Interactive critical shear stress	104.2	972	2.16

Based on the results of the eigenvalue buckling analysis, it is worthwhile investigating the post buckling behaviour of the sidewall assembly. To investigate the post buckling behaviour, a nonlinear elastic buckling analysis is needed as discussed in the literature. In Section 4.2.3, a Riks analysis performed in ABAQUS was described for the corner columns. The same approach will be adopted for the stiffer sidewall configuration. As previously mentioned, steel plate shear walls are sensitive to initial imperfections because of manufacturing. According to EN 1993-1-5 (2006), the geometric imperfection considered for corrugated plates should be equal to b/200, where b is the smallest panel dimension. The material property definition was amended to include the plasticity of the steel while the critical buckling loads listed in Table 5-2 were applied as reference loads for the Riks analysis. The results of the Riks analyses are shown in Table 5-4.

Table 5-4: Results for the Riks analysis of the sidewall.

Flange thickness (mm)	Stiffener thickness (mm)	Nonlinear elastic capacity (kN)
Unstiffened wall		171.7
10	20	1052
20	-	1485
30	-	1651
40	-	1692
20	10	1378
-	20	1485

Stellenbosch University https://scholar.sun.ac.za

-	30	1486
-	40	1487

Comparing the values in Table 5-4 to those listed in Table 5-2. a decrease in shear buckling capacity is observed. The load proportionality factors were high ranging between 0.870 and 0.957. The high load proportionality factors initially seem to be in good agreement with the extreme slenderness of the sidewall panel as it is expected for buckling to occur before yielding of the steel takes place. Based on the results of the nonlinear elastic buckling analysis, it is evident that an increase in flange thickness for a given stiffener thickness, i.e. 20 mm, corresponds to a rise in capacity. Figure 5-8 shows the deformed shape for the nonlinear elastic buckling analysis considering a flange and stiffener thickness of 20 mm. The mode of failure corresponds to that of web buckling which agrees well with the high load proportionality factors as mentioned previously.

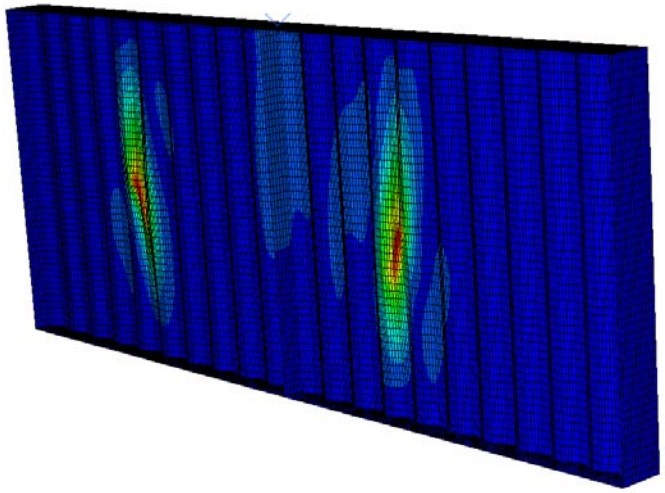

Figure 5-8: Deformed shape for the nonlinear elastic buckling analysis for a flange and stiffener thickness of 20 mm.

Based on the results listed in Table 5-4 for a varying stiffener thickness, the capacity of the side wall for 20, 30 and 40 mm thick stiffeners were the same while the 10 mm thick stiffeners showed a 7% reduction in capacity. The deflected shapes for the 10 and 40 mm stiffener models are illustrated in Figure 5-9. It is evident that two different modes of failure occur. The lower capacity of the 10 mm thick stiffener can be attributed to a bearing failure in the form of web and stiffener crippling which corresponds to a lower load proportionality factor of 0.87 compared to the rest of the stiffener thicknesses considered. For the 20, 30 and 40 mm thick stiffeners, the deflected shapes corresponded to that of a buckling failure as seen in Figure 5-9 (b). It is therefore concluded that thicker flanges and stiffeners not only increase the elastic buckling capacity of the stiffened sidewall but can also dictate the type of failure that occurs when plasticity is included in the model.

The lowest predicted capacity of the sidewall according to the Riks analysis occurred for a flange and stiffener thickness of 10 and 20 mm respectively. This capacity is still greater than the critical global and interactive buckling loads as listed in Table 5-3. From these results it is

Stellenbosch University https://scholar.sun.ac.za

concluded that the theoretical formulae can conservatively predict the capacity of the strengthened sidewall assembly assuming the capacity to be governed by shear buckling behaviour. A study performed by Faegh and Fanaie (2018) investigated several formulae used to predict shear strength of typical plate girders and their applicability to corrugated shear walls. Their results showed that these developed formulae conservatively predict the shear buckling stress of corrugated shear wall systems. Using theoretical formulae derived for plate girders should still be used with great caution especially for the unstiffened sidewall due to fundamental differences in boundary conditions and the influence of surrounding stiffness.

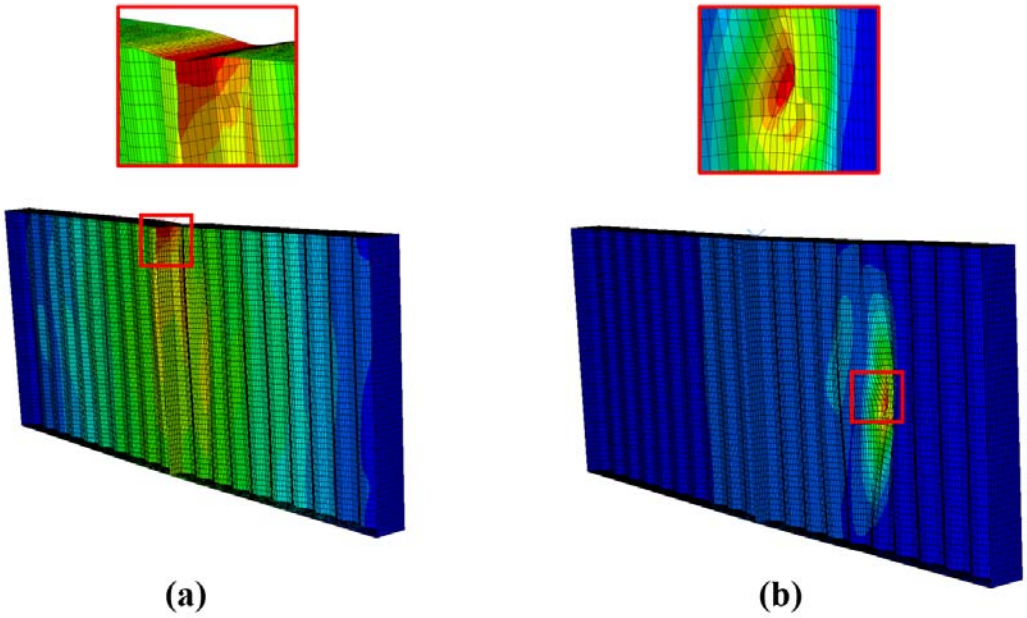

Figure 5-9: Elastic buckling modes of the side wall with (a) 10mm stiffener, (b) 40mm stiffener.

5.5 Conclusions

Several finite element models were developed in this section to determine the capacity of the sidewall of the 20 ft ISO shipping container due to a change in load path because of loads applied to the mid-span of walls. Both a stiffened and unstiffened sidewall were considered while the numerical results were compared to those predicted by theoretical formulae.

The elastic buckling capacity of the unstiffened sidewall was 317 kN according to the numerical model. The deflected shape corresponded to that of compressive buckling as opposed to shear buckling which is the case for typical plate girders. The analytical results were conservative in relation to the numerical results due to an overprediction of the effective length of the pitch configurations considered. The inclusion of plasticity in the material definition led to failure of the top side beam. Further validation is needed to verify this result, although the failure mode appears sensible based on the geometry and load position. As a result of the top beam failing, an updated numerical model was proposed to investigate possible ways of strengthening the sidewall should high loads need to be applied to walls in the case of multi-storey structures.

Stellenbosch University https://scholar.sun.ac.za

The corrugated wall was strengthened by the addition of flange and stiffener plates. A series of models were considered with different flange and stiffener thicknesses. The deflected shapes for the strengthened models indicated global shear buckling behaviour for the eigen value buckling analysis. The numerical capacities for these models ranged between 1099 and 1561 kN which is significantly higher than the elastic buckling capacity of the unstiffened sidewall. The theoretically predicted capacity for global shear buckling of the sidewall was found to be 1020 kN and was therefore considered conservative. The theoretical formulation derived for plate girder buckling does not consider the effect of stiffer surrounding members and therefore it should still be used with caution. For the nonlinear elastic buckling analyses, the reduction in capacity was generally small as load proportionality factors ranging between 0.87 and 0.957 were observed. Although this is the case, the mode of failure was found to be dependent on the thickness of the stiffener as 10 mm thick stiffeners showed a bearing failure while web buckling was induced when thicker stiffeners were implemented.

The analytical formulae used in this work are fundamentally based on theoretical and dimensional conditions applicable to plate girders. Due to the fundamental differences regarding the geometry and boundary conditions of the 20 ft ISO shipping container sidewall, designers need to apply theoretical formulae with extreme caution as it may over or underestimate the capacity of the sidewall configuration subject to a monolithic load. The results show that there is a clear need for new independent formulae to calculate the strength of corrugated wall systems such as the sidewall considered in this study.

Stellenbosch University https://scholar.sun.ac.za

6 Thermal and structural fire finite element analyses of shipping containers

6.1 Introduction

Chapters 4 and 5 provided an in-depth discussion on the structural capacity of a modified shipping container at ambient temperature. As mentioned in the literature, large-scale fire testing provides significant insight into both the thermal and structural behaviour of real structures. Due to the high costs and logistical challenges involved with these tests, the finite element method was implemented in this work instead to predict the structural fire resistance of the 20 ft ISO shipping container. As with the models developed previously in this study, ABAQUS was the preferred software due to its capabilities supporting the development of the thermal and elevated temperature structural models described below (Dassault-Systemes, 2020). The aim of this section is to predict the capacity of the main load bearing elements of the shipping container, namely the corner columns, when exposed to a fire. The reduced capacities of the columns can then be used to evaluate the stability failure criteria as outlined in Section 2.6.1. The results of the finite element analyses performed in this study will provide useful information to consider when designing modular structures for fire resistance. The specific models developed in this chapter are:

(1) Four thermal models of different sections of the container to calculate temperatures and thermal gradients. Models of the top and bottom side beams are used to determine the updated stiffness of column boundary conditions, while the back and front corner column models are used to determine the temperature of the corner columns and the corrugated sheeting.

(2) Structural models of the corner columns at varying elevated temperatures, employing the updated boundary conditions and material temperatures based on the thermal models.

This chapter comprises a detailed discussion on the development of the finite element models. The heat transfer models are used to predict the temperature profile of the necessary structural elements while thermal material properties, boundary conditions and thermal interactions are considered. The results of the heat transfer analysis are briefly looked at in terms of temperature gradients before the results of these models are implemented in models like those developed in Chapter 4 to predict the capacity of the corner columns at elevated temperature. This chapter concludes by highlighting important considerations to consider with regard to multistorey modular construction.

6.2 Development of FE models

To overcome the fire prevention deficiencies associated with unprotected steel, passive fire protection measures are needed. The finite element models discussed further in this section considered a worst-case scenario where the steel was unprotected while protected models were

Stellenbosch University https://scholar.sun.ac.za

also developed. For this study, only an internal fire, i.e. within the shipping container, was considered.

Due to the planar nature of the shipping container elements, it was deemed satisfactory to only consider two-dimensional heat transfer models to obtain the necessary time-temperature relationships for the walls, beams and columns. The two-dimensional heat transfer models for the beams are used to predict the reduction in axial and rotational restraint to be applied at the column ends. On the other hand, the heat transfer models for the corner columns are necessary to determine the adjusted constitutive relationship needed for the material definition in the buckling models. The heat transfer models for the columns are also used to obtain the temperature of the corrugated sidewalls which is ultimately needed to determine the reduced lateral stiffness along the length of the columns.

Figure 6-1 shows the cross-sectional geometries considered for the finite element heat transfer models. The cross sections enclosed in the red and black borders depict the plan and elevation view of the columns and beams respectively. As depicted in Table 3-3, the geometry of the bottom side and end beams are slightly different. Only the bottom side beam was modelled while the time-temperature relationship for this model was considered for the bottom end beams as well. The bottom side beam was modelled by considering a cross section which included the web of the cross beam as shown in Figure 6-1. Even though the plywood floor system will reduce the rate of temperature increase in the bottom beams and cross beams, it is a combustible material where charring needs to be considered. The thermal behaviour of timber is beyond the scope of this study and therefore the plywood floor system was conservatively omitted in the heat transfer model considered for the unprotected bottom side beam. The top side and end beams consist of the same cross section and even though the cross-sectional geometry of the corrugated ceiling differs orthogonally, the steel temperature over time was assumed to be the same. Therefore, only the top side end beam assembly was considered during the heat transfer modelling.

Stellenbosch University https://scholar.sun.ac.za

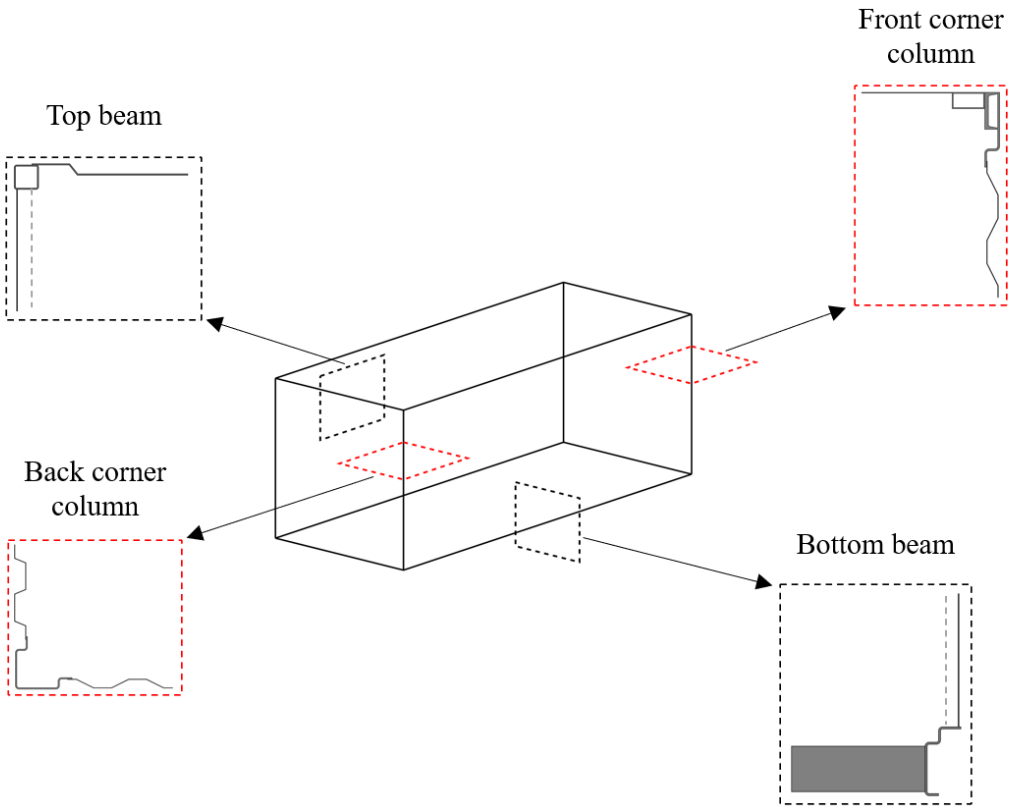

Figure 6-1: Schematic showing the two-dimensional models considered for the heat transfer analyses.

The cross-sectional geometries considered for the beam vary with respect to the out-of-plane dimension due to the corrugation of the walls and therefore these cross sections are not entirely planar. A worst-case scenario was considered by modelling the geometry in such a way that the largest possible areas of the beams were exposed to the fire. This was achieved by considering the fold widths of the corrugated sheeting welded closest to the unexposed face of the beams as illustrated in Figure 6-1.

As outlined in the literature, several different fire curves exist which can be used for fire design depending on the scenario at hand. For the heat transfer models considered in this thesis, the standard ISO 834 temperature curve was applied (ISO, 1999). As mentioned previously, this curve is not representative of a real fire which is dependent on fuel load characteristics and ventilation openings. It is possible that a real fire could result in a more severe fire, however the standard fire curve serves as a useful benchmark for determining fire ratings due to the correspondence with furnace-based fire tests (Buchanan and Abu, 2017).

All three modes of heat transfer were considered namely conduction, convection, and radiation. The specifics with respect to the thermal properties and interactions considered in these models are discussed in the following sections.

6.2.1 Thermal modelling considerations and configuration factors

It is evident that the cross-sectional geometries of the heat transfer models depicted in Figure 6-1 possess a non-uniform surface geometry. As a result, configuration factors had to be

Stellenbosch University https://scholar.sun.ac.za

determined so that the correct emissivity values could be used when defining the radiation due to the standard fire exposure. Although the depth of the corrugated panels is small, the varying distance between the surface geometry and flames were assumed to have an influence on the configuration factors. A further simplification was made by assuming the heat from the standard fire curve to be directly emitted onto the fold widths of the panel closest to the fire.

To aid the computation of the configuration factors, a datum line was implemented as illustrated in Figure 6-2. Surfaces that fall on the datum line had a configuration factor of 1. The datum lines were used to compute the configuration factors for all surfaces not falling on the datum by using Equation 2.32 (EN 1991-1-2, 2002). The configuration factors calculated for the respective cross sections depicted in Figure 6-2 are listed in Appendix C. These configuration factors were multiplied by the emissivity of the steel before implementing separate radiative interactions on each corresponding surface.

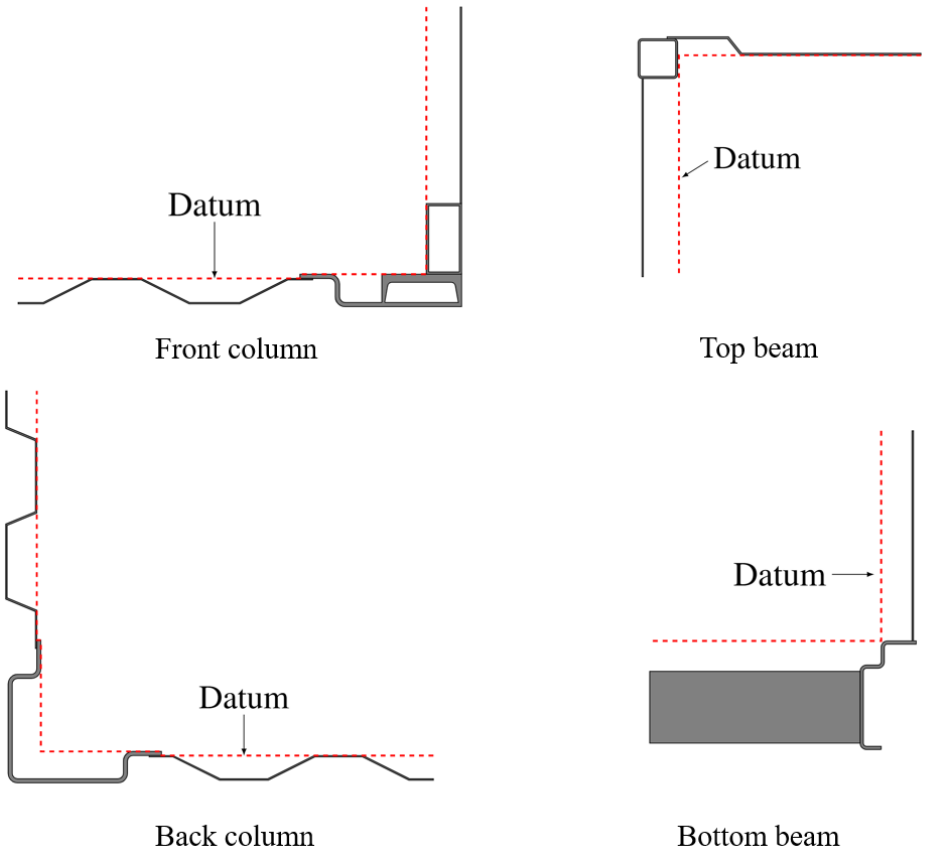

Figure 6-2: Datums considered for the determination of the configuration factors

At the beginning of this study two important means of passive fire protection were highlighted, namely that of intumescent paints and protective board systems. The study performed by Shuttleworth *et al.* (2020) showed that protective board systems can be used to great effect to satisfy insulation requirements for passively protected shipping containers. Protective board systems not only reduce the rate of temperature increase in steel structures, but they also have the added benefit in terms of aesthetics.

Stellenbosch University https://scholar.sun.ac.za

The heat transfer models considered for the protected shipping container only considered protective board systems with a thickness of 10 and 20 mm respectively as these thicknesses are typical for passive fire protection installations. There are many different types of board systems currently available, while the majority are manufactured from calcium silicate or gypsum plaster (Buchanan and Abu, 2017). The passive fire protection board systems used in this study were generic with thermal and material properties corresponding to typical values listed in product catalogues. Figure 6-3 depicts the passively protected models considered for determining the time-temperature histories of the steel beams and columns. The protective boards are fixed to the container walls and ceiling via steel channel brackets with dimensions of 51 x 35 x 0.5 mm, based on specifications used in practice in South Africa. The plywood floor system was also assumed to be contained by a layer of protective boarding. As seen in Figure 6-3, the plywood floor system has been included in the bottom side beam model. It is assumed that the protective boarding covering the plywood floor system will prevent it from reaching temperatures where charring starts to occur. As a result of the buoyant gases within the shipping container fire, the top beams and columns are expected to heat up quicker than the floor system. Only once enough buoyant gases have accumulated beneath the ceiling, will the radiant heat flux from the hot upper layer start to increase the temperature of the floor system. Even if charring of the protected plywood occurs, the temperatures of the bottom beams should be insensitive towards the violation of this assumption. In real structures it will often not be feasible to have passive protection on top of floors, except if a cementitious screed is used. Hence, the boards may have to be moved to be underneath the floor or be supported by an independent frame underneath the floor. However, the analyses for now provide preliminary estimates of behaviour that can be adapted to suit specified configurations.

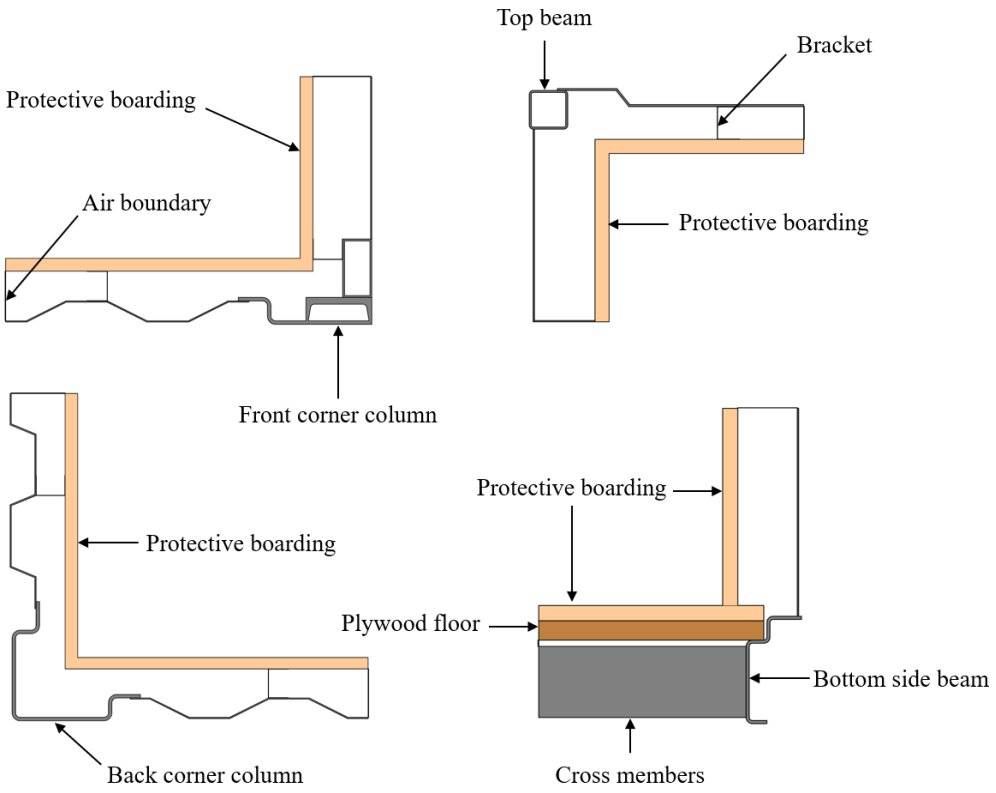

Figure 6-3: Passive protection systems considered for the protected heat transfer models.

Stellenbosch University https://scholar.sun.ac.za

In contrast to the unprotected models, the uniform surface geometry of the protective boards prevents any shielding of the emitting gases, and therefore the exposed surface of the boarding coincides with the datum. The configuration factor was, therefore, taken as unity for all the protected models when defining the radiative interactions along the exposed surface.

From Figure 6-3, it is apparent that voids occur between the protective boarding and the elements of the shipping container. Radiation and convection within these voids are to be accounted for to accurately determine the temperatures of the beams and columns.

To determine the capacity of the corner columns at elevated temperature, finite element models were developed in a similar way to those described in Section 4.2.3. Theoretically speaking, the steel columns will have some capacity once the steel temperatures exceed 600 ℃. Once the steel reaches temperatures in this range, the assumptions of boundary conditions can no longer be relied upon and as a result the effective length of the columns increase markedly. The capacities of the corner columns were determined via a series of points from the onset of a reduction in stiffness until the columns reached a temperature of 600 ℃, or the duration of the standard fire exposure was reached.

Figure 4-16 depicted the model considered for determining the end conditions of the columns according to the axial and rotational stiffness of the beams. The results of the finite element models for the top and bottom beams were used to compute the reduced axial and rotational stiffness because of a decreasing Young's modulus. As with the ambient models considered in Chapter 4, the ceiling and cross beams were assumed to have a negligible effect on the axial and rotational stiffness provided by beams.

6.3 Input parameters for structural finite element models

The accuracy of the heat transfer models considered in this thesis is dependent on several factors which must be defined to match the conditions of the containers as constructed. The sections to follow provide a brief discussion on the element type, material thermal properties as well as the thermal boundary conditions and interactions considered.

6.3.1 Model and element description

As discussed in the previous section, the heat transfer models were developed in two-dimensional space to allow for shorter computational time while still yielding accurate results. Each heat transfer model was analysed using shell elements, namely a 4-node linear heat transfer quadrilateral (DC2D4).

6.3.2 Material properties

In practice the material properties of the steel and protective boarding could vary depending on the materials utilised in manufacturing the products. The protective boarding used to protect the shipping container would need to have similar characteristics to those of the generic protective board used in this work otherwise the model parameters would need to be adjusted accordingly.

Stellenbosch University https://scholar.sun.ac.za

The required thermal properties of the steel, namely density, thermal conductivity and specific heat, are used as defined in Section 2.8.2 as proposed by EN 1993-1-2 (2005). To perform the nonlinear elastic buckling analysis in ABAQUS, the constitutive relationship for the steel at elevated temperature was determined according to the model proposed for carbon steel as outlined in EN 1993-1-2 (2005). The model consists of a linear stress-strain relationship until the limit of proportionality is reached. The transition from the proportionality limit to the yield stress of the steel is defined by an ellipse up to a 2% strain. The Eurocode states that a yield plateau occurs up until a strain of 15% is reached before the stress reduces linearly to zero at 20% strain. For this study, the yield plateau was modified to a strain of 18% which corresponds to that of weathered steel for the shipping container as discussed in Section 4.2.1. The equations used to compute the stress strain relationship for carbon steel at elevated temperature are listed in Appendix D. Figure 6-4 shows the stress strain relationship for carbon steel according to EN 1993-1-2 (2005) for a steel temperature of 20 and 600 ℃.

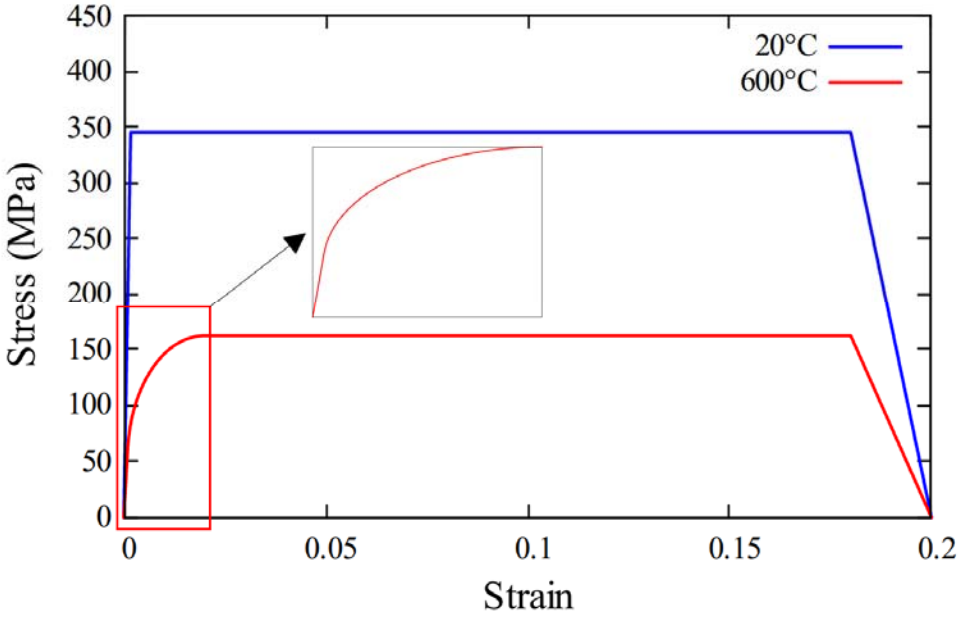

Figure 6-4: Stress-strain relationship for carbon steel at elevated temperature, showing graphs at 20 and 600 °C as examples.

Protective board manufacturing companies namely Gyprock, Promat and MagnaStruct provide thermal properties in their technical specifications. In general these properties are temperature dependent as discussed in a study performed by Feng *et al.* (2003) on the thermal performance of cold-formed thin-walled steel panel systems. The manufactures listed above only provide values for the specific heat and thermal conductivity at a specific temperature. As a result, the thermal properties of the generic boards were modelled as constant values when defining the material for the protective boards in ABAQUS. If the temperature dependent thermal properties for a specific board product are known, a more accurate finite element model can be developed. The manufacturing companies also provide information on the integrity relating to the fire resistance as discussed in the literature. Integrity ratings of up to 4 hours can be achieved for certain configurations. For this study, it is assumed that the protective boards will not fail the integrity criteria, while the results of the unprotected models will provide useful insight if this

Stellenbosch University https://scholar.sun.ac.za

assumption is violated, i.e. if boards crack allowing steel to be exposed to hot gases and radiation.

Pitts and Sissom (1977) list the thermal properties of some common materials applicable to structural fire engineering. The thermal properties for the generic boards considered in the heat transfer models were taken approximately to be the average of the values listed for gypsum and fibre insulating boards.

According to Buchanan & Abu (2017), the thermal properties of wood are not well defined as moisture is driven off at 100 ℃ before charring takes place at 300 ℃. EN 1995-1-1 (2004) provides temperature dependent values for both the thermal conductivity and specific heat of wood while published values are still considered to vary significantly. For the protected models, a constant thermal conductivity and specific heat were considered for the plywood floor corresponding to the values listed by Pitts and Sissom (1977) for oak.

To model cavity radiation as discussed in the following section, it is necessary to have a closed cavity. Additional boundary conditions were added to the open ends of the cavities for the protected models in the form of separate two-dimensional shell elements as shown in Figure 6-3. The material definition for these additional boundary conditions corresponded to that of air to minimise the effect it has on conduction and convection at the edges, thereby simulating radiation within the cavity as accurately as possible.

Table 6-1: Thermal properties considered for the heat transfer models.

Material name	Density (kg/m^3)	Conductivity (W/mK)	Specific heat (J/kgK)
Steel	7850	Equation 2.47	Equation 2.46
Protective board	1000	0.22	900
Plywood floor	800	0.17	2380
Air boundary	1.1	0.026	1040

6.3.3 Boundary conditions and thermal interactions of heat transfer models

The boundary conditions for the unprotected models were defined on the exposed and unexposed surfaces while further interactions were modelled within the voids of the protected models. The ambient temperature was assumed to be 20 ℃ for all heat transfer models. The ambient temperature was applied to all surfaces within the models by creating a predefined field variable in the initial step. The heat transfer was simulated by assuming a 2-hour standard fire which was applied to the corrugated sheeting, column and beam surfaces for the unprotected models as described in Section 6.2. For the protected models, the standard fire was simply applied along the face of the protective boards.

The time-temperature history of the ISO 834 standard fire was added as an amplitude in the finite element model. When defining the convective and radiative heat transfer interactions

Stellenbosch University https://scholar.sun.ac.za

along the exposed surfaces of the models, this amplitude was used as an input temperature. Convection was modelled as a surface film condition while radiation due to the standard fire was defined according to surface radiation in ABAQUS. For the protected models, radiative and convective heat transfer within the voids were considered according to the cavity radiation and surface film condition interactions. In Section 2.7.2, the concept of convective heat transfer was discussed while appropriate convective heat transfer coefficients were introduced based on EN 1991-1-2 (2002). The convective heat transfer coefficient for the exposed surface had a value of 25 W/m^2K as stated in EN 1991-1-2 (2002). The Eurocode provides an analytical formulation for determining the steel temperature over time for both protected and unprotected steel sections exposed to fire (EN 1993-1-2, 2005). Where radiation is considered separately from convection, the convective heat transfer coefficient is taken as 4 W/m^2K, while a value of 9 W/m^2K is recommended when radiation is considered with convection. For simplicity's sake, the latter value was used by defining a surface film condition on the unexposed surface, thereby eliminating the need to define an additional interaction namely surface radiation. The additional boundary conditions described in Section 6.3.2 allowed heat to be transferred through convection with a convective heat transfer coefficient of 9 W/m^2K.

Even though a study performed by Marx (2018) showed that convective heat transfer within the voids of a sandwich floor system has a negligible influence on steel beam temperatures, a convective heat transfer coefficient of 4 W/m^2K was still assigned along the internal surfaces of the voids for the protected models. As the temperature within the voids vary over time, two models for each protected model were generated. The sink temperature of the first model was constant at 20 ℃ while the average time-temperature history within the voids was used to define an additional amplitude for the sink temperature in the second model so that convective heat transfer within the voids could be modelled accurately.

The emissivity of the standard fire exposure was conservatively taken as unity. According to EN 1993-1-2 (2005), an emissivity value of 0.7 is to be adopted for carbon steel while a value of 0.8 was considered for the protective boards (ECCS TC3, 2001). The resultant emissivities due to self-radiation between the respective surfaces were computed according to Equation 2.30. Table 6-2 and Figure 6-5 provide a summary of the interactions considered for the protected finite element models while only the red and green surfaces are applicable to the unprotected models. The individual parts were connected via tie constraints to account for conductive heat transfer. To prevent any further conduction from occurring within the models, no ties were assigned between the air boundaries and the rest of the model.

Table 6-2: Heat transfer coefficients for protected finite element models.

Location	Colour	Emissivity	Convective heat transfer coefficient (W/m^2K)	Sink temperature (℃)
Exposed surface	Red	0.7	25	ISO 834
Unexposed surface	Green	-	9	20
Cavity (mixed)	Orange	0.6	4	avg. temp

Stellenbosch University https://scholar.sun.ac.za

Cavity (steel only)	Cyan	0.54	4	avg. temp
Air boundary	Blue	-	9	avg. temp

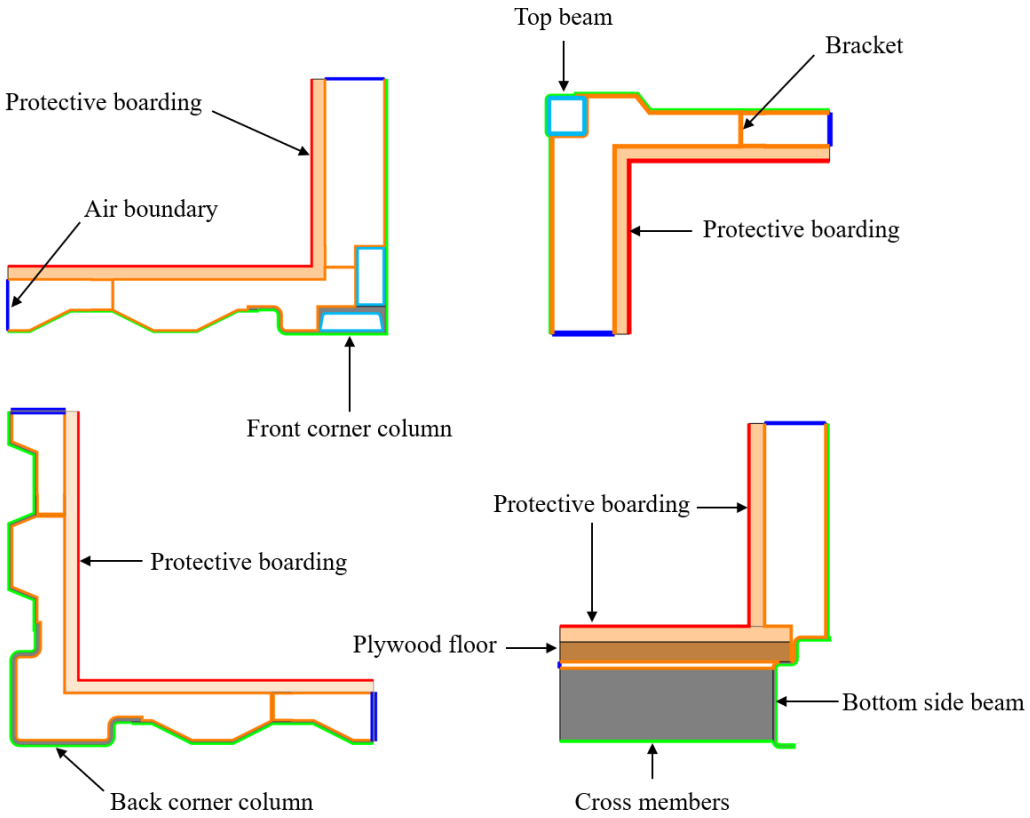

Figure 6-5: Surfaces considered for modelling the interactions. Colours of items are as defined in Table 6-2.

6.4 Results of finite element analyses

The temperatures obtained from the heat transfer models described in the previous section serve as an input for the structural models to predict the capacity of the corner columns at elevated temperature. The results for the heat transfer and buckling models are described separately in the sections below.

6.4.1 Finite element heat transfer results

As previously mentioned, only an internal fire is considered meaning that the columns are not uniformly heated as assumed by many design codes (Agarwal *et al.*, 2014). Columns may have non-uniform temperature distributions through the cross section or along the length. Thermal gradients along the length of the column were assumed to be excluded in this study. This assumption is considered reasonable in the case of a post flashover fire where turbulence and mixing of hot gases will maintain a uniform temperature throughout the height of the shipping container. Temperatures have been determined at several points on the column and beam cross sections so that the thermal gradients can be investigated. The minimum and maximum temperatures after a 2-hour standard fire exposure are depicted in Figure 6-6 for the beams and columns. For all the curves depicted below, the rearrangement of the molecular structure of the

Stellenbosch University https://scholar.sun.ac.za

steel is evident once the steel temperature reaches 700 °C. Another interesting observation from the graphs depicted below is the fluctuation in the differential between the minimum and maximum temperatures for the duration of a 2-hour standard fire exposure.

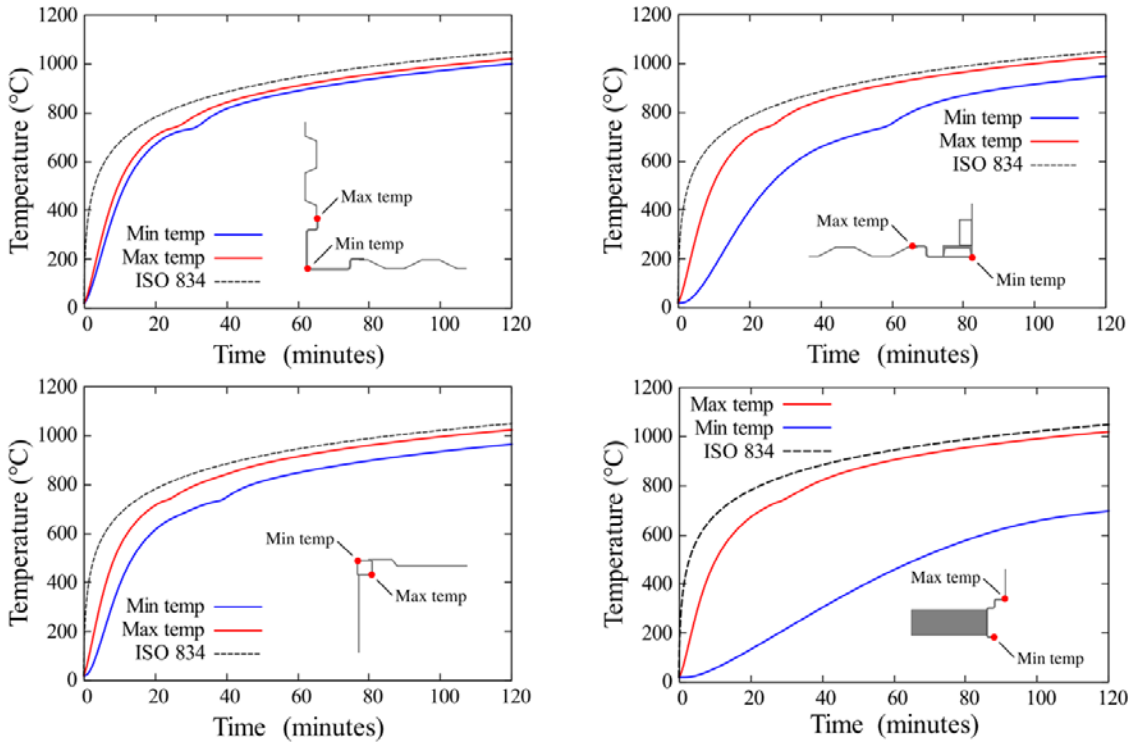

Figure 6-6: Maximum and minimum temperatures for the beams and columns after a 2-hour standard fire exposure with no passive protection.

From Figure 6-6 it is evident that the back corner column does not have a significant thermal gradient present through the cross section. The temperature differential for the duration of the fire exposure is constant. Even though the back corner column is only exposed to fire on the internal surface, the high thermal diffusivity of the steel in combination with the thin-walled nature of the column leads to a nearly uniform temperature distribution. Based on the literature as discussed in Section 2.8.3, the back corner column should not be susceptible to additionally induced moments caused by a shift in the neutral axis or thermal bowing.

The geometry of the front corner column is considerably different to that of the back corner column, due to practical reasons regarding the container doors. A larger thermal gradient is observed for the front corner column in relation to the back corner column. The higher thermal gradient as shown in Figure 6-7 is attributed to the greater distance through which conductive heat transfer takes place. The thermal gradient is not solely dependent on the thermal conductivity of the steel but rather the thermal diffusivity which is related to transient heat transfer. For the back corner column, the entire internal face was exposed to the fire meaning that conduction occurred over a maximum distance equal to the thickness of the section before reaching the unexposed surface where the minimum temperature was recorded. The minimum temperature was recorded on the unexposed corner of the front column as shown in Figure 6-6. Intuitively this makes sense, as the distance through which conductive heat must travel is

Stellenbosch University https://scholar.sun.ac.za

furthest to this point. To investigate the effect of cavity radiation on the thermal gradient through the cross section, an additional heat transfer model was run where cavity radiation within the voids was omitted. As expected, lower temperatures were observed on the unexposed side of the void when cavity radiation was omitted. The omission of cavity radiation also led to higher thermal gradients across the section. This highlights the fact that the thermal distribution is dependent on both conduction across the section and radiative heat transfer within the void. It can therefore be concluded that the minimum temperature through the cross section is due to conductive heat transfer as well as radiation from the void surface closest to the fire exposure.

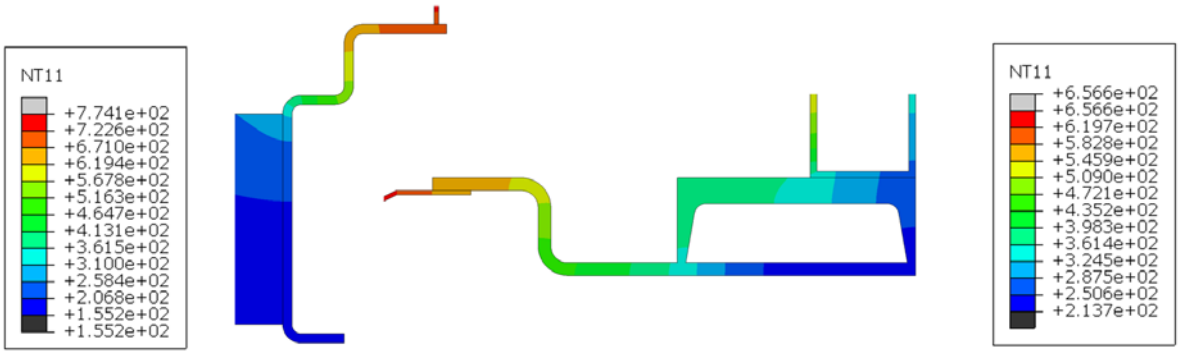

Figure 6-7: Temperature gradients for the bottom side beam and front corner column after a 2-hour standard fire exposure. Values provided in ℃.

Like the back corner column, a relatively small thermal gradient was observed for the top beam. Even though the box section possesses a large void in a similar way to that of the front corner column, the temperature gradient through the cross section was considerably less. The lack of thermal gradient is attributed to the thermal diffusivity of the steel in combination with the relatively small section thickness of the member.

The results of the bottom side beam considered in the heat transfer analysis showed a large thermal gradient as depicted in Figure 6-6. As mentioned in Section 6.2, a specific cross section was investigated by considering the web of the cross beam. Even though the steel is considered to have a high thermal diffusivity, the presence of the cross beam slows down the rate of conductive heat transfer for the portion of the beam below the top fibre of the cross beam. Therefore, the model considered for the bottom side beam is considered a worst-case scenario as the omission of the cross beams will result in a less significant thermal gradient. As mentioned previously, the thermal gradient along the length of the beams and columns is assumed to be uniform for this study. Due to the presence of the cross beams welded to the bottom side beam, it can be argued that a three-dimensional heat transfer model is necessary to capture the non-planar geometry. Considering the large spacings between the cross beams relative to the web thickness, only concentrated areas along the length of the beam will be subject to the thermal gradient highlighted in Figure 6-7. Therefore, it is assumed that a more uniform thermal distribution occurs along most of the length of the bottom side beam where the cross beams are absent. The thermal gradients depicted in Figure 6-7 occur at the time when the maximum differential occurred between the minimum and maximum temperatures

Stellenbosch University https://scholar.sun.ac.za

throughout the 2-hour standard fire exposure.

According to EN 1993-1-2 (2005), the buckling resistance of a column susceptible to thermal gradients should be determined using the same design equations as for a uniformly heated column. The maximum temperature through the cross section of the column is then used to compute the reduced material properties. The maximum temperature material properties introduce a level of conservatism which counterbalances the fact that thermal bowing and shifting of the neutral axis have been neglected in the design equations proposed by the Eurocode. As a result of this conservatism, it was decided to not include the thermal strain which is related to thermal bowing in the finite element models. Depending on the degree of freedom allowed in terms of thermal expansion, thermally induced forces could increase the applied loads which could accelerate the buckling phenomena.

It was decided to use the maximum temperature through the cross section of the columns to determine the adjusted material properties for the constitutive model. A similar approach was adopted for determining the axial and rotational stiffness of the top and bottom beams. Based on previous discussions, the top and bottom beams did not display considerable thermal gradients. As a result, the Young's modulus of the beams was computed based on the maximum temperature. The moment of inertia at ambient conditions was equal to that at elevated temperatures due to the lack of significant thermal gradients and hence no shifting of the neutral axis occurred.

The time-temperature histories for the protected and unprotected models are displayed in Figure 6-8. For an unprotected shipping container, it is evident that the salient elements considered in this study heat up rapidly. Even though radiative and convective heat losses have been accounted for in all the finite element models, the high thermal diffusivity of the steel leads to temperatures which almost coincide with the standard fire gas temperature.

Stellenbosch University https://scholar.sun.ac.za

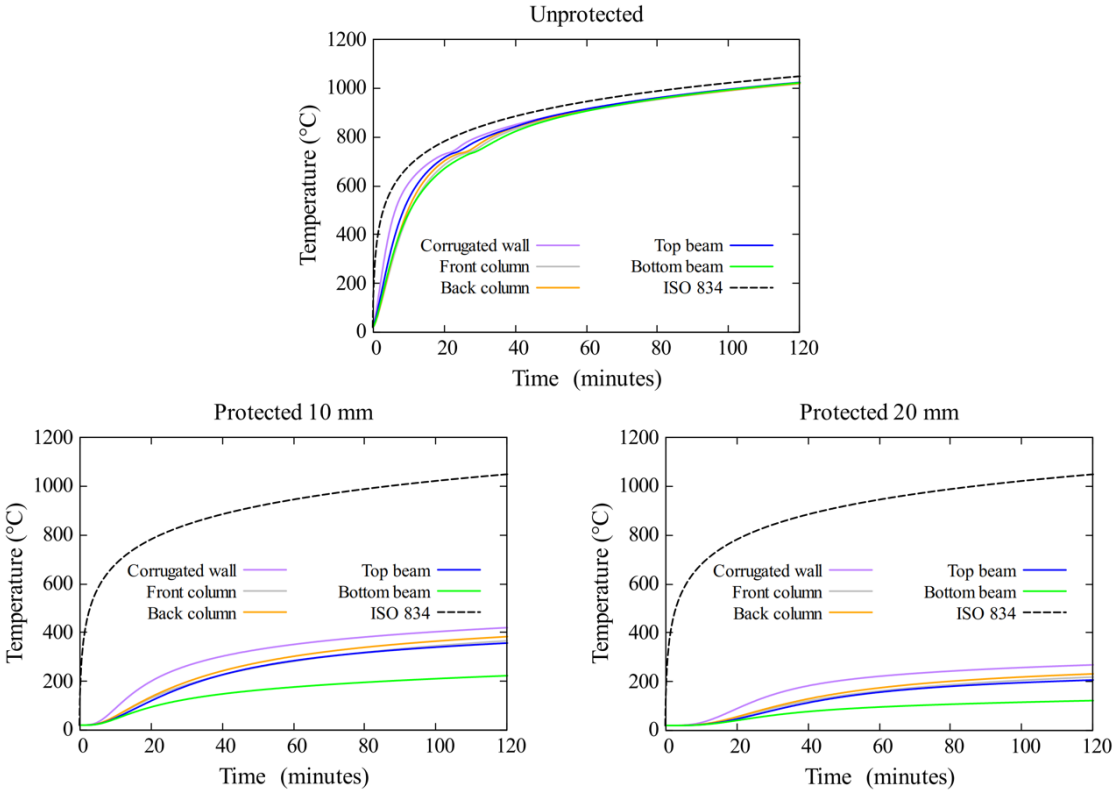

Figure 6-8: Time-temperature histories for the salient features considered in the protected and unprotected models.

The temperatures observed for the protected models are significantly lower, while a definite delay in temperature increase is observed as opposed to the unprotected models. The low thermal diffusivity of the protective boards results in a slow rate of heat transfer through the medium. Only once the temperatures on the unexposed side of the protective board increase will radiation and convection within the void start to increase the temperatures of the beams and columns. Furthermore, the channel brackets conduct heat from the unexposed side of the protective boards which in turn transfer heat to the corrugated sheet via conduction. The thicker protective boards lead to a further reduction in steel temperatures. An extended delay in the start of temperature rise in the steel is apparent as the heat travels through a thicker section. The rate of change in temperature increases on the unexposed side of the protective boards is also less as highlighted by the lower amplitudes for the 20 mm board. These results agree well with the nature of the second order differential equation which describes transient heat transfer as was discussed in the literature.

The discussion on temperature gradients only considered the unprotected heat transfer models. Due to the lower temperatures reflected for the protected models, the presence of temperature gradients was not considered detrimental and therefore further investigation was not necessary.

6.4.2 Elevated temperature buckling results

Using the temperatures determined in the previous section the elevated temperature models are now used to predict the capacity of columns, with updated boundary stiffnesses from the

Stellenbosch University https://scholar.sun.ac.za

adjacent structural elements. Figure 6-9 presents the results of the buckling analyses performed for the back and front corner column for the 2-hour standard fire exposure. In Section 3.3 an imposed loading of 3 kN/m^2 was assumed for the shipping container while the weight of the empty unit was listed as 48.8 kN in Table 3-2. Considering the fire limit state load combination as stated by EN 1991-1-2 (2002), each corner column needs to carry a load of 17.4 kN per overhead storey. Based on this, an additional feature has been added to the graphs below showing the capacity required for a given multistorey configuration assuming regular stacking on the loading blocks.

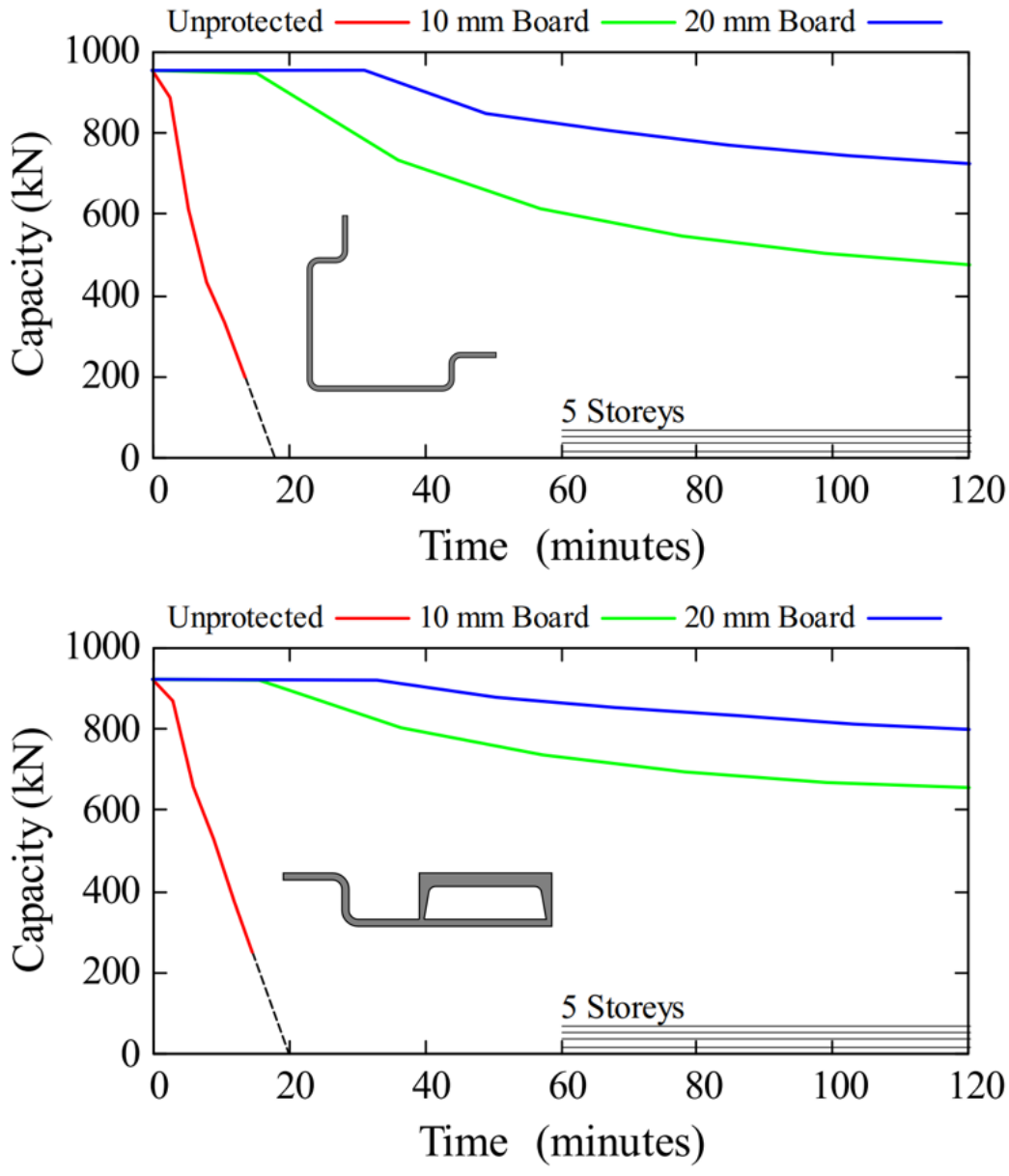

Figure 6-9: Load bearing capacities for the corner columns at elevated temperature.

As mentioned previously, the capacities of the columns were determined at a series of discrete points. As expected, the unprotected models show a rapid decline in load bearing capacity. The back and front corner columns reached a temperature of 600 ℃ at approximately 14 minutes,

Stellenbosch University https://scholar.sun.ac.za

while the capacity beyond this point was considered negligible as highlighted by the dashed line in Figure 6-9. These results agree well with the literature as the vulnerability of unprotected steel structures is once again highlighted. It should be noted that the same level of severity as that of the standard fire is unlikely to occur in a closed container due to lack of ventilation openings. As discussed previously the occurrence of an internal fire pose little threat to the structural stability of a fully closed shipping container (Eberly, 1977). When used as a habitable structure, the time-temperature history of the fire will depend on the ventilation factor and the fuel loads associated with a given container unit.

The effectiveness of the passive fire protection boards is clearly visible from the graphs depicted in Figure 6-9. After a 2-hour standard fire exposure, both the back and front corner columns have significant residual capacity. For the 10 mm thick protective boards, the back and front corner columns showed a reduction in capacity of 50 and 29% respectively. The reduction in capacity for the thicker protective board was lower while values of 24 and 13% were recorded. Even though the capacity at ambient temperature for both columns are similar, it is worth noting that the rate at which the capacity of the back corner column reduces is higher than that of the front corner column. The steel temperature for the back corner column at a given point in time is slightly higher than that of the front corner column as highlighted in Figure 6-8. Even though this is the case, the discrepancy between the capacity reduction rates is unlikely due to this small change in the time-temperature histories. After further investigation it was observed that the load proportionality factor remained approximately constant for an increase in temperature for the front corner column. In contrast to the front corner column, the load proportionality factor for the back corner column decreased as the temperature increased. Figure 6-10 shows the load proportionality factors according to the Riks analyses performed for the duration of the 2-hour standard fire exposure.

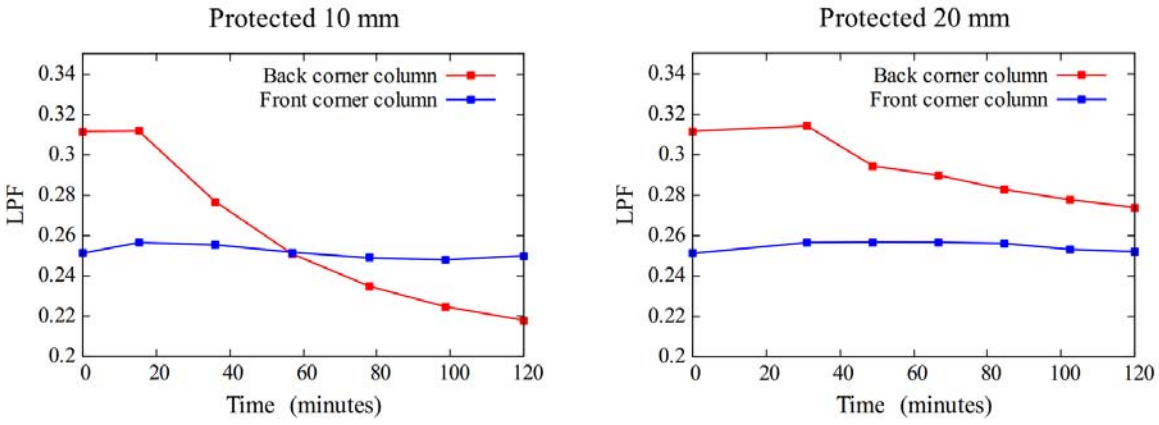

Figure 6-10: Load proportionality factors (LPF) for the Riks analysis showing the reduction in capacity with time for the protected columns.

Based on the results and discussion for the load bearing capacity of the corner columns at ambient temperature, it was clear that the buckling failure mode for the back and front corner columns were considerably different. However, even after a 2-hour standard fire exposure, the axial and rotational stiffness provided by the beams and corrugated wall were still considered to be high in relation to the required demand of modified container homes. As a result, the

Stellenbosch University https://scholar.sun.ac.za

effective length of the front corner column was not reduced significantly. The reduced capacity of the front corner column is therefore mainly due to a reduction in the material properties of the column itself. At ambient conditions, the back corner column was not considered sensitive towards the end conditions of the columns due to local buckling dominating failure. As stated in the literature, the Riks algorithm considers several variables to predict the buckling or collapse behaviour for a given system. The reduction in the load proportionality factor for the back corner column can therefore be due to several reasons. A possible explanation for the reduced load proportionality factor for the back corner column is a sensitivity towards the geometrical imperfection included in the model. Furthermore, the back corner column might be sensitive towards local buckling at elevated temperature.

Based on the results for the protected columns, the concept of using these modular units for both single and multistorey construction is promising with regard to the stability criteria for fire resistance. The study performed by Shuttleworth *et al.*, (2020) highlighted that the use of passive fire protective boards can provide adequate fire resistance to satisfy the necessary insulation requirements. For this study it was assumed that the protective boards remain in place for the entire duration of the 2-hour standard fire and therefore satisfy the integrity requirement based on manufacturers ratings. The discussion to follow introduces some key aspects to consider for multistorey modular construction.

Overall, it appears that column capacity will not be the limiting factor when specifying passive protection for fire resistance, but rather the passive requirements of modified containers will be determined by insulation requirements of walls. However, this may not necessarily be the case when thermal restraint is considered, as will now be addressed.

6.4.3 Multistorey considerations

As mentioned in the literature, the occurrence of thermal strain is generally not considered for simply supported members while this phenomenon needs to be investigated for complex structural buildings. Axial restraint of columns and beams can be influential if a fire is contained within one shipping container assuming the containers above and below remain close to ambient temperature and are able to resist the restraint forces, i.e. boundary conditions remain stiff. One major challenge with respect to axial restraint members is the thermally induced forces which may arise. Axial restraint members are considered detrimental for concrete and masonry buildings while steel buildings generally have enough ductility to prevent a very stiff surrounding environment. If a given multistorey configuration results in a structure allowing no thermal expansion of the corner columns, then according to Equation 2.37, the thermal strain is equal to the stress induced strain but acting in the opposite direction. The force induced in the corner columns, because of thermal expansion, is equal to the force that would be required to cause the same elongation as the thermal effect and can be computed according to Equation 6.1.

$$N_T = \varepsilon_T E_T A \qquad 6.1$$

where:

Stellenbosch University https://scholar.sun.ac.za

ε_T	=	thermal strain at temperature T (°C)
E_T	=	Young's modulus at temperature T (°C)
A	=	cross sectional area of column

The equivalent thermally induced forces for the corner columns have been computed based on the heat transfer results for the 10 and 20 mm thick protective boards. The thermal strain was computed based on the linear expansion coefficient as discussed in Section 2.8.2 by using the maximum temperature through the cross section. Figure 6-11 depicts the thermally induced forces for the duration of the 2-hour standard fire. From these results it is evident that full axial restraint of the corner columns leads to extremely high compressive forces.

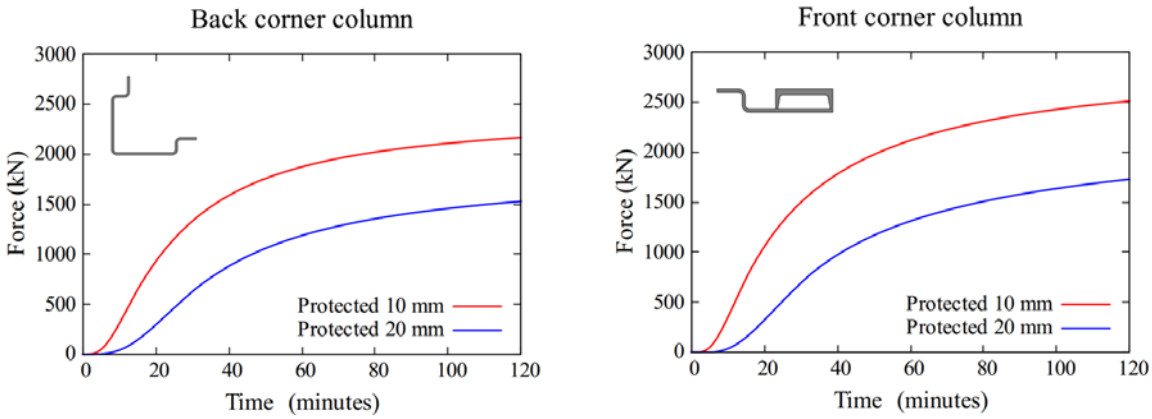

Figure 6-11: Axial restraint forces for the protected configurations considered.

Based on the time-temperature histories determined in the previous section, it is reasonable to assume an equivalent thermal expansion for the corner columns and the corrugated wall. Therefore, the corrugated wall will not provide additional axial restraint to the column during the event of a fire. By allowing some degree of thermal expansion for the corner columns, the thermally induced forces can be reduced significantly. Equation 6.1 can be rearranged to compute the magnitude of thermal expansion required to prevent the occurrence of the thermally induced forces. The values listed in Table 6-3 indicate how much thermal expansion is required for the columns to prevent any thermally induced forces from occurring. By designing connections to allow for a vertical slippage of these magnitudes, restraint forces can be minimized. The results listed below highlight that the rate of thermal expansion for both the back and front corner columns are nearly the same. If one of the columns were to expand at a faster rate, it is possible that bending moments exceeding the flexural capacity of the side beams could arise which could ultimately affect the capacity of the corner columns due to a change in boundary conditions.

Table 6-3: Thermal expansion required to prevent thermally induced forces for protected shipping container.

Time (minutes)	Thermal expansion (mm)			
	Back corner column		Front corner column	
	10mm	20mm	10mm	20mm
30	5.8	2.5	5.4	2.3

Stellenbosch University https://scholar.sun.ac.za

60	9.2	5.0	8.6	4.6
90	10.9	6.2	10.2	5.8
120	11.9	6.9	11.3	6.5

The assumption of full axial restraint is considered over-conservative for the case where container units have only been stacked in the Y-direction (i.e. vertically on top of each other) as seen in Figure 6-13 (a). The significantly smaller imposed loads associated with the habitable container unit considered in this study are considered almost negligible with regard to full axial restraint while the concept of a lightly loaded structure is deemed to be more applicable (Buchanan and Abu, 2017). Based on the imposed loading depicted in Figure 6-9 for multistorey buildings, it is inevitable that thermal expansion of the corner columns will occur during the event of a fire for the configuration shown in Figure 6-13 (a). The rotational and axial stiffnesses computed for the elevated temperature models only considered the beams applicable to the container under consideration. Referring to the multistorey configuration shown in Figure 6-13 (a), the additional restraint provided by the container units above and below the fire exposed container will depend on how these modular units have been connected at the corners. Special connections which allow for movement in the X and Z-directions can be implemented between the loading blocks to allow for thermal expansion of the side and end beams thereby reducing thermally induced forces. Figure 6-12 depicts the loading block of the 20 ft ISO shipping container while connections allowing vertical slip can be installed via the slotted holes. If the connections allow no thermal expansion in the respective lateral directions, the axial and rotational stiffness at the column ends will increase due to the stiffness from the containers above and below assuming connections do not fail.

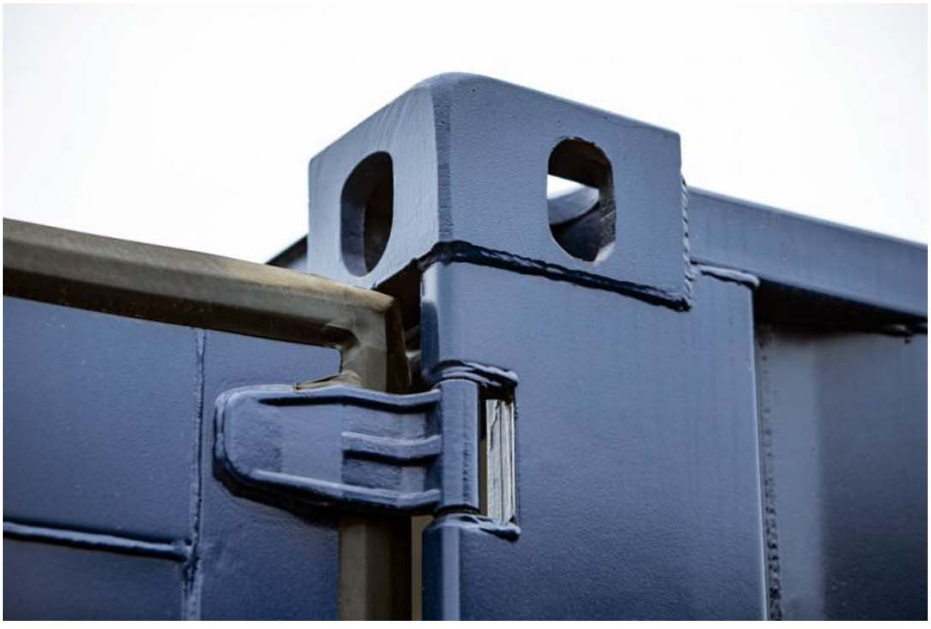

Figure 6-12: Loading block for the 20 ft ISO shipping container with slotted holes visible (Steel Forging, 2018).

The multistorey configuration depicted in Figure 6-13 (b) poses an additional problem with respect to axial restraint as discussed in Section 2.8.1. Assuming the fire to only be contained

Stellenbosch University https://scholar.sun.ac.za

within one container, the columns in adjacent container units will provide some stiffness resulting in thermally induced axial forces in the fire exposed columns. The axial stiffness of the surrounding columns and the temperature differential between the exposed and unexposed columns will ultimately determine the magnitude of the axial force generated. To develop an understanding of the magnitude of the axial force generated for a configuration similar to that shown in Figure 6-13 (b), the equation derived by Ali *et al.* (1997) as discussed in the literature was adopted. The stiffness from the surrounding structure was assumed to be provided by one adjacent corner column at ambient temperature, while the surrounding stiffness could be more than this depending once again on connection behaviour. Figure 6-14 shows the axial force generated in the corner columns after being exposed to the standard fire for 2 hours.

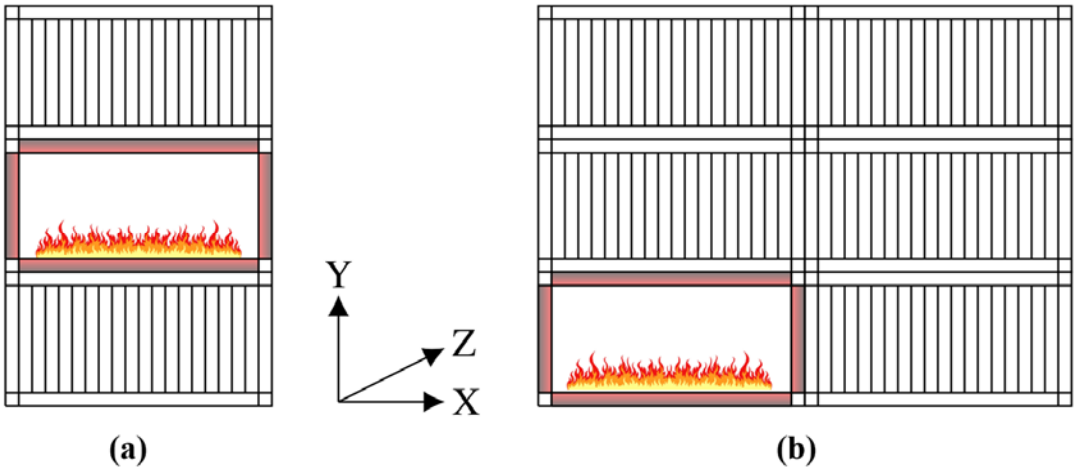

Figure 6-13: (a) Fire in vertically only stacked configuration, (b) Fire in horizontal and vertically stacked configuration.

The axial force generated in the corner columns are high even though the surrounding stiffness has only been based on one corner column. The y-intercept values depicted in Figure 6-14 are smaller than the axial forces shown in Figure 6-11 after a 2-hour standard fire exposure. This discrepancy is explained by the difference in axial stiffness assumed where the axial force generated in Figure 6-14 is based on an infinitely stiff surrounding structure as opposed to stiffness provided by only one column. The benefit of an axially restrained column in fire is clearly visible as the axial force generated in the columns reduce as the imposed loads increase. Unfortunately, the magnitude of the imposed loads considered in Figure 6-14 is unrealistic with regard to the typical loading associated with a multistorey modular building. Based on these results some degree of thermal expansion should be allowed for in design both in the lateral and vertical directions. It is highly unlikely that connections allowing no movement will be able to resist the high axial forces generated in the corner columns. If the connections are to fail before buckling is induced within the columns, thermal expansion will be permitted to some extent thereby relieving the axial force generated. A connection failure between the container units in the event of a fire may lead to partial collapse while further research on this topic is required.

Stellenbosch University https://scholar.sun.ac.za

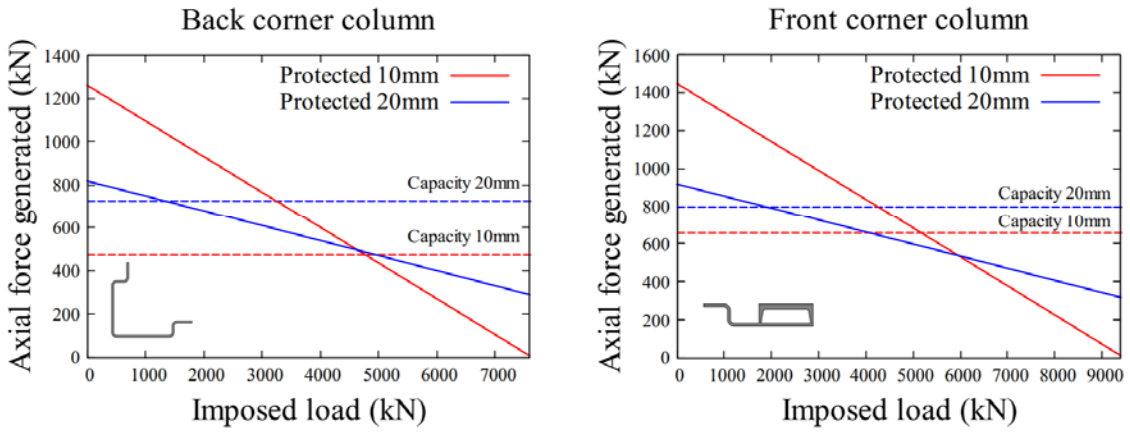

Figure 6-14: Axial force generated after a 2-hour standard fire exposure for the corner columns, also showing the capacity of the columns after a 2-hour fire.

6.5 Conclusion

This chapter presented a detailed discussion on the development and analysis procedures for determining the capacity of the corner columns for the 20 ft ISO shipping container when exposed to elevated temperature. Both protected and unprotected models were developed, where the protected models considered a generic passive board system with thermal properties corresponding to average tabulated values. Initially heat transfer models were developed to determine the time-temperature histories of the beams and columns exposed to a 2-hour standard fire. The results of the heat transfer models where then used to determine the reduced axial and rotational restraint of the beams to be applied at the column ends while the material definition was adjusted for the corner columns.

The maximum and minimum temperatures through the beams and columns were recorded for the duration of the standard fire exposure so that the thermal gradients could be investigated. For the beams and the back corner column, the thermal gradients were insignificant due to the high thermal diffusivity of the thin-walled steel sections. The only element which showed a considerable thermal gradient through the section was the front corner column. The front corner column had a slightly thicker section than the other elements considered while the exposed surface was small in relation to the unexposed surface meaning that the heat had to travel a longer distance to reach certain unexposed areas. Based on the model proposed by EN 1991-1-2 (2002), it was decided to use the maximum temperature through the cross sections of the elements to determine the necessary parameters for the buckling analysis of the corner columns.

The time-temperature histories of the salient features for the unprotected shipping container highlighted the vulnerability of an unprotected shipping container as the temperatures were almost equal to that of the gas temperature considered for the duration of the 2-hour standard fire. The inclusion of the passive fire protective boards reduced the temperatures of the salient features significantly emphasising the importance of using passive fire protection to protect a steel structure during the event of a fire.

Stellenbosch University https://scholar.sun.ac.za

For the unprotected models, the capacities of the corner columns were considered negligible after 14 minutes as the assumptions of the boundary condition behaviour beyond 600 ℃ can no longer be relied upon. For the 10 mm thick boards, the back and front corner columns showed a reduction in capacity of 50 and 29% respectively after a 2-hour standard fire exposure. For the 20 mm thick board, the reduction in capacity was even less as values of 24 and 13% were recorded. To prevent high thermally induced axial forces from occurring in the corner columns, it is necessary to allow for some degree of thermal expansion when considering multistorey construction. Assuming the integrity criteria of the passive fire protective boards do not fail, and that thermal expansion of the corner columns is permitted, the corner columns are still considered to have sufficient load bearing capacity for the design loads associated with a multistorey modular structure.

Overall, the capacity demands of modified shipping container columns are low and the columns typically have significant additional capacity. Wall insulation requirements are likely to govern passive protection requirements, rather than to ensure structural strength. If columns are fully restrained high forces are induced, although if connections are designed to allow slippages of the magnitudes calculated in this chapter, restraint forces will be dissipated for most structural geometries.

Stellenbosch University https://scholar.sun.ac.za

7 Conclusions and recommendations

7.1 General overview

The main objective of this thesis was to investigate the structural capacity of the load bearing elements for a modified shipping container at ambient conditions, while the structural capacity at elevated temperature was also investigated. Due to an advancement in modular construction, the work performed in this thesis serves as a steppingstone for developing standards to ensure the safe design of modular structures both single and multistorey. Finite element models including buckling and heat transfer analyses were developed to gain an understanding of the reduction in capacity for a weakened container unit. The objectives of this thesis, as discussed in Chapter 1, have been addressed according to the discussions below.

An extensive literature review was conducted in Chapter 2 to gain an understanding of the behaviour of steel structures at ambient conditions with specific focus on failure modes of compression elements applicable to the 20 ft ISO shipping container. A background on the behaviour of steel structures in fire as well as important heat transfer principles were discussed to aid the understanding by which heat is transferred according to the different mechanisms for an unprotected and protected shipping container unit.

Chapter 3 identified possible modes of weakening due to modifications of the shipping container unit while the details regarding loads applied to the walls of containers, was also introduced. As this thesis focused solely on load bearing elements, and in this case the corner columns, one of the weakening mechanisms considered was the removal of the side and end walls. With respect to load paths opposing the original design, the scenario where a concentrated point load applied to the top beam of the shipping container needed further investigation. Chapter 3 also identified three studies which included analytical and numerical methods applicable to the work performed in this study. The results of these studies were validated according to finite element models developed in ABAQUS.

Finite element models were developed in Chapter 4 to determine the capacity of the corner columns for both a modified and unmodified shipping container unit at ambient conditions. A detailed discussion on the development of these models was provided including the material definition applicable to the 20 ft ISO shipping container. A sensitivity analysis was performed on parameters considered relevant to the accuracy of the predicted capacities of the corner columns. These parameters included mesh size, influence of rounds and fillets, boundary end conditions, imperfection magnitudes and number of springs needed to model lateral restraint. Based on the findings of the sensitivity analysis, final models were proposed followed by a comparison between the numerical and analytical results.

The load bearing capacity of the side wall due to mid-span loads, as mentioned previously, was investigated in Chapter 5. Once again, the development of these models was discussed followed by a brief sensitivity analysis on the effect of the members surrounding the corrugated side wall. The numerical results were compared to the analytical formulations as outlined in

Stellenbosch University https://scholar.sun.ac.za

the literature.

The penultimate chapter included the development of the elevated temperature models to predict the capacity of the corner columns when exposed to a 2-hour standard fire. Four heat transfer models were developed, namely those for the back and front corner columns as well as the top and bottom beams. The results of the heat transfer analyses were discussed with specific focus on thermal gradients. The time-temperature histories obtained from the results of the heat transfer analyses were used to determine the adjusted material properties and boundary conditions to predict the capacity of the corner columns for the duration of a 2-hour standard fire.

7.2 Project findings

The findings of this thesis are summarised in this section. This includes the numerical results for the weakened mechanisms highlighted in Chapter 3 at ambient temperature as well as the results for the elevated temperature scenario considered in this work. Only the most important findings are highlighted here, while the reader is encouraged to refer to the respective chapters for an in-depth discussion.

7.2.1 Preliminary verification results

The preliminary verification studies considered in Chapter 3 included the lateral rigidity of a modular side wall by Yu and Chen (2018), shear buckling behaviour of a plate girder by Sayed-Ahmed *et al.* (2003) as well as the development of insulation time reference curves for shipping containers exposed to fire (Shuttleworth *et al.*, 2020). Finite element models were developed in ABAQUS for each of the above-mentioned studies to validate the different modelling procedures applicable to the work in this thesis. The numerical results were promising as they not only agreed well with those of the authors, but also agreed well with the analytically predicted values.

7.2.2 Results for corner column capacities at ambient conditions

The finite element models developed to predict the capacity of the corner columns considered both a laterally restrained and a laterally unrestrained model where the presence of the corrugated sheeting was neglected for the latter. The eigenvalue buckling analyses performed served as an input to model the geometric imperfections considered for the nonlinear elastic buckling analyses.

For the sensitivity analysis, elements with a size of 12.5 mm were deemed satisfactory as a finer mesh resulted in negligible difference in the load bearing capacity of the corner columns. The following parameter investigated was the influence of the rounds and fillets. The back corner column was more sensitive to the inclusion of the rounds and fillets as opposed to the front corner column. A reduction in load bearing capacity of 11% was observed for the back corner column while a reduction of only 3% was observed for the front corner column. The higher reduction for the back corner column was attributed to the occurrence of local buckling

Stellenbosch University https://scholar.sun.ac.za

of the flanges while global buckling about the weak axis was dominant for the front corner column.

From a theoretical buckling point of view, the effect on the load bearing capacity of the corner columns needed to be investigated with respect to the end conditions. Three cases were considered, namely fixed, partially fixed and a pinned connection. Opposed to the results described for the previous parameter, the front corner column showed a higher drop in load bearing capacity than the back corner column. Intuitively this makes sense since local buckling is dependent on the cross-sectional geometry of the column, while global buckling is highly dependent on the rotational and axial restraint provided at the ends of the column.

Both the back and front corner columns were sensitive with regard to the geometrical imperfections included in the model. Using the 1st eigenmode to predict the geometrical imperfections in conjunction with a scaling factor of L/250 led to the most severe reduction in load bearing capacity of the corner columns. A scaling factor of L/250 was considered to be overly conservative, and therefore the geometrical imperfection model proposed by EN 1993-1-2 (2005) was implemented when developing the final models.

The final parameter investigated served merely as a convergence study to determine how many springs are needed to accurately model the lateral restraint provided by the corrugated panel. Based on the results, it was decided to use 20 axial springs along the length of the columns.

The numerical results for the unmodified corner columns were within 10 % of the capacity values listed by ISO 668 (1995). The capacities for the back and front corner columns reduced by 20 and 34% respectively. The absence of the corrugated side and end walls do not influence the load bearing capacity of the corner columns as severely in the context of using the 20 ft ISO shipping container for modular buildings. The significantly smaller imposed loads within the habitable container unit reduces the payload to such an extent that the concept of multistorey construction is reasonable assuming the load transfer between the units do not oppose the original design. The lateral stiffness of the corrugated side and end walls have been used to model the correct effective length of the columns to predict the change in load bearing capacity of the corner columns. As shown by Yu and Chen (2018) in their study on the rigidity of corrugated plate sidewalls, the removal of the corrugated side and end walls reduces the lateral rigidity significantly and therefore some form of bracing needs to be installed to ensure adequate capacity to resist horizontal loads.

7.2.3 Results for different load paths

The finite element model developed to investigate the capacity due to mid-span loads, as mentioned in the general overview section, considered the sidewall configuration of the 20 ft ISO shipping container. Two models were developed for each sidewall configuration, one with the standard beams and columns in place, also referred to as the unstiffened case, and another with stiffer surrounding elements.

For the unstiffened model, the buckling behaviour was found to be more representative of

Stellenbosch University https://scholar.sun.ac.za

compression buckling as opposed to shear buckling. Hence, the numerical results were verified according to analytical formulations outlined in the literature for compression members. The numerical capacity for the eigenvalue buckling analysis was 317 kN. The analytically predicted capacity was lower due to a conservative effective length assumed for the pitch configurations. The inclusion of plasticity in the unstiffened model highlighted failure of the top side beam as the capacity reduced significantly to a value of 171.7 kN. Even though these capacities are considered high in the context of modular construction, further models were proposed with the aim of strengthening the sidewall for the loading considered. For the stiffened case, a series of models were developed with varying flange and stiffener thickness combinations. The deflected shapes of the eigenvalue buckling analyses for the stiffer models developed were in better agreement with shear buckling behaviour. The numerical capacities for the eigenvalue buckling analyses ranged between 1099 and 1561 kN while global shear buckling was evident. Even though these values were higher than the analytically predicted capacity of 1020 kN, the capacity is highly dependent on the stiffness of the surrounding members which is not explicitly accounted for in the shear buckling formulae used in this study.

Further models were produced to include the plasticity of the material as well as the geometric imperfections according to EN 1993-1-5 (2006). The observed reductions in capacities were relatively small and ranged from 4 to 11%. The reason for this was based on the deflected shapes of the results as the dominant mode of failure was global shear buckling due to the high slenderness of the corrugated web. Even though a small reduction in capacity occurred when plasticity was included in the models, the mode of failure was found to be sensitive towards the thickness of the stiffeners. For a 10 mm thick stiffener, crippling of the web and stiffener occurred while stiffeners with thicker sections induced web buckling in the corrugated panel as was the case for the 40 mm thick stiffener.

Although the analytical formulae used in this work to predict the shear buckling capacities led to conservative results for the stiffened model, these formulae need to be adapted to account for the stiffness of the surrounding elements as well as the slenderness associated with the 20 ft ISO shipping container.

7.2.4 Results for corner column capacities at elevated temperature

The capacity of the corner columns at elevated temperature were determined for both a protected and unprotected case. The protected models considered passive fire protection boards with thicknesses of 10 and 20 mm respectively.

Due to the thin-walled nature of the salient elements of the shipping container, large thermal gradients were not encountered for the beams, sheeting and the back corner column. The lack of temperature gradients observed for these elements can also be attributed to the fact that steel has a high thermal diffusivity meaning that heat travels from the exposed side to the unexposed side relatively quickly. The thermal distribution of the front corner column highlighted significant thermal gradients. The reason for this is due to the small, exposed surface area in relation to the unexposed surface area. As a result, heat must travel along the length of the section to reach certain areas of the unexposed surface as opposed to only through the thickness

Stellenbosch University https://scholar.sun.ac.za

of the element. Based on the literature, the front corner column could very well be subjected to thermal bowing. The model proposed by EN 1991-1-2 (2002) was used to determine the adjusted mechanical properties based on the maximum temperature through the cross-section. This approach has been deemed conservative as it compensates for the omission of thermal bowing and shifting of the neutral axis in the numerical models developed.

The vulnerability of an unprotected shipping container was first highlighted in this study by the time-temperature histories for the unprotected models which nearly coincided with that of the standard fire curve. The rate at which the temperatures of the salient elements increased in this study was reduced significantly by the inclusion of the passive fire protective boards. This led to a less severe reduction in the Young's modulus and the yield strength of the steel elements and ultimately a higher capacity for the main load bearing elements at a given point in time relative to the unprotected models.

For the unprotected corner columns, the residual capacities after 14 minutes were considered negligible as the steel temperatures exceeded 600 ℃. For the 10 mm thick protective boards, the load bearing capacity of the back and front corner columns reduced by 50 and 29% after being exposed to a 2-hour standard fire. As expected, these reductions were even less for the 20 mm thick protective boards as the capacities only dropped by 24 and 13%. Based on these findings, the protected corner columns had sufficient capacity to resist the imposed loading from multiple container units above supporting the idea of multistorey construction assuming the containers are stacked on their corners. It is not possible to assume that the protective boards will never fail with regard to integrity especially considering the unpredictable nature of a fire. The worst-case scenario namely the unprotected models served as an example of what could happen if the protective boards were to fail during the event of a fire.

The capacities computed as discussed above where only compared to the imposed loading and own weight of the container units. However, thermally induced axial forces also need to be accounted for in design. Analytical methods outlined in the literature were used to investigate the effect of axially restraint columns. For a fully restraint corner column, the axial force that would be generated after a 2-hour standard fire exposure would lead to buckling of the columns. Connections between shipping containers in multistorey configurations need to be designed in such a way to allow for thermal expansion, thereby reducing the axial force generated in the corner columns.

7.3 Recommendations and future research

An extensive study has been conducted in this thesis on the structural capacity of load bearing elements for both a modified and unmodified 20 ft ISO shipping container. Several finite element models were created to gain a good understanding of the behaviour of such elements in modified shipping container buildings for ambient and elevated temperature conditions. Due to a lack of design guidance for modular construction, a substantial amount of further research is needed while this thesis only covered certain aspects.

This thesis only considered numerical modelling and analytical formulations. Experimental

Stellenbosch University https://scholar.sun.ac.za

testing would be useful to further validate the results obtained in this thesis especially for the elevated temperature models.

The results of the buckling behaviour for the corrugated sidewall showed that the capacity is dependent on several factors which are currently neglected in analytically derived formulae. Further research is required in conjunction with extensive parametric studies so that new formulae can be derived to accurately predict the capacity of the side wall assembly when a load is applied to the top side beam.

For the elevated temperature analyses, the ISO 834 standard fire was chosen as the design fire. Depending on the extent to which the shipping containers are modified with respect to ventilation openings, it is worthwhile investigating the behaviour of the corner columns when subjected to a parametric design fire curve as outlined in EN 1991-1-2 (2002).

In the literature it was mentioned that two of the most dangerous failure mechanisms in steel structures at both ambient and elevated temperature is that of connection and compression member failure. This thesis only considered the capacity of compression members while a few recommendations were made with regard to connection behaviour between shipping container units in a multistorey configuration when exposed to fire. Further numerical modelling is required on this topic specifically to answer the question as to whether connection failure will lead to collapse of such a structure.

Stellenbosch University https://scholar.sun.ac.za

Bibliography

Absolute Containers. (2021), "Container Buildings", available at: https://absolutecontainers.co.za/products/mobile-solutions/container-buildings/.

Agarwal, A., Choe, L. and Varma, A.H. (2014), "Fire design of steel columns: Effects of thermal gradients", *Journal of Constructional Steel Research*, Elsevier Ltd, Vol. 93, pp. 107–118.

Ali, F., Sirnms, I. and O'connor, D. (1997), "Behaviour Of Axially Restrained Steel Columns During Fire", *Fire Safety Science*, Vol. 5, pp. 1105–1116.

Amouzegar, H., Amirzadeh, B., Zhao, X. and Schafer, B.. (2015), "Statistical analysis of the impact of imperfection modes on collapse behaviour of cold-formed steel members", *Annual Stability Conference Structural Stability Research Council*, pp. 1–15.

Australian Steel Institute. (2005), "Structural Fire Engineering", available at: https://www.steel.org.au/focus-areas/steel-and-fire/structural-fire-engineering/ (accessed 21 May 2020).

Bathe, K.J. (1996), *Finite Element Procedures*, *Englewood Cliffs New Jersey*, 2nd ed., United States of America, available at: http://www.amazon.com/Finite-Element-Procedures-Part-1-2/dp/0133014584.

Becker, R. (2002), "Structural behaviour of simple steel structures with non-uniform longitudinal temperature distributions under fire conditions", *Fire Safety Journal*, Vol. 37, pp. 495–515.

Beer, F.P., Johnston, E.R., DeWolf, J.T. and Mazurek, D.F. (2014), "Section 11.13 'Deflections by Castigliano's Theorem'", *Mechanics of Materials*, 7th ed., McGraw-Hill Education.

Bisby, L., Gales, J. and Maluk, C. (2013), "A contemporary review of large-scale non-standard structural fire testing", *Fire Science Reviews*, Vol. 2 No. 1.

Buchanan, A.H. and Abu, A.K. (2017), *Structural Design for Fire Safety*, Second., Wiley, New Zealand.

Cadoni, E., Forni, D., Gieleta, R. and Kruszka, L. (2018), "Tensile and compressive behaviour of S355 mild steel in a wide range of strain rates", *The European Physical Journal*, Vol. 43, pp. 29–43.

Conor, J. and Faraji, S. (2013), "Fundamentals of Structural Engineering", Vol. 1 No. 1, pp. 32–122.

Dassault-Systemes. (2020), "Abaqus Analysis User's Manual", *Dassault Systemes Simulia Corporation*.

De Koker, N. (2021), *The Finite Element Method - Mathematical Foundations and Computer Implementation*, Stellenbosch University, available at:https://doi.org/10.1007/978-3-642-23099-8__2.

Stellenbosch University https://scholar.sun.ac.za

Delcourt, D. and Garis, L. (2014), "Intermodal Shipping Container Fire Safety", No. July 2014.

Delgado Ojeda, O., Maljaars, J. and Abspoel, R. (2016), "Fire exposed steel columns with a thermal gradient over the cross-section", *Thin-Walled Structures*, Elsevier, Vol. 98, pp. 103–110.

Ding, Y., Deng, E., Zong, L., Dai, X., Lou, N. and Chen, Y. (2017), "Cyclic tests on corrugated steel plate shear walls with openings in modularized-constructions", *Journal of Constructional Steel Research*, Elsevier Ltd, Vol. 138, pp. 675–691.

Dinis, P.B. and Camotim, D. (2006), *On the Use of Shell Finite Element Analysis to Assess the Local Buckling and Post-Buckling Behaviour of Cold-Formed Steel Thin-Walled Members*, *III European Conference on Computational Mechanics*, Springer Netherlands, Dordrecht.

Driver, R.G., Abbas, H.H. and Sause, R. (2006), "Shear Behavior of Corrugated Web Bridge Girders", *Journal of Structural Engineering*, Vol. 132 No. 2, pp. 195–203.

Drysdale, D. (2011), "An Introduction to Fire Dynamics", *An Introduction to Fire Dynamics*, Vol. 3 No. 1.

Eberly, R. (1977), "Fire Performance Of Intermodal Shipping Containers", *Department of Transportation United States Coast Guard*, Vol. 1 No. 1, pp. 1–27.

ECCS TC3. (2001), "Model Code on Fire Engineering", *European Convention for Constructional Steelwork*, Brussels.

EL-Metwally, A.. and Loov, R.. (1999), "Composite Prestressed Concrete Beams with Courrugated Webs", *Proceedings of the Annual Conference of the Canadian Society for Civil Engineers (CSCE)*, Vol. 1, pp. 305–314.

Elgaaly, M. (1998), "Thin steel plate shear walls behaviour and analysis", *Thin-Walled Structures*, Vol. 32 No. 1–3, pp. 151–180.

Ellobody, E. (2014), "Finite Element Analysis of Steel and Steel-Concrete Composite Bridges", *Finite Element Analysis and Design of Steel and Steel-Concrete Composite Bridges*.

EN 10025-5:2019. (2019), "Hot rolled products of structural steel Technical delivery conditions for structural steels with improved atmospheric corrosion resistance", *The European Union*, pp. 24–35.

EN 1990:2002+A1. (2011), "Eurocode - Basis of structural design", *The European Union*, Vol. 1 No. 2005.

EN 1991-1-2. (2002), "Eurocode 1: Actions on structures - Part 1-2. General actions - actions on structures exposed to fire", *The European Union*.

EN 1993-1-1. (2005), "Eurocode 3: Design of steel structures - Part 1-1: General rules and rules for buildings", *The European Union*, Vol. 1.

EN 1993-1-2. (2005), "Eurocode 3: Design of steel strucutres - Part 1-2: General rules -

Stellenbosch University https://scholar.sun.ac.za

Structural fire design", *The European Union*, Vol. 1.

EN 1993-1-5. (2006), "Eurocode 3: Design of steel structures - Part 1-5: Plated structural elements", *The European Union*, Vol. 1.

EN 1995-1-1. (2004), "Eurocode 5: Design of timber structures - Part 1-1: General - Common rules and rules for buildings", *The European Union*, Vol. 1.

Eröz, M., White, D.W. and DesRoches, R. (2008), "Direct Analysis and Design of Steel Frames Accounting for Partially Restrained Column Base Conditions", *Journal of Structural Engineering*, Vol. 134 No. 9, pp. 1508–1517.

European Convention for Constructional Steelwork (ECCS). (1995), *European Recommendations for the Publication of Metal Sheeting Acting as a Diaphragm.*, Brussels.

Faegh, S.S. and Fanaie, N. (2018), "Comparative Study on Shear Strength of Corrugated Steel Plate Shear Walls", *Conference: 3rd International Conference on Steel & Structure*, No. December, available at:https://doi.org/COI code: ISSS09_013.

Fazzolari, F.A. (2017), "Sandwich Structures", *Stability and Vibrations of Thin Walled Composite Structures*.

Feng, M., Wang, Y.C. and Davies, J.M. (2003), "Thermal performance of cold-formed thin-walled steel panel systems in fire", *Fire Safety Journal*, Vol. 38 No. 4, pp. 365–394.

Franssen, J.. and Vila Real, P. (2012), "Actions on structures; Part 1-2: General actions - Actions on structures exposed to fire", *Fire Design of Steel Structures Eurocode 1*, No. 1, pp. 24–27.

Frost, R. (2018), "The Importance of Structural Steel in Constructing Buildings", *Construction 21 International*, available at: https://www.construction21.org/articles/h/the-importance-of-structural-steel-in-constructing-buildings.html.

Galambos, T.. (1988), *Guide to Stability Design Criteria for Metal Structures*, John Wiley and Sons, New York, USA.

GDV. (2021), "Container Handbook - Cargo loss prevention information from German marine insurers", available at: https://www.containerhandbuch.de/chb_e/stra/index.html?/chb_e/stra/stra_02_03_01.html.

Gil, H. and Lee, H.-E. (2005), "Shear buckling strength of trapezoidally corrugated steel webs for bridges", *Transportation Research Board - 6th International Bridge Engineering Conference: Reliability, Security, and Sustainability in Bridge Engineering*, No. February 2017, pp. 473–480.

Giriunas, K., Sezen, H. and Dupaix, R.B. (2012), "Evaluation , modeling , and analysis of shipping container building structures", *Engineering Structures*, Elsevier Ltd, Vol. 43, pp. 48–57.

Gross, J.L., Phan, L.T., Therese, P.M. and Morgan, J.H. (2010), "Summary of best practice

Stellenbosch University https://scholar.sun.ac.za

guidelines for structural fire resistance design of concrete and steel buildings", *NIST Technical Note 1681*, available at:https://doi.org/10.1061/41130(369)215.

Gyprock. (2017), "Rhinoboard firestop", available at: https://www.gyproc.co.za/products/walls/rhinoboard-firestop-0.

Harish, A. (2020), "Finite Element Method - What Is It? FEM and FEA Explained", *Simscale*, Vol. 1, available at: https://www.simscale.com/blog/2016/10/what-is-finite-element-method/.

Hibbeler, R.C. (2017), *Mechanics of Materials, 10th Edition*, Pearson.

Hibbeler, R.C. (2018), *Structural Analysis, 10th Edition*, Pearson.

Hibbitt, H.D. (1984), "ABAQUS / EPGEN – A GENERAL PUR- POSE FINITE ELEMENT CODE WITH EMPHASIS ON NONLINEAR APPLI- CATIONS", *Structural Integrity Research of the Electric Power Research Institute*.

Home Containers. (2019), "Building houses in containers", available at: https://home-containers.com/en/building-houses-in-containers/.

Hosseinpour, E., Baharom, S. and Yadollahi, Y. (2015), "Evaluation of steel shear walls behavior with sinusoidal and trapezoidal corrugated plates", *Advances in Civil Engineering*, No. April, available at:https://doi.org/10.1155/2015/715163.

Howard, B.C. (2017), "45 Amazing Homes and Offices Built from Shipping Containers", *Popular Mechanics*, available at: https://www.popularmechanics.com/home/how-to/g172/shipping-container-homes-460309/.

Hurley, M.J., Gottuk, D., Jr., J.R.., Harada, K., Kuligowski, E., Puchovsky, M., Torero, J.L., *et al.* (2016), *SFPE Handbook of Fire Protection Engineering*, New York.

Islam, M., Ali, R. Bin and Billah, M. (2019), "Strengthening Techniques of Steel Structure : An Overview", *World Scientific News*, Vol. 118, pp. 181–193.

Ismail, R.E.. and Hesham, A.Z.E.D. (2015), "Effect of the first local buckling mode on the behaviour of steel I-section beam-columns", *Alexandria Engineering Journal*, No. November 2000.

ISO. (1999), "Iso 834 fire-resistance tests", *Elements of Building Construction*, Vol. 1–12, p. 13.

ISO 668. (1995), *ISO 668:1995 Series 1 Freight Containers-Classification, Dimensions and Ratings*, International Organization for Standarization, Geneva (Switzerland).

Kirby, B.. and Preston, R.. (1988), "High temperature properties of hot-rolled structural steels for use in fire engineering design studies", *Fire Safety Journal*, Vol. 13, pp. 27–37.

Laizhou Dingrong Steel Structure CO. LTD. (2019), "Container Homes Houses", available at: https://containerhomeshouses.en.made-in-china.com/product/tSUxRwrdgOpE/China-Prefab-Flat-Pack-Mobile-Modular-Steel-Shipping-Container-Frames.html.

Stellenbosch University https://scholar.sun.ac.za

Lallanilla, M. (2019), "The New Wave of Shipping Container Homes", *The Spruce*, available at: https://www.thespruce.com/new-wave-shipping-container-homes-1708537.

Liu, Y., Chen, Z., Liu, J., Bai, Y., Zhong, X. and Wang, X. (2020), "Thin-Walled Structures Lateral stiffness evaluation on corner-supported thin walled modular steel structures", *Thin-Walled Structures*, Elsevier Ltd, Vol. 157 No. June, pp. 1–18.

MagnaStruct. (2019), "MagnaBoard Wall Panel - Technical Specifications", Cape Town, available at: https://www.magnastruct.co.za/technical-data.

Marx, H. (2018), *Thermal Behaviour of a Novel Cellular Beam Structural System in Fire*, available at: https://scholar.sun.ac.za.

Megahed, M. (2015), *Buckling of Pretwisted Steel Columns*, *Master of Science in Civil Engineering*, American University of Sharaj.

Midwest Steel. (2016), "The Importance of Steel in Today's Construction", available at: https://www.midweststeel.com/about/news/The-Importance-of-Steel-in-Todays-Construction_AE21.html.

Narang, V. (2005), "Heat transfer analysis in steel structures", *Worcester Polytechnic Institute: Civil and Environmental Engineering*, pp. 1–173.

Nemer, S. and Papp, F. (2021), "Influence of imperfections in the buckling resistance of steel beam-columns under fire", *Pollack Periodica*, Vol. 16 No. 2, pp. 1–6.

Nseir, J., Hayeck, M., Saloumi, E. and Boissonnade, N. (2016), "Influence of imperfections on the local buckling response of hollow structural shapes", *Proceedings of the Annual Stability Conference Structural Stability Research Council*, Orlando, Florida.

Paul, A. (2014), "Buckling of Columns - Euler Theory for Elastic Buckling", available at: https://civildigital.com/buckling-columns-euler-theory-elastic-buckling/.

Pitts, D.. and Sissom, L.. (1977), *Schaum's Outline Series: Theory and Problems of Heat Transfer*, McGraw Hill, New York.

Promat. (2016), "PROMATEC-H MATRIX ENGINEERED MINERAL BOARD - Product properties", available at: https://etexassets.azureedge.net/-/dam/promat-promatect-h-datasheet-en-au/pi9192/original/promat-promatect-h-datasheet-en-au.pdf?v=-230113597.

S Jones Containers. (2021), "How Many Shipping Containers Can You Stack", available at: https://www.sjonescontainers.co.uk/contact-us/.

SABS. (2005), "SANS 10177-2", *Fire Testing of Materials, Components, and Elements Used in Buildings*, Vol. Pretoria No. Part 2: Fire resistance for buildings elements.

SABS. (2011a), "The structural use of steel", *SANS 10162-1:2011*, Vol. Pretoria No. Part 1: Limit-states design of hot-rolled steelwork.

SABS. (2011b), "Basis of structural design and actions for buildings and industrial structures", *SANS 10160-1:2011*, Vol. 1.1, pp. 36–38.

Stellenbosch University https://scholar.sun.ac.za

Sadiq, H., Wong, M.B., Tashan, J., Al-Mahaidi, R. and Zhao, X.L. (2013), "Determination of steel emissivity for the temperature prediction of structural steel members in fire . A numerical method , with which experimental results were processed , was adopted to", *Journal of Materials in Civil Engineering*, Vol. 25 No. 2, pp. 167–173.

Sadowski, A.J. and Rotter, J.M. (2013), "Solid or shell finite elements to model thick cylindrical tubes and shells under global bending", *International Journal of Mechanical Sciences*, Vol. 74 No. May, pp. 143–153.

Sayed-Ahmed, E.Y., Hancock, G.J., Bradford, M.A., Wilkinson, T.J., Uy, B. and Rasmussen, K.J.R. (2003), "Girders with corrugated steel webs: buckling modes and numerical modelling", *Advances in Structures*, Vol. 2, available at: http://gateway.webofknowledge.com/gateway/Gateway.cgi?GWVersion=2&SrcAuth=ORCID&SrcApp=OrcidOrg&DestLinkType=FullRecord&DestApp=WOS_CPL&KeyUT=WOS:000184437600114&KeyUID=WOS:000184437600114.

Schafer, B. and Peköz, T. (1996), "Geometric imperfections and residual stresses for use in the analytical modeling of cold-formed steel members", *International Specialty Conference on Cold-Formed Steel Structures: Recent Research and Developments in Cold-Formed Steel Design and Construction*, pp. 649–664.

Seaburg, P.A. and Carter, C.J. (2003), "Torsional Analysis of Structural Steel Members", United States of America.

Secer, M. and Uzun, E.T. (2017), "Corrosion Damage Analysis of Steel Frames Considering Lateral Torsional Buckling", *Procedia Engineering*, Vol. 171 No. 1, pp. 1234–1241.

Shuttleworth, S.M., De Koker, N. and Walls, R.S. (2020), "Fire Technology Fire Resistance Time Reference Curves for Specifying Passive Protection for Modular Structures from Shipping Containers Fire Resistance Time Reference Curves for Specifying Passive Protection for Modular Structures from Shipping Containers", *Fire Technology*, Vol. 1 No. 1.

Singamas. (2018), "Technical specification for 20'x8'x8'6'' ISO 1CC type steel dry cargo container", *Singamas Management Services Ltd*.

Skotny, L. (2019), "Linear vs nonlinear buckling explained", *Enterfea*, available at: https://enterfea.com/linear-vs-nonlinear-buckling-explained/.

Speed Spares. (2019), "Speedspares-Full-Catalogue", Rustenburg.

Steel Construction Institute. (2013), *HANDBOOK OF STRUCTURAL STEELWORK - EUROCODE EDITION*.

Steel Forging. (2018), "Shipping Container Door Hinge", *Steel Forging*, available at: http://www.steelforging.org/shipping-container-door-hinge/.

Stewart Lumber and Hardware. (2020), "The Most Common Types of Building Materials Used in Construction", *Building Materials*.

Subramanian, L. and White, D.W. (2017), "Improved Noncompact Web-Slenderness Limit for Steel I-Girders", *Journal of Structural Engineering*, Vol. 143 No. 4.

Stellenbosch University https://scholar.sun.ac.za

Usmani, A.S., Rotter, J.M., Lamont, S., Sanad, A.M. and Gillie, M. (2001), "Fundamental principles of structural behaviour under thermal effects", *Fire Safety Journal*, Vol. 36 No. 8, pp. 721–744.

Wankhede, A. (2021), "A Guide to Shipping Container Dimensions", *Maritime Law*.

Wolff, M., Bo, M. and Helm, D. (2008), "Material behavior of steel – Modeling of complex phenomena and thermodynamic consistency", Vol. 24, pp. 746–774.

Yang, G. and Bradford, M.A. (2015), "Thermoelastic buckling and post-buckling of weakened columns", *Structures*, pp. 12–19.

Yu, Y. and Chen, Z. (2018), "Rigidity of corrugated plate sidewalls and its effect on the modular structural design", *Engineering Structures*, Elsevier, Vol. 175 No. April, pp. 191–200.

Zha, X. and Zuo, Y. (2016a), "Theoretical and experimental studies on in-plane stiffness of container structure with holes", *Advances in Mechanical Engineering*, Vol. 8 No. 6, pp. 1–17.

Zha, X. and Zuo, Y. (2016b), "Theoretical and experimental studies on in-plane stiffness of integrated container structure", *Advances in Mechanical Engineering*, Vol. 8 No. 3, pp. 1–20.

Zhao, X.-L., Wilkinson, T. and Hancock, G. (2005), *Cold-Formed Tubular Members and Connections*.

Stellenbosch University https://scholar.sun.ac.za

APPENDIX A

The information listed in this appendix describes the geometric properties of the salient features for the 20 ft ISO shipping container.

Back-corner column

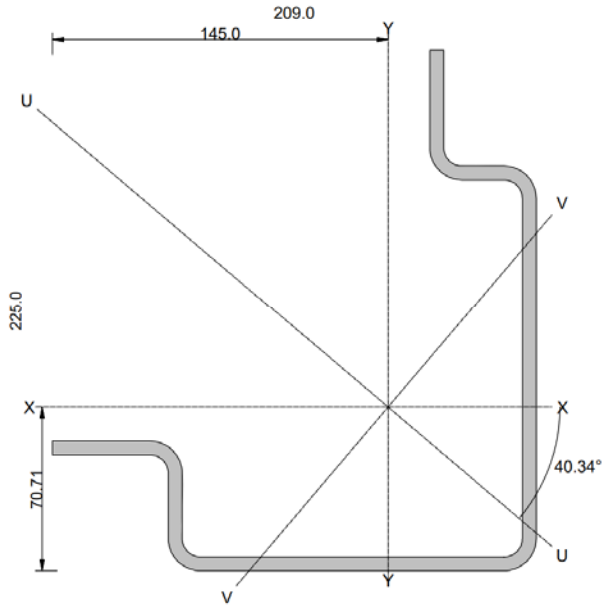

$A\ (10^3)$	2.97	[mm^2]
$I_{xx}\ (10^6)$	14.5	[mm^4]
$I_{yy}\ (10^6)$	12.7	[mm^4]
$I_{xy}\ (10^6)$	5.36	[mm^4]
$I_{uu}\ (10^6)$	19.0	[mm^4]
$I_{vv}\ (10^6)$	8.18	[mm^4]
$I_r\ (10^6)$	27.2	[mm^4]
$Z_{plx}\ (10^3)$	169	[mm^3]
$Z_{ply}\ (10^3)$	158	[mm^3]
Y_c	70.7	[mm]
X_c	145	[mm]

Stellenbosch University https://scholar.sun.ac.za

$J\ (10^3)$	37.9	[mm^4]
$C_w\ (10^{36})$	1.53	[mm^6]

Front-corner column

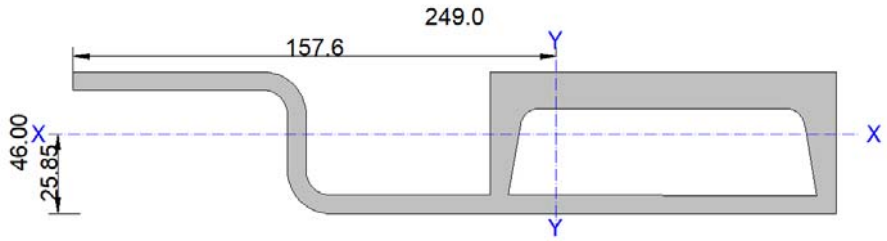

$A\ (10^3)$	3.53	[mm^2]
$I_{xx}\ (10^6)$	1.02	[mm^4]
$I_{yy}\ (10^6)$	15.7	[mm^4]
$I_{xy}\ (10^6)$	-0.352	[mm^4]
$I_{uu}\ (10^6)$	15.7	[mm^4]
$I_{vv}\ (10^6)$	1.01	[mm^4]
$I_r\ (10^6)$	16.8	[mm^4]
$Z_{plx}\ (10^3)$	52.8	[mm^3]
$Z_{ply}\ (10^3)$	193	[mm^3]
Y_c	25.9	[mm]
X_c	158	[mm]
$J\ (10^6)$	1.84	[mm^4]
$C_w\ (10^9)$	4.39	[mm^6]

Stellenbosch University https://scholar.sun.ac.za

Bottom-side beam

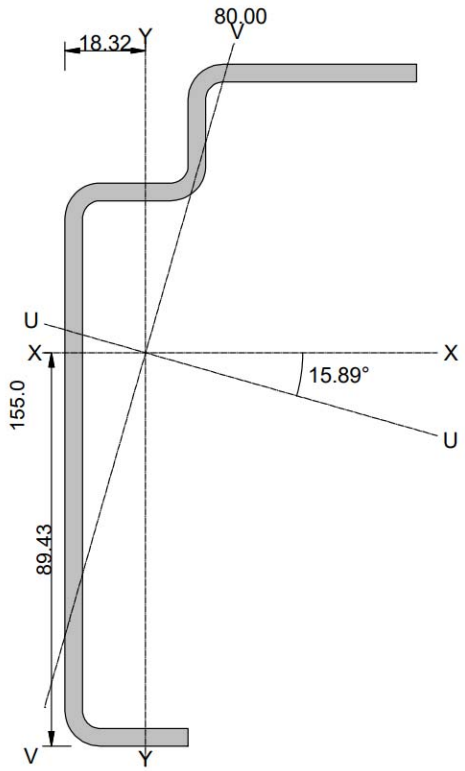

$A\ (10^3)$	0.978	[mm^2]
$I_{xx}\ (10^6)$	2.84	[mm^4]
$I_{yy}\ (10^6)$	0.465	[mm^4]
$I_{xy}\ (10^6)$	0.735	[mm^4]
$I_{uu}\ (10^6)$	3.05	[mm^4]
$I_{vv}\ (10^6)$	0.255	[mm^4]
$I_r\ (10^6)$	3.30	[mm^4]
$Z_{plx}\ (10^3)$	46.4	[mm^3]
$Z_{ply}\ (10^3)$	15.9	[mm^3]
Y_c	89.4	[mm]

Stellenbosch University https://scholar.sun.ac.za

X_c	18.3	[mm]
$J\ (10^3)$	5.19	[mm^4]
$C_w\ (10^6)$	272	[mm^6]

Bottom-end beam

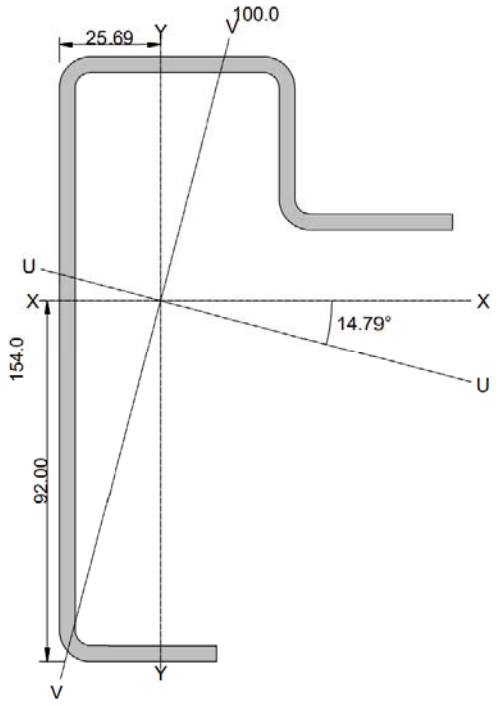

$A\ (10^3)$	1.26	[mm^2]
$I_{xx}\ (10^6)$	3.48	[mm^4]
$I_{yy}\ (10^6)$	1.06	[mm^4]
$I_{xy}\ (10^6)$	0.687	[mm^4]
$I_{uu}\ (10^6)$	3.66	[mm^4]
$I_{vv}\ (10^6)$	0.876	[mm^4]
$I_r\ (10^6)$	4.54	[mm^4]
$Z_{plx}\ (10^3)$	54.4	[mm^3]
$Z_{ply}\ (10^3)$	29.5	[mm^3]

Stellenbosch University https://scholar.sun.ac.za

Y_c	92.0	[mm]
X_c	25.7	[mm]
$J\ (10^3)$	6.73	[mm^4]
$C_w\ (10^9)$	1.49	[mm^6]

Top side and end beam

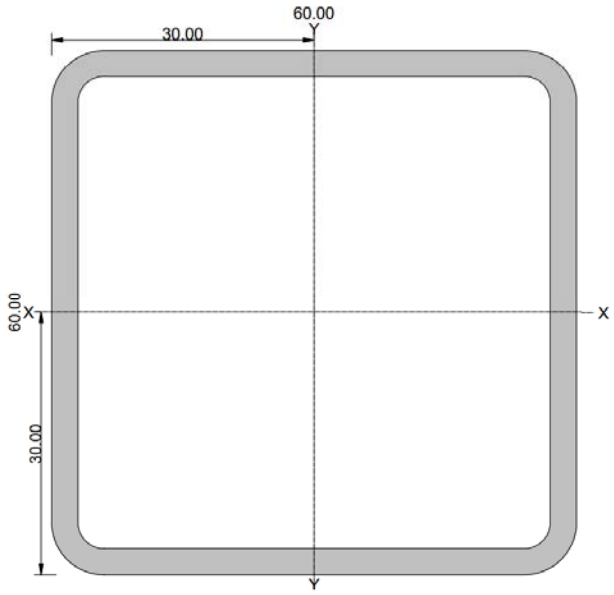

$A\ (10^3)$	0.661	[mm^2]
$I_{xx}\ (10^6)$	0.351	[mm^4]
$I_{yy}\ (10^6)$	0.351	[mm^4]
$I_{xy}\ (10^6)$	0.00	[mm^4]
$I_{uu}\ (10^6)$	0.351	[mm^4]
$I_{vv}\ (10^6)$	0.351	[mm^4]
$I_r\ (10^6)$	0.703	[mm^4]
$Z_{plx}\ (10^3)$	13.9	[mm^3]
$Z_{ply}\ (10^3)$	13.9	[mm^3]

Stellenbosch University https://scholar.sun.ac.za

Y_c	30.0	[mm]
X_c	30.0	[mm]
$J\ (10^3)$	565	[mm^4]
$C_w\ (10^3)$	226	[mm^6]

Cross beam

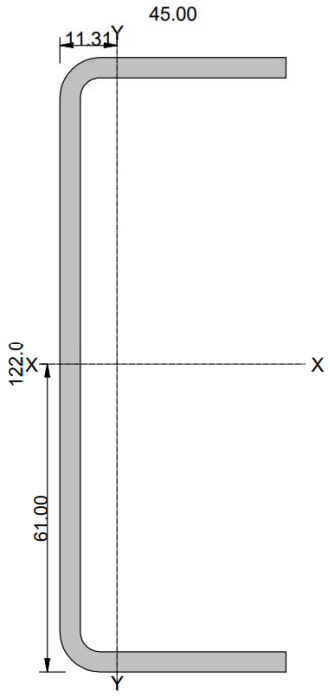

$A\ (10^3)$	0.795	[mm^2]
$I_{xx}\ (10^6)$	1.67	[mm^4]
$I_{yy}\ (10^6)$	0.144	[mm^4]
$I_{xy}\ (10^6)$	0.00	[mm^4]
$I_{uu}\ (10^6)$	1.67	[mm^4]
$I_{vv}\ (10^6)$	0.144	[mm^4]
$I_r\ (10^6)$	1.82	[mm^4]
$Z_{plx}\ (10^3)$	33.0	[mm^3]

Stellenbosch University https://scholar.sun.ac.za

Z_{ply} (10^3)	7.60	[mm^3]
Y_c	61.0	[mm]
X_c	11.3	[mm]
J (10^3)	4.20	[mm^4]
C_w (10^3)	338	[mm^6]

Stellenbosch University https://scholar.sun.ac.za

APPENDIX B

The steps listed below are used to perform a nonlinear elastic material buckling analysis (Riks) in ABAQUS. Steps 1-6 are used to compute the critical buckling load (Euler buckling capacity) while the remainder of the steps describe the process of including plasticity and geometric imperfections in the model to ultimately compute the nonlinear elastic material buckling capacity.

1. Define geometry of columns.
2. Discretise the column into an adequate number of finite elements.
3. Define material properties, boundary conditions, interactions and load.
4. Create a linear perturbation step namely Buckle.
5. Edit the keyword script by creating a *NODE FILE before *End step to store the deflections of the eigen modes.
6. Run the eigen value buckling analysis so that the *NODE FILE is generated and record the critical buckling load for the first eigen mode.
7. Create a copy of the model developed up until step 6.
8. Modify material parameters to include plasticity.
9. Delete the Buckle step and define a static Riks step.
10. Apply critical buckling load from eigen value buckling analysis
11. Edit the keyword script to import the initial imperfection file obtained from the eigen value buckling analysis as follows:
    - Remove the *NODE FILE from the copied model.
    - Add *IMPERFECTION before the first step and provide the name of the job associated with the eigenvalue buckling analysis as well as the mode to be scaled including its scaling factor i.e., $L/1000$.
12. Run the analysis and obtain the full load-deflection response via the load proportionality factor to ultimately determine the nonlinear elastic buckling capacity.

Stellenbosch University https://scholar.sun.ac.za

APPENDIX C

This appendix includes the configuration factors as determined for the unprotected models discussed in Chapter 6. S and C refer to the flat and chamfered surfaces respectively.

Back corner column configuration

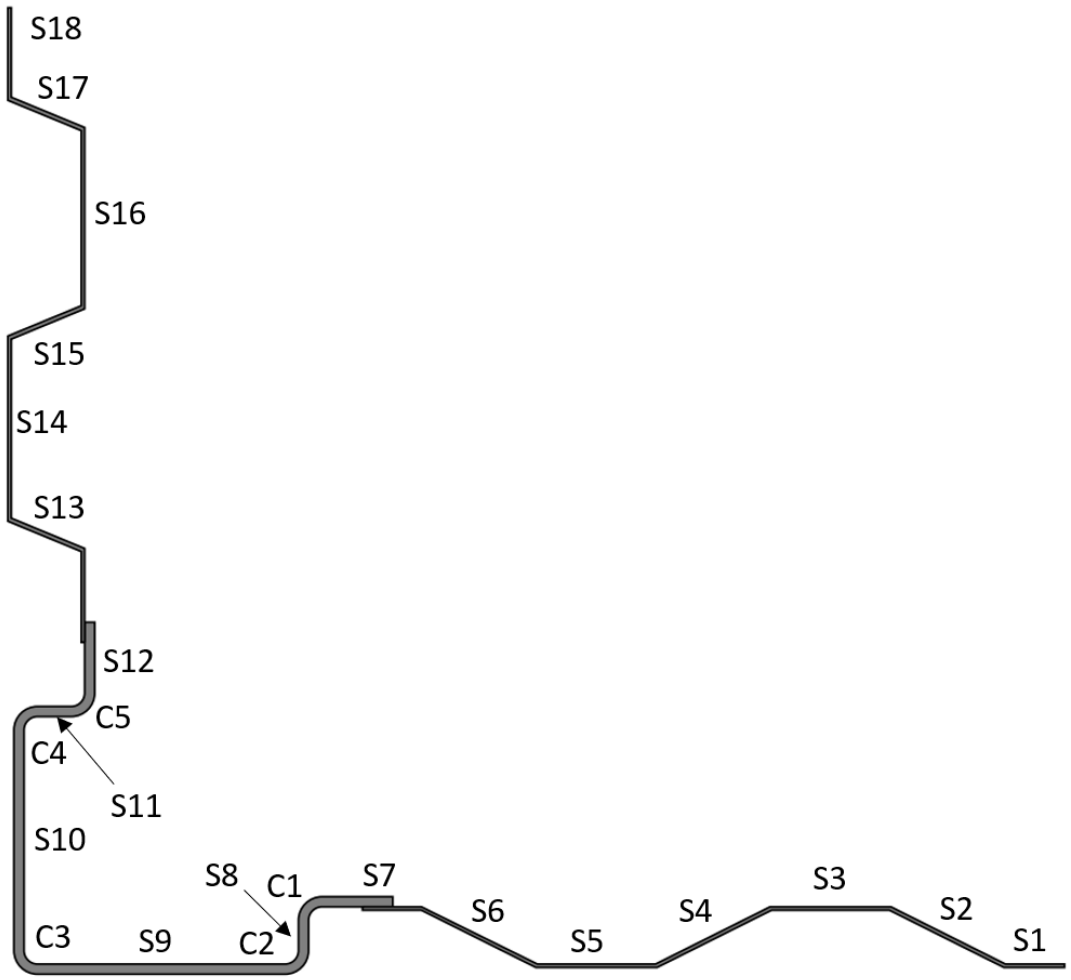

Surface	Configuration factor
S1	0.48
S2	0.60
S3	0.70
S4	0.64
S5	0.66

Stellenbosch University https://scholar.sun.ac.za

S6	0.64
S7	0.7
S8	0.22
S9	0.42
S10	0.41
S11	0.35
S12	0.7
S13	0.43
S14	0.56
S15	0.43
S16	0.7
S17	0.54
S18	0.41
C1	0.46
C2	0.32
C3	0.42
C4	0.38
C5	0.53

Stellenbosch University https://scholar.sun.ac.za

Front corner column configuration

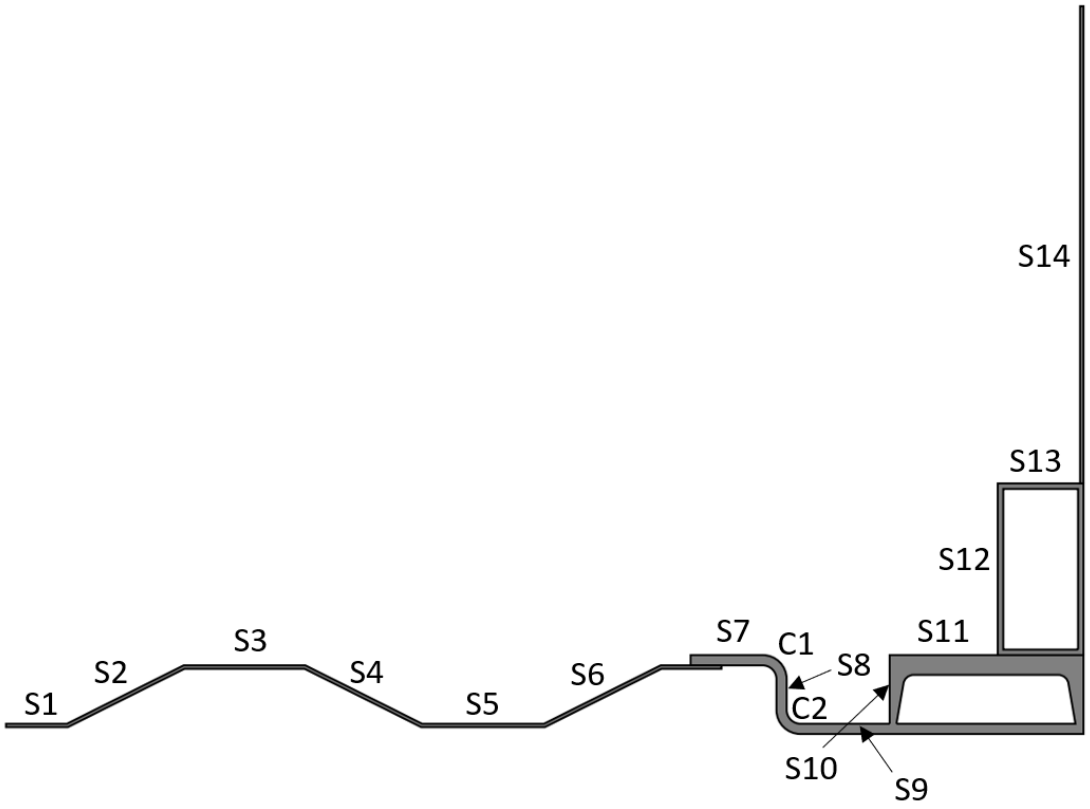

Surface	Configuration factor
S1	0.47
S2	0.6
S3	0.7
S4	0.64
S5	0.66
S6	0.64
S7	0.7
S8	0.23
S9	0.37
S10	0.24

Stellenbosch University https://scholar.sun.ac.za

S11	0.7
S12	0.7
S13	0.32
S14	0.59
C1	0.57
C2	0.10
Bottom beam configuration	
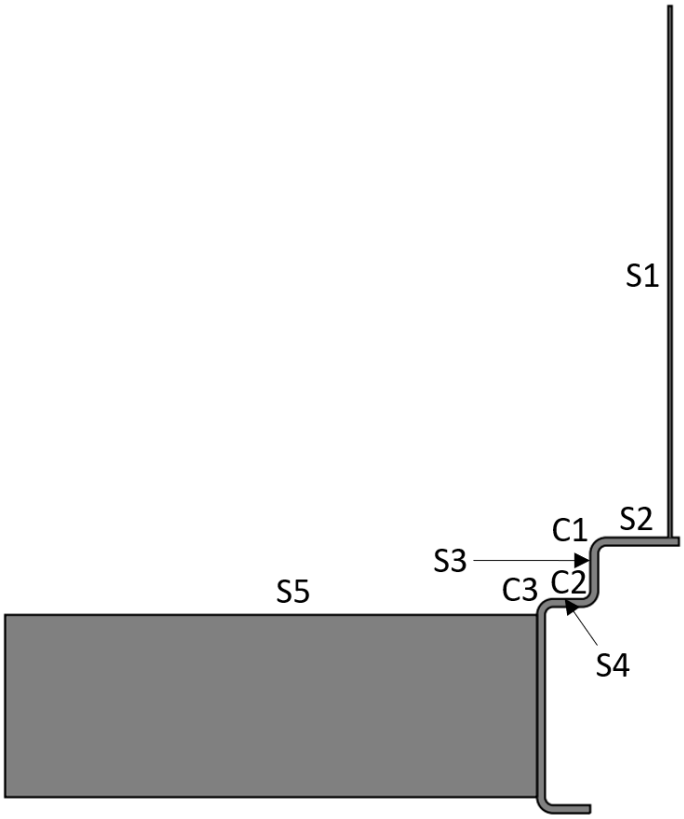	
Surface	Configuration factor
S1	0.60
S2	0.32
S3	0.33
S4	0.56

Stellenbosch University https://scholar.sun.ac.za

S5	0.63
C1	0.33
C2	0.45
C3	0.59
Top beam configuration	
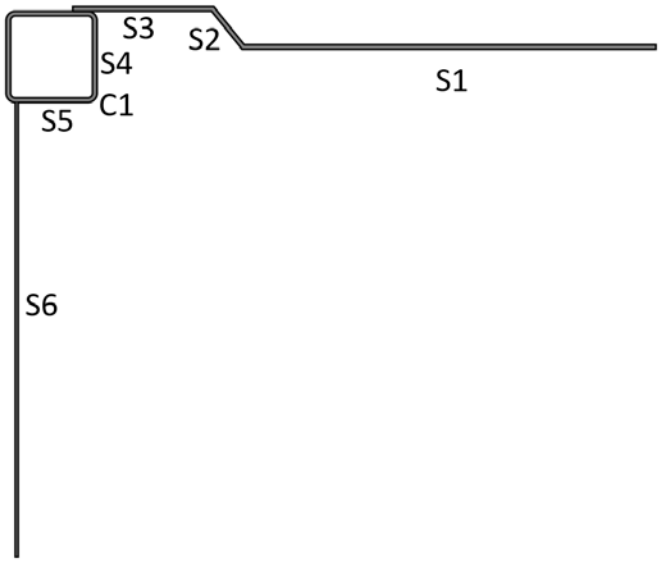	
Surface	Configuration factor
S1	0.7
S2	0.525
S3	0.52
S4	0.7
S5	0.36
S6	0.59
C1	0.53

Stellenbosch University https://scholar.sun.ac.za

APPENDIX D

The following equations are used to compute the stress-strain relationship for carbon steel at elevated temperatures according to EN 1993-1-2 (2005).

$$\sigma = \varepsilon E_{a,\theta} \qquad \varepsilon \leq \varepsilon_{p,\theta}$$

$$= f_{p,\theta} - c + (b/a)[a^2 - (\varepsilon_{y,\theta} - \varepsilon)^2]^{0.5} \qquad \varepsilon_{p,\theta} < \varepsilon < \varepsilon_{y,\theta}$$

$$= f_{y,\theta} \qquad \varepsilon_{y,\theta} \leq \varepsilon \leq \varepsilon_{t,\theta}$$

$$= f_{y,\theta}[1 - (\varepsilon - \varepsilon_{t,\theta})/(\varepsilon_{u,\theta} - \varepsilon_{t,\theta})] \qquad \varepsilon_{t,\theta} \leq \varepsilon \leq \varepsilon_{u,\theta}$$

$$= 0 \qquad \varepsilon = \varepsilon_{u,\theta}$$

with:

$$\varepsilon_{p,\theta} = f_{p,\theta} / E_{a,\theta}$$

$$\varepsilon_{y,\theta} = 0.02$$

$$\varepsilon_{t,\theta} = 0.15$$

$$\varepsilon_{u,\theta} = 0.2$$

$$a^2 = (\varepsilon_{y,\theta} - \varepsilon_{p,\theta})(\varepsilon_{y,\theta} - \varepsilon_{p,\theta} + c/E_{a,\theta})$$

$$b^2 = c\,(\varepsilon_{y,\theta} - \varepsilon_{p,\theta})E_{a,\theta} + c^2$$

$$c = (f_{y,\theta} - f_{p,\theta})^2/((\varepsilon_{y,\theta} - \varepsilon_{p,\theta})E_{a,\theta} - 2(f_{y,\theta} - f_{p,\theta}))$$

where:

$f_{y,\theta}$	=	effective yield strength
$f_{p,\theta}$	=	proportional limit
$E_{a,\theta}$	=	effective elastic modulus
$\varepsilon_{p,\theta}$	=	strain at the proportional limit
$\varepsilon_{y,\theta}$	=	yield strain
$\varepsilon_{t,\theta}$	=	limiting strain for yield strength
$\varepsilon_{u,\theta}$	=	ultimate strain

Stellenbosch University https://scholar.sun.ac.za